



**CALIFORNIA
ENERGY COMMISSION**



**CALIFORNIA
natural
resources
AGENCY**

Energy Research and Development Division

FINAL PROJECT REPORT

Renewable Natural Gas Production from Woody Biomass via Gasification and Fluidized-Bed Methanation

Gavin Newsom, Governor
August 2020 | CEC-500-2020-055

PREPARED BY:

Primary Author:

Dr. Reinhard Seiser, UC San Diego
Dr. Robert Cattolica, UC San Diego
Michael Long, UC Davis

University of California, San Diego
Department of Mechanical and Aerospace Engineering
9500 Gilman Dr. #0411, La Jolla, CA 92093
(858) 692-4143
<http://maeweb.ucsd.edu>

Contract Number: PIR-14-023

PREPARED FOR:

California Energy Commission

Kevin Uy
Project Manager

Jonah Steinbuck, Ph.D.
Office Manager
ENERGY GENERATION RESEARCH OFFICE

Laurie ten Hope
Deputy Director
ENERGY RESEARCH AND DEVELOPMENT DIVISION

Drew Bohan
Executive Director

DISCLAIMER

This report was prepared as the result of work sponsored by the California Energy Commission. It does not necessarily represent the views of the Energy Commission, its employees or the State of California. The Energy Commission, the State of California, its employees, contractors and subcontractors make no warranty, express or implied, and assume no legal liability for the information in this report; nor does any party represent that the uses of this information will not infringe upon privately owned rights. This report has not been approved or disapproved by the California Energy Commission nor has the California Energy Commission passed upon the accuracy or adequacy of the information in this report.

ACKNOWLEDGEMENTS

The primary authors acknowledge the other authors who wrote sections of this report:

- Elija Talebi, TU-Munich (Chapter 4: Methanation and Appendix G)
- Jonathan Christiani and James Easterly, Black and Veatch (Appendices A and B)
- Hui Liu, UC San Diego (Appendix I)
- Tinku Baidya, UC San Diego (Appendix J)
Tilman Schildhauer, Jörg Schneebeli, Alwin Frei, and Serge Biollaz, Paul-Scherrer
Institute (Appendices K and L)

The authors acknowledge other contributors involved in the project:

- University of California San Diego
 - Zachariah McCaffrey
 - Tinku Baidya
 - Shane Plant-Mason
 - Hui Liu
- University of California Davis
 - Bryan Jenkins
 - Li Wang
- West Biofuels
 - Peter Paul
 - Matthew Summers
 - Matthew Hart
 - Brandon Bruning
 - Chang-hsien Liao
 - Matthew Hoffman
 - George Loveday
 - John Lipinski
 - Andrew Ramirez
 - Briain Dennis
 - Cody McCallum
 - Anthony Roca
- Paul Scherrer Institut, Switzerland
 - Serge Biollaz
 - Tilman Schildhauer
 - Joerg Schneebeli
 - Frank Schillinger
- Technical University Munich, Germany
 - Elija Talebi
 - Felix Fisher
 - Sebastian Fendt
- Bioenergy 2020+, Austria
 - Reinhard Rauch
 - Markus Gölles
 - Benjamin Paul

- Technical Advisory Committee
 - Joergen Held, Renewable Energy Technology International AB
 - Paul Vergnani, CHA Corporation
 - Ron Kent, Sempra Energy
 - Valentino Tiangco, SMUD

The authors also thank the corporations that have contributed match funds or other equipment and materials to the project.

- West Biofuels for providing the operational time on the gasifier and associated equipment.
- SMUD for providing in-kind match funds to evaluate costs and benefits and contribute to the techno-economic analysis.
- UC Davis for providing Prof. Jenkins' time and helpful guidance for the project.
- Parker Hannifin Veriflo Division - for donating the compressor for the compression of producer gas.
- SulfaTrap for donating adsorbent materials and their help in specifying proper operating conditions.

PREFACE

The California Energy Commission's (CEC) Energy Research and Development Division manages the Natural Gas Research and Development Program, which supports energy-related research, development, and demonstration not adequately provided by competitive and regulated markets. These natural gas research investments spur innovation in energy efficiency, renewable energy and advanced clean generation, energy-related environmental protection, energy transmission and distribution and transportation.

The Energy Research and Development Division conducts this public interest natural gas-related energy research by partnering with research, development, and demonstration entities, including individuals, businesses, utilities and public and private research institutions. This program promotes greater natural gas reliability, lower costs and increases safety for Californians and is focused in these areas:

- Buildings End-Use Energy Efficiency.
- Industrial, Agriculture and Water Efficiency.
- Renewable Energy and Advanced Generation.
- Natural Gas Infrastructure Safety and Integrity.
- Energy-Related Environmental Research.
- Natural Gas-Related Transportation.

Renewable Natural Gas Production from Woody Biomass via Gasification and Fluidized-Bed Methanation is the final report for Contract Number PIR-14-023 conducted by the University of California, San Diego. The information from this project contributes to the Energy Research and Development Division's Natural Gas Research and Development Program.

For more information about the Energy Research and Development Division, please visit the [CEC's research website](http://www.energy.ca.gov/research/) (www.energy.ca.gov/research/) or contact the CEC at 916-327-1551.

ABSTRACT

Converting forest waste to renewable natural gas for pipeline injection has the potential to reduce the carbon footprint of the natural gas system and provide a beneficial use for abundant forest waste in California. However, there are significant cost and technological barriers to enabling the conversion pathway. One barrier is the cleanup and methanation processes to convert gas derived from woody biomass into pipeline-quality renewable natural gas since there are no successfully demonstrated methods for performing this difficult chemical conversion. Through laboratory and pilot-scale testing, this study developed novel gas cleanup and methanation methods to convert woody biomass to renewable natural gas. In particular, this study focused on fluidized bed methanation, a highly efficient form of methanation that can reduce the operating costs of the methanation process. The research team tested two different feedstocks, seven adsorbents, and two methanation catalysts. Researchers developed and tested new methods to measure trace contaminants in the product gas, new gas cleanup methods, and production of renewable natural gas from fluidized bed methanation. Finally, the researchers performed technical and economic analysis for a full-scale, 60 megawatt renewable natural gas facility. Researchers found the fluidized bed methanation technology could deliver a levelized cost of renewable natural gas of \$26 per million British thermal units a fully commercialized, full-scale scenario. Further improvements, outlined in the recommendations section, could further reduce this cost. Overall, this study found fluidized bed methanation to be a viable technology to produce renewable natural gas from woody biomass.

Keywords: gasification, fluidized-bed methanation, sulfur analysis, gas cleanup, nickel catalyst

Please use the following citation for this report:

Seiser, Reinhard, Robert Cattolica, and Michael Long. 2020. *Renewable Natural Gas Production from Woody Biomass via Gasification and Fluidized-Bed Methanation*. California Energy Commission. Publication Number: CEC-500-2020-055.

TABLE OF CONTENTS

	Page
ACKNOWLEDGEMENTS.....	i
PREFACE	iii
ABSTRACT	iv
EXECUTIVE SUMMARY	1
Introduction.....	1
Project Purpose.....	1
Project Process	2
Project Results.....	2
Technology/Knowledge Transfer	3
Benefits to California	3
CHAPTER 1: Introduction	5
CHAPTER 2: Operation of the Gasifier	7
Gasifier Overview	7
Gasifier Subsystems	7
Biomass-Feeding System	8
Heat-Recovery System.....	10
Steam Generator	11
Insulation of Refractory Sections	12
Feedstocks.....	13
Summary of Gasifier Tests	16
Gasification Parameters	16
Producer Gas Composition	17
Collection of Producer Gas	24
Compression of Producer Gas.....	24
Producer Gas Cylinders	26
Composition of Collected Producer Gas	27
CHAPTER 3: Gas Cleanup	29
Chilled Biodiesel Scrubber	29
Design and Construction of Scrubber	29
Adsorbent Studies	32
Materials and Methods.....	32

Test Plan	34
Test Results	36
Gas Cleanup of Producer Gas Before Methanation	45
CHAPTER 4: Methanation	46
Catalyst Development.....	46
Catalyst Support.....	46
Fluidization Tests.....	46
Fluidized-bed Catalyst.....	49
Fixed-Bed Characterization.....	50
Methanation Testing Experimental Setup	51
Gas-Generation Unit	52
Gas Cleaning Unit	53
Axial Sampling Unit.....	54
Post Reactor	56
Control	56
Methanation Experiments	66
Gas Composition Throughout Fluidized-Bed Methanation Reactor	68
Catalyst Comparison	69
Parameter Study	70
Operation on Synthesis Gas From Gasifier.....	71
Catalyst Surface Analysis	72
Modeling of Fluidized-Bed Reactor.....	72
Concluding Remarks.....	74
CHAPTER 5: Project Benefits and Production Readiness Plan	75
Qualitative Project Benefits	75
Job Creation.....	75
Reduction of Operations and Maintenance (O&M) Costs.....	75
Reduction of Capital Costs	75
Non-Energy Economic Benefits.....	75
Energy Security	76
Greenhouse Gas (GHG) Emissions Reductions	76
Criteria Air Pollution Emission Reductions.....	76
Habitat Area Disturbance Reductions	76
Quantitative Benefits for a Single 60MW _{RNG} Plant	76

Potential Project Benefits to California	77
Production Readiness Plan	77
Levelized Costs of RNG	77
Sensitivity Analysis of Costs	80
Comparison to Conventional Systems	81
Scale-up of Gasification System.....	82
CHAPTER 6: Knowledge Transfer	84
Conferences.....	84
Meetings.....	86
Webinars	87
Publications	87
Collaboration with Paul-Scherrer Institute	88
Collaboration with TU Munich.....	89
CHAPTER 7: Conclusions	90
LIST OF ACRONYMS.....	93
REFERENCES	94
APPENDICES.....	A-1

LIST OF FIGURES

	Page
Figure 1: Process of Thermochemical RNG Production	5
Figure 2: Schematic of Gasifier Pilot Plant.....	8
Figure 3: Process Flow Diagram for the Gasifier Pilot Plant	9
Figure 4: Picture of Roto-Disk Valve	9
Figure 5: Gas Composition Affected by Feeding Cycles	10
Figure 6: Heat-Recovery System	11
Figure 7: Steam Generator	12
Figure 8: Replacement of Insulation on Combustor Section	13
Figure 9: Photograph of Forest Thinnings	14
Figure 10: Testing of Orifice Plate with Nitrogen	16
Figure 11: CAD Drawing of Pilot Gasification Plant	18
Figure 12: Gas-Sampling Points after Chilled Scrubber.....	18

Figure 13: Major Gas Components in Producer Gas	19
Figure 14: Portable Tar Sampling Equipment	20
Figure 15: Tar Sampling During Operation.....	21
Figure 16: Sampling Equipment for Tars and Sulfur Tars	21
Figure 17: GC-SCD for Sulfur Analysis	22
Figure 18: Measured Sulfur Compounds in Producer Gas	23
Figure 19: Testing of Gas Compressor	25
Figure 20: Producer Gas Compression during Gasifier Operation	25
Figure 21: Schematic of Producer Gas Compression	26
Figure 22: Use of Compressed Producer Gas.....	26
Figure 23: Major Gas Components in Producer Gas Cylinders.....	27
Figure 24: Sulfur Components in Producer Gas Cylinders	27
Figure 25: Design of a Multi-Stage Version of a Scrubber	30
Figure 26: Construction and Installation of a Single-Stage Scrubber	30
Figure 27: Installed Chilled Scrubber	31
Figure 28: Results from Chilled Scrubber	32
Figure 29: Schematic of Adsorbent Testing	33
Figure 30: Installed Adsorption Vessel.....	33
Figure 31: Definition of Quantities in Adsorbent Studies	34
Figure 32: Sulfur Analysis Before and After SulfaTreat Adsorbent.....	40
Figure 33: Sulfur Analysis Before and After Brightblack Adsorbent	41
Figure 34: Adsorbent Results on Activated Biochar	42
Figure 35: Adsorbent Capacities for Circledraft Biochar.....	43
Figure 36: Adsorbent Capacities for SulfaTrap R8C.....	44
Figure 37: Adsorbent Capacities for Biochar (Fluidized Bed).....	45
Figure 38: Catalyst Support Material.....	47
Figure 39: Size Distribution of Bed Material.....	47
Figure 40: Cold-Flow Experiment	48
Figure 41: Determination of Minimum Fluidization.....	48
Figure 42: Bulk Density of Fluidized Bed Catalyst	49
Figure 43: Fixed-bed Flow Reactor	50

Figure 44: Catalyst Screening Results.....	50
Figure 45: Process Flow Diagram for the Laboratory Fluidized-Bed Methanation Setup	51
Figure 46: Gas and Steam Generation Components for the Laboratory Methanation Setup	52
Figure 47: Installation of Two Adsorbent Vessels Before the Fluidized-Bed Methanation Reactor	53
Figure 48: CAD Figures of the Engineered Main Reactor	54
Figure 49: Diagram of sampling probe locations.....	55
Figure 50: Axial Sampling Unit for Two Combined Gas-Sampling/Temperature Probes.....	55
Figure 51: Screenshot of Software	56
Figure 52: Control of Reactor Cooling by Compressed Air	57
Figure 53: External Reactor Cooling Using an Air Knife	58
Figure 54: Ceramic Heater for Preheating of Laboratory Methanation Reactor	59
Figure 55: Computer-Controlled Selector Valve for Gas Sampling Location.....	60
Figure 56: Laboratory Methanation Setup with Gas Sampling to Gas-Chromatograph	60
Figure 57: Engineering Design and Fabrication of Fluidized-Bed Methanation Reactor	61
Figure 58: Catalytic Synthesis Unit Fabrication and Assembly.....	62
Figure 59: Determination of Minimum Fluidization.....	63
Figure 60: Model Curves Compared to Experimental Data for UCSD and Meth134 Catalyst ...	64
Figure 61: Differential Temperature Versus Probe Height	65
Figure 62: Gas Phase Composition Versus Bed Height	68
Figure 63: Comparison of UCSD and a Commercial Fixed-Bed Type Catalyst.....	69
Figure 64: Effect of H_2/CO Equivalence Ratio	70
Figure 65: Influence of Steam Addition on Methane Concentration.....	72
Figure 66: Modeling of Fluidized Bed	73
Figure 67: Modeling of Fluidized Bed With Reaction and Heat Transfer	73
Figure 68: Calculation of Levelized Costs	79
Figure 69: Projected Levelized Cost of RNG	80
Figure 70: Sensitivity Analysis of Costs of RNG.....	81
Figure 71: Modeling of Pilot FICFB Gasifier	82
Figure 72: Modeling of Scaled-Up FICFB Gasifier.....	83
Figure 73: Modeling of Air Injection in Scaled-Up FICFB Gasifier	83
Figure 74: Presentation at TCBIomass 2015	84

Figure 75: Presentation at TCS Symposium 2016	85
Figure 76: Poster Presentation at TCBIomass 2015.....	86
Figure 77: Presentation at a DOE Biomass Committee Meeting	87
Figure 78: PSI microBFB Reactor	88
Figure 79: Workshop During BaCaTeC Summer School.....	89

LIST OF TABLES

	Page
Table 1: Proximate Analysis of Feedstocks.....	13
Table 2: Ultimate Analysis of Feedstocks	15
Table 3: Elemental Analysis of Ash (w%).....	15
Table 4: RCRA Metals in Ash.....	15
Table 5: Volatile Metals in Feedstock.....	15
Table 6: Overview of Gasifier Results	17
Table 7: Test Results of Tar and Particulate Measurements	22
Table 8: Results of Draeger Tube Measurement.....	24
Table 9: Summary Adsorbent Tests.....	35
Table 10: Adsorbent Testing Results	37
Table 11: Summary of Minimum Fluidization.....	49
Table 12: Range of Experimental Conditions.....	67
Table 13: Experimental Conditions for Bed Sampling Experiment	68
Table 14: Experimental Conditions for the Comparison of the Catalysts	69
Table 15: Experimental Conditions for the Investigation of Steam Addition	71
Table 16: Summary of Experimental Parameters.....	74
Table 17: Quantitative Benefits for a 60MW _{RNG} Plant.....	77

EXECUTIVE SUMMARY

Introduction

California has adopted ambitious goals to move from fossil to renewable energy sources for power, heating, and transportation fuels. Natural gas is an efficient energy carrier that is widely used in all three of these sectors and has a well-developed infrastructure for distribution and end use. Renewable natural gas (RNG) is similar to fossil natural gas and can serve as a drop-in replacement, and it can be produced from renewable biomass resources such as forest and agricultural residues. Other potential feedstocks are trees that have died from drought and bark-beetle infestations and pose a fire hazard, or biomass from orchard removal that is otherwise burned in open fires on fields. Most types of woody (also known as lignocellulosic) feedstocks are suitable for thermo (heat) chemical conversion, and can be converted to the desired fuel quickly (within minutes), efficiently (60 percent), and is scalable to larger plant sizes (greater than 30 megawatts [MW]).

For decades, technology has been available to convert coal to natural gas on a large scale (1 gigawatt [GW]) using gasification, a process that converts solid materials into an intermediate gas containing hydrogen, carbon monoxide, and hydrocarbons (producer gas), followed by methanation, a process which converts producer gas into methane. This technology can be adapted to biomass which, due to its distributed availability and logistics, is characterized by smaller plant sizes (less than 100 MW). For these smaller sizes, new technologies need to be developed that significantly reduce the specific costs compared to simply scaling down existing technologies.

Currently, California uses approximately 2 GW of biomass in solid fuel combustors and boilers to produce electricity. Alternatively, these plants could be modified to produce 1.2 GW of renewable natural gas equivalent to 30 trillion British thermal units (Btu) per year.

Project Purpose

Emerging technologies to convert biomass to RNG include fluidized-bed gasification and fluidized-bed methanation. They were pioneered in Europe and have the potential to match up with the size required for a commercial biomass-to-RNG plant. In fluidized-bed methanation, catalyst particles are suspended and can move freely between different zones, providing excellent heat and mass transfer. In conventional fixed-bed methanation, catalyst particles are larger and do not move around in the reactor. With fluidized-bed methanation, the capital and operating costs can be reduced by eliminating or simplifying several process steps. For example, only a single fluidized-bed methanation reactor is required instead of using several fixed-bed vessels in series. Further, fluidized-bed methanation is less sensitive to the producer gas composition, requiring fewer unit operations to adjust the gas properties. A process to remove sulfur-containing compounds is required, however, for all nickel-based methanation systems, and this is one of the steps that should be simplified and optimized depending on the plant size.

This project explored improving and testing several of the process steps to convert biomass to RNG. If the capital and operating costs can be reduced, the California natural gas industry could use this technology to construct several of these plants and produce significant amounts of RNG from domestic renewable resources.

During the project, it was also important to test the process in a setting where (a) actual biomass was converted to an intermediate producer gas, (b) the producer gas was cleaned of contaminants such as tar and sulfur species to prepare for methanation, and (c) the methanation was tested on the cleaned producer gas. This test is necessary to demonstrate that the technology would also work in a real-world application. A further goal was to derive costs for commercial-size production of RNG from biomass.

Project Process

The research team improved a pilot-plant gasifier (the system which converts woody feedstock to producer gas and precedes methanation) that operated on almond prunings and forest thinnings (mixture of soft wood such as pine and hard wood such as oak). The team recorded the operational parameters and the producer gas was analyzed for its applicability to conversion into renewable natural gas. During this process, the producer gas was cleaned and compressed into gas cylinders for later use in the methanation system. Further gas-cleanup studies were also conducted to remove key sulfur compounds before the producer gas was routed to the fluidized-bed methanation, which requires a low level of sulfur to ensure a long lifetime of the catalyst. Several adsorbent materials were tested that have the potential to reduce the cost of sulfur removal for small-to-medium-sized plants.

A laboratory-scale fluidized-bed methanation system was constructed and operated to prove that the cleaned producer gas from the gasifier can be converted into a mixture of methane and carbon dioxide. A number of operational parameters were tested to optimize the process. At the end of the project, the catalyst was analyzed to determine its integrity.

Analyzing all results from gasifier operation, gas cleanup, and fluidized-bed methanation was used to update the mass and energy balances for a commercial-size RNG plant. Based on those numbers, consulting firm Black & Veatch provided financial estimates for capital and operating costs for a projected commercial-scale biomass-to-RNG plant.

Project Results

A laboratory-scale fluidized-bed methanation unit was successfully operated using two different catalysts and producer gas collected from the gasifier as the feedstock. A two-stage adsorbent bed was used for sulfur removal before the methanation process, and no adverse effects or surface contamination by sulfur were found on the catalyst.

A new catalyst formulation was developed to extend the operating window for preventing coke formation. Coke, a hard carbon-containing substance, if formed during the process, may build up over time and inhibit gas-catalyst contact, significantly slowing the reaction speed. With the new catalyst, the required amount of steam for preventing coke is reduced, and this lowers the operating costs in a commercial plant. The catalyst was successfully tested against two other nickel-based catalysts, and improved stability against coke formation was found.

Analysis of a future commercial 60MW plant showed that the levelized cost of RNG, before any incentives or subsidies, is \$26/MMBtu. This is \$4/MMBtu less than a comparable plant based on fixed-bed methanation, due to simplification of several unit operations. The major price components of the RNG costs are capital costs (\$12/MMBtu, including interest, equity returns, and associated taxes), fixed and variable operating costs (\$10/MMBtu, including materials and labor), and feedstock costs (\$4/MMBtu). The capital costs include permitting, safety

equipment, and many auxiliary units that are required in such a thermochemical plant. Because of the associated complexity of the plant, an estimated staff of 72 is required (accounting for around-the-clock operation). This indicates that the main efforts for future cost reduction should be focused on further simplifying the process and improving automation. Costs at the current state of technology could be projected to be below \$20/MMBtu if the feedstock was provided for free as part of a forestry management program, and if credits were included (GHG reduction credits, tax credits.)

Technology/Knowledge Transfer

Interim and final results of the project were shared via conferences, webinars, publications, collaboration with research institutes and universities, and site tours of the facility. Prominent highlights include presentations at prominent international biomass conferences (TC Biomass 2015 and 2016), a published article in Chemical Engineering Science, and research collaboration with the Paul-Scherrer Institute (Switzerland) and the Technical University of Munich (Germany).

Benefits to California

The team identified technological and economic challenges for building commercial plants to convert woody biomass to RNG on a large scale. Because of the many unit operations within a thermochemical plant, capital and operating costs hold the potential to be further reduced if individual steps can be simplified, improved, and automated. Gasification, gas cleanup, and methanation are technologies that can be improved over time. The results of this study focusing on the current configuration to produce RNG from biomass has provided baseline data on the performance of this integrated biomass methanation system and new approaches for future cost reduction of RNG.

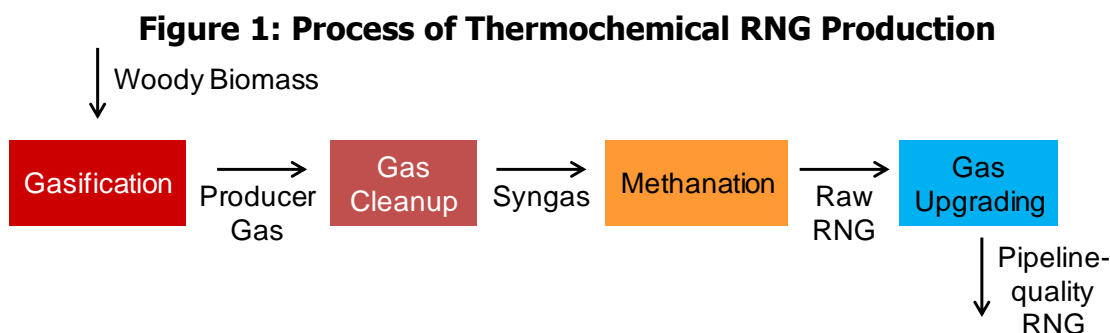
Natural gas is a major energy source in California used in power generation, industry, households, and transportation. Evaluating the thermochemical conversion of biomass to RNG can be beneficial to California ratepayers, because it would use abundant forest-waste resources that can be converted to RNG, significantly displacing fossil natural gas. A significant reduction in GHG emissions could be achieved by substituting RNG for fossil natural gas.

Using the technical availability of forest and urban biomass (26 million dry tons/year), 150 plants would provide 60 MW each, for a total production of 260 petajoule per year (245 million MMBtu/yr). Each plant would bring benefits with GHG reductions, wildfire reduction, energy security, jobs, and other economic activity. GHG reductions per plant would be an estimated 86,658 metric tons of CO₂ per year for a total of 13 million metric tons CO₂ per year in California. Each plant would further provide estimated benefits in wildfire prevention of \$650,000/year, energy security of \$1.5 million/year, and 2,400 direct and indirect jobs.

CHAPTER 1:

Introduction

Thermochemical conversion of biomass resources via gasification creates producer gas (also called synthesis gas or syngas), which can be further converted to RNG, a pipeline-quality gas, by the process of methanation. Because the syngas needs to be very clean before the methanation step, this process is still expensive. The conversion of producer gas by methanation, however, provides the opportunity to convert large amounts of available biomass in California into pipeline-quality renewable gas. Figure 1 shows the process steps for converting woody biomass to pipeline-quality RNG.



Source: UC San Diego

The goals of the proposed project were to reduce the costs of cleanup of producer gas and to reduce the costs of methanation. The current project investigated the methanation process using a fluidized-bed system design. This process is not yet commercial but has the potential to improve the economics of methanation compared to more costly processes with many cleanup steps (such as the GoBiGas project in Gothenburg, Sweden). Fluidized-beds have the advantage of excellent heat-transfer and can avoid hot spots in the presence of exothermic methanation reactions which can negatively impact catalysts (Kopyscinski, 2013). Fluidized-bed methanation is also not subject to olefin-whisker formations as in current commercial fixed-bed-methanation systems that generally require an additional olefin-removal process. At lower costs, fluidized-bed methanation could be economical at scales less than 60 MW_{RNG}, which is important because it matches the scale of the logistics of transporting biomass feedstocks.

The success of methanation is closely linked to the success of producer-gas cleanup, since small amounts of contaminants in the gas can deactivate the catalysts used in the process. Nickel-based methanation catalysts are sensitive to sulfur poisoning. Since a large part of the sulfur in the biomass is transferred to the producer gas, economical methods have to be found to remove these gaseous sulfur compounds. The project first quantified which sulfur compounds are present in the producer gas, and then studied various sulfur removal techniques.

To generate the producer gas from biomass, the FICFB gasifier at West Biofuels was used for this project. This type of gasifier converts chipped woody biomass into producer gas with a high efficiency (>80%). Several improvements were made to the gasifier and its subsystems, such as biomass feeding, steam generation, and heat recovery.

The project started in June 2015 and ended in May 2018. During the first year, planning and construction took place, while in the remaining two years, the experiments were conducted.

In addition to UC San Diego, partners in the project were West Biofuels, UC Davis, SMUD, and Black and Veatch. West Biofuels was responsible for the gasifier operation and maintenance and for the construction and setup of larger-scale equipment such as scrubbers, chillers, compressors, and gas storage. UC Davis served as measurement and verification provider and was responsible for many of the gas measurements and verification of flow rates. SMUD contributed techno-economic analysis to the project as match funds provider. This analysis was performed in collaboration with Black and Veatch, a consulting firm that specializes in energy projects.

CHAPTER 2:

Operation of the Gasifier

The purpose of the gasifier is to convert biomass to producer gas. Producer gas is a mixture of hydrogen, carbon monoxide, methane, ethylene, carbon dioxide, water, nitrogen, and other organic and inorganic contaminants. Producer gas, after appropriate gas cleaning, is suitable for fluidized-bed methanation, which converts hydrogen and carbon monoxide to methane (plus water and carbon dioxide).

Gasifier Overview

The fast-internally-circulating-fluidized-bed (FICFB) gasifier was developed by the Technical University Vienna [Hofbauer (2002), Rauch (2004)], and built together with Repotec Inc. at various demonstration scales throughout Europe. The CHP demonstration plant in Güssing has regularly achieved above 80 percent availability between 2006 and 2012. The FICFB gasifier achieves a high efficiency, requires no oxygen plant, and generates a producer gas with a high ratio of hydrogen to carbon monoxide (1.6-1.8). The dry gas contains already large amounts of methane (>20 percent by heating value), which is the main constituent in renewable natural gas (RNG). Since the gasifier is a fluidized bed, it allows for a wide range of biomass properties, including particle size and chemical composition.

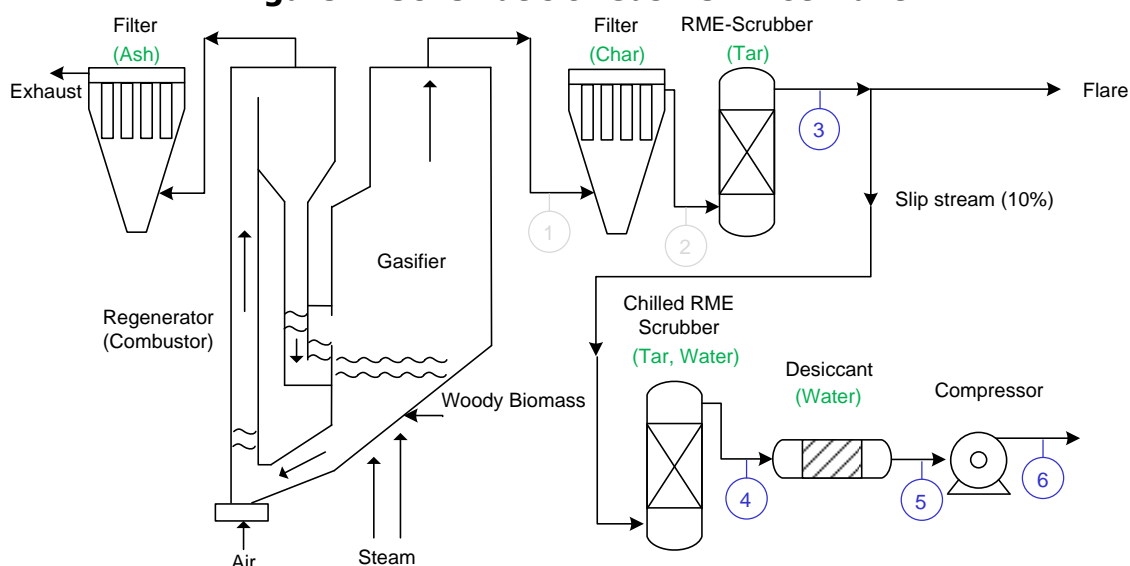
The operating principle of the FICFB gasifier is as follows (Figure 2). Biomass enters the gasifier vessel, which is a bubbling bed of hot bed material, fluidized by steam. The biomass thermally decomposes into producer gas and char by the heat provided from the bed material. Char and bed material are then carried to the regenerator section which is a riser using pneumatic transport with air. Here, the char is oxidized and the bed material reheated. A cyclone separates the flue gases from the hot bed material, and via a loop seal, the bed material flows back to the gasifier.

The producer gas leaves the gasifier on top and is cooled, filtered, and scrubbed of tars and water, and in this state it is clean enough for being combusted in a burner or internal combustion engine. For catalytic synthesis processes, the producer gas requires further cleaning. In the current project, the gas was initially cleaned by a second scrubbing and a drying process. This way, it could be compressed for further use and investigation. The compressed gas was then cleaned of sulfur before using it in the methanation reactor.

Gasifier Subsystems

Besides the main gasifier, additional unit operations and sub-systems are necessary for the plant to operate. The main unit operations after the gasifier are a filter that removes sent to the steam generator. The main other subsystems of the plant are the feeding system, the heat-recovery system, and the steam generator. Figure 2 shows the process flow diagram (PFD) of the entire pilot plant and indicates several of the subsystems.

Figure 2: Schematic of Gasifier Pilot Plant



Schematic of gasifier pilot plant and sampling locations. Sampling locations 3-6 were used for the measurement of sulfur compounds. Locations 1-3 were used for tar sampling.

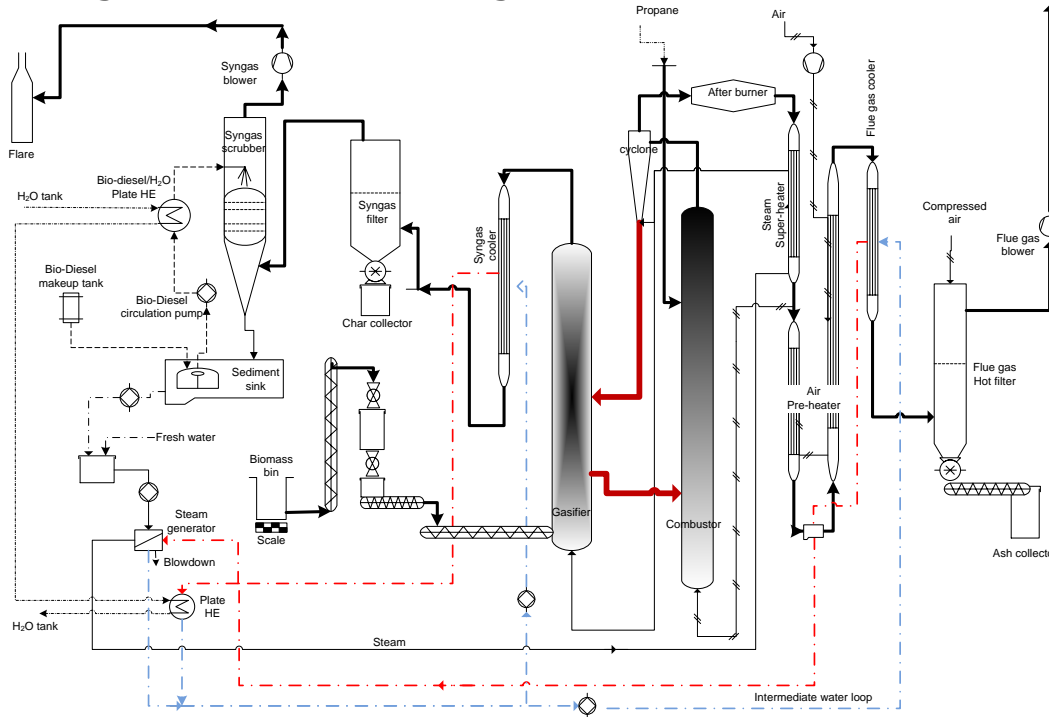
Source: UC San Diego

Biomass-Feeding System

Feeding systems often provide challenges to the operation, because feedstocks come in a variety of shapes, sizes, and moistures, and a blockage anywhere along the feed train for longer than a few minutes would disrupt the operation of the gasifier. Over the years, many lessons were learned among operators of gasification plants, and in the course of this project, the feeding system was reviewed and improved. A review of problems occurring in feeding systems led to the compilation of a list of failure modes that need to be avoided with any improved feed-system design. A table of these identified failure modes is provided in Appendix C. Some of the features of the improved feed system are detailed in the following paragraphs.

Figure 3 includes the schematic layout of the feeding system, starting with the biomass bin. The bin sits on a scale for determining of the overall feed rate between fillings. A bucket elevator transports the biomass intermittently to a lock hopper, that employs two roto-disc valves. Figure 4 shows a picture of a roto-disc, or dome valve, that was employed at the pilot plant. The advantage of the roto-disc valve over a knife-gate valve is that during closing, small wood debris is swiped in a tangential motion along the seals and not jammed into a narrow gap between the surfaces around the knife. Sealing of both valves is important, since at times, only one of them is closed, and if it were to leak, producer gas from the gasifier would flow backwards through the feeding system. Small leaks can be overcome with additional purge fluids (nitrogen), and also the lock-hopper needs to be compressed with a purge fluid during every cycle (combustor exhaust gas). A further improved version of the roto-disc valve employs an inflatable gasket, and this version would be recommended for future upgrades or scale-up of the plant.

Figure 3: Process Flow Diagram for the Gasifier Pilot Plant



Schematic of the gasifier system including subsystems such as feeding system, heat recovery system, and steam generation, and gas cleanup.

Source: UC San Diego

Figure 4: Picture of Roto-Disk Valve



Photograph of Roto-disc valve used for the lock hopper of the biomass feeding system. The Roto-disc valve was used to replace a knife-gate valve and provided better sealing at moderate pressures. It was also less susceptible to jamming by fine feedstock particles.

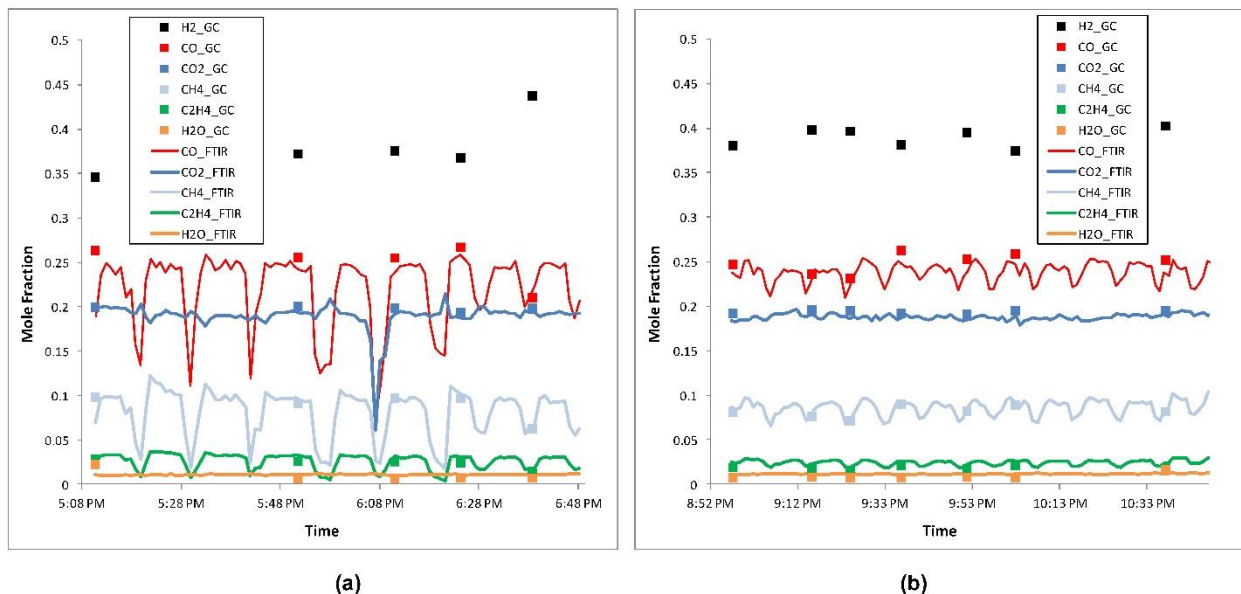
Source: UC San Diego

After the lock hopper, biomass falls into a small bin of a (converging) compression screw. The screw compresses the feedstock into a plug that, while not perfectly gas tight, reduces any diffusive or convective flows from the gasifier backwards through the screw. After the compression screw, blades mounted on a vertical shaft (not shown in Figure 3) loosen the

biomass from the plug, and biomass chips fall into the final screw transporting the biomass into the gasifier.

The operation of the lock hopper (and bucket elevator) is depending on the biomass level in the bin before the compression screw. As the biomass in the bin drops below a certain level (measured with a vibratory sensor), a new charge is refilled from the lock hopper. During the operation, it was discovered that unsteady feeding can affect the producer gas composition. As the biomass level in the compression-screw bin drops, the feed rate slows down. This slows down the gas production, but since there is circulating char in the gasifier system, the gas production is not slowed down proportionally to the feed rate. Since char contains less volatiles than fresh biomass, the composition of producer gas also changes. Percentage wise, the change is most pronounced in the mole fractions of methane and ethylene (Figure 5a). The concentration of these compounds can therefore be used to monitor the steadiness of biomass feeding. During the test, increasing the minimum level in the compression-screw bin decreased the drop of the feed rate during this part of the feeding cycle, and this steadied the gas composition (Figure 5b).

Figure 5: Gas Composition Affected by Feeding Cycles



Producer-gas composition (dried) during two phases of a gasifier test (20160330). Symbols show the measurements using a Micro GC and lines show those using an FTIR. (a) Period of high fluctuations in gas composition due to cycles in biomass feeding. (b) Period of reduced fluctuations after raising minimum level in compression-screw bin.

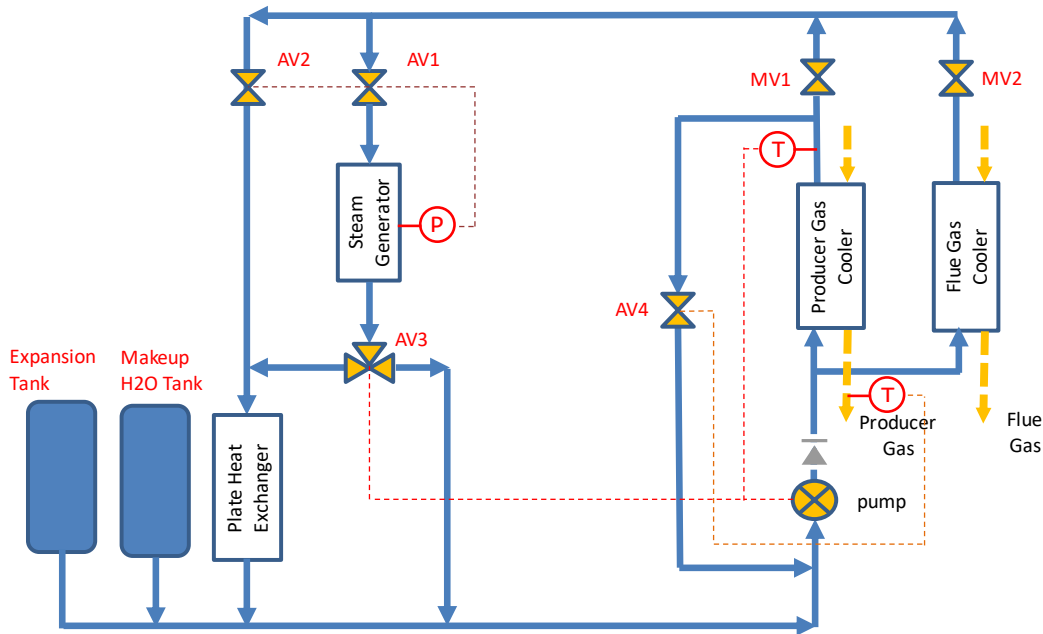
Source: UC San Diego

Heat-Recovery System

Product gas from the gasifier and exhaust gas from the combustor are cooled down in heat exchangers using pressurized water. The heated water is then used to generate steam for the gasifier, and any additional heat can be removed with ambient air or water. Figure 6 shows the entire heat-recovery system with a single pump and several valves for controlling the flows through various components. To control the water temperature exiting the two gas coolers, the pump speed is controlled. Two manual valves (MV1 and MV2) can be used to select the relative coolant flows through the gas coolers if the temperatures are too unequal. A valve in a

recycle loop around the producer gas cooler (AV4) is used to increase the water temperature at the heat-exchanger inlets. This is used to control the producer gas exit temperature which should be near 200C to avoid condensation of tars. The heated water is used to generate steam in an unfired steam generator. If less steam is required, some water may bypass the steam generator through AV2. If further cooldown is necessary, for example if the pump is operating at its maximum, some water can be routed through a final heat exchanger before it returns to the gas coolers (using AV3). This system was improved from a previous version employing two individual pumps for the product-gas cooler and exhaust gas cooler, respectively. In that system, the control of each pump also influenced the flow through the other pump, making the system difficult to control.

Figure 6: Heat-Recovery System



Schematic of heat recovery system with a single water pump. The producer gas- and flue gas coolers provide heat, and the steam generator and plate heat exchanger remove heat.

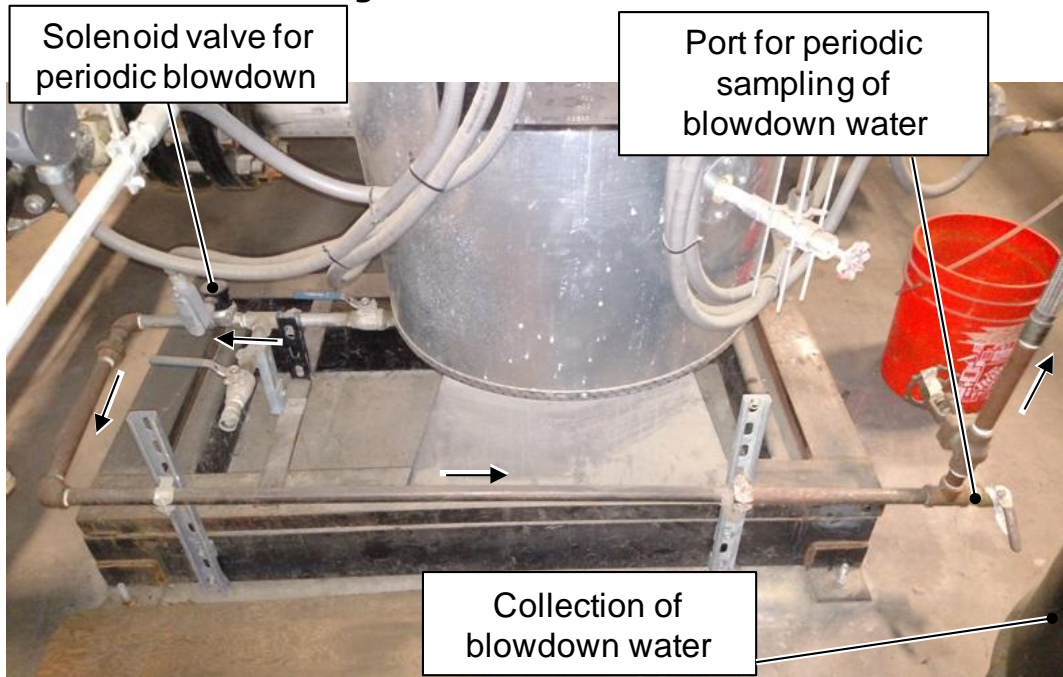
Source: UC San Diego

Steam Generator

Besides controlling the hot water flow on the heating side (hot side) of the steam generator, there are also several controls on the heated side (steam side, cold side). A solenoid valve controls the inlet of pressurized water to keep the water level inside the steam generator at a certain height. There is another solenoid valve at the bottom of the vessel to let out water/brine. This is called blowdown and is used periodically to remove minerals from the system. Since the water mostly comes from the condensate in the biodiesel scrubber, it contains various minerals that do not evaporate as steam is produced. In fact, these minerals would coat the heat-exchanger surface as scale and impact the heat transfer. Figure 7 shows the arrangement of the solenoid valve for blowdown and the drum used to collect the blowdown water. There is also a tee for taking a sample of the blowdown water to evaluate how close the brine is to saturation. During operation, it was attempted that the mineral concentration in the blowdown water is near half of the saturation point. This was achieved by opening the solenoid valve for 20 seconds every hour. It resulted in a blowdown water

collection of approximately one barrel per 24-hour operation. This water is one of the few waste streams generated from the plant and must be disposed.

Figure 7: Steam Generator



Photograph of steam generator with blowdown system. The solenoid valve is opened periodically to remove brine from the steam generator to avoid scaling of the heat exchanger surfaces. The blowdown water is collected in a barrel.

Source: UC San Diego

Insulation of Refractory Sections

Over time, some of the solid insulation around the refractory in the combustor was eroded and flow was able to bypass the inner refractory tubes. Several sections had to be repaired, and they were improved in two ways. First, a slightly denser poured insulating refractory was used to replace the solid foam insulation used previously. Second, stainless baffle plates were welded on the inside of the steel flanges, preventing the gas and particle flow from traveling around the inner refractory tubes and damaging the insulation. Figure 8 shows the installation of the repaired bottom section of the combustor.

Figure 8: Replacement of Insulation on Combustor Section



Photograph during installation of a newly repaired combustor section of the FICFB gasifier. The solid foam insulation was replaced with a poured refractory insulation, and baffle plates were welded inside the main flanges. This is to prevent gas flow near the metal walls.

Source: UC San Diego

Feedstocks

Table 1 shows the feedstocks considered for this project; all are woody biomass feedstocks, and the proximate analysis shows similar properties.

Table 1: Proximate Analysis of Feedstocks

	Moisture [kg / kgbiomass (a.r.)]	Ash (dry) [kg / kgbiomass (dry)]	Fixed carbon [kg / kgbiomass (dry)]	Volatiles [kg / kgbiomass (dry)]
Almond Prunings	7.1%	2.17%	21.30%	76.50%
Forest Thinnings	25.5%	1.04%	18.61%	80.41%
Forest Tops/Limbs	11.6%	1.82%	20.62%	78.33%
Forest Residue	20.1%	0.55%	22.36%	77.08%
Redwood	34.4%	0.23%	19.33%	80.61%
Average	20.1%	1.09%	20.65%	78.39%

Source: UC San Diego

The main differences are in the ash content which ranges from 0.23 percent to 2.17 percent. In general, a higher ash content leads to a lower efficiency, and often feedstocks with higher ash can also have a lower melting point. On the other hand, potassium and calcium in the ash can provide an important catalytic function in the gasifier, and therefore some ash content is desired. All the feedstocks listed here are within the desired range. Regarding moisture

content, there is also an optimal range. Too high moisture reduces the energy efficiency of the plant, but some moisture is desired in steam gasification. The demonstration plant in Güssing reported that 25 weight- percent moisture was a good compromise for low tar production. It is expected that a larger commercial plant may be able to handle 30 percent moisture, but feedstocks with a higher moisture content than that will need to be dried before use. Dry feedstocks may require additional makeup water in the steam generation, while very wet feedstocks may generate some waste water within the gasification plant. Since California has a relatively dry climate, feedstocks may dry during storage, transport, and handling. In the pilot plant, almond prunings and a mixture of almond prunings and forest thinnings were used, and no major problems were encountered. Figure 9 shows a photograph of the forest thinnings after screening to 1/4"-plus and 1"-minus with a deck screener. This feedstock was provided by Soper-Wheeler Co from thinning operations in the northern Sierra Nevada. The feedstock is made up of both soft wood and hard wood, as both trees grow in the mid-altitude forest.

Figure 9: Photograph of Forest Thinnings



Forest thinnings from the northern Sierra Nevada, provided by Soper-Wheeler Co. The feedstock was screened with a deck screener to 1/4"-plus and 1"-minus.

Source: UC San Diego

Table 2 shows the results of the ultimate analysis of the feedstocks considered for this project. The amounts of carbon, hydrogen, and oxygen are very similar between the different feedstocks. There is some variability in the amounts of nitrogen and sulfur. Both of these atoms are to be expected to occur in biomass. Nitrogen will preferentially form ammonia in the gasifier, which will be absorbed in the scrubber condensate and made back into steam. In fact, ammonia in the steam loop will prevent corrosion. Sulfur from the biomass is the main source for the sulfur compounds in the producer gas, and the quantification of these sulfur compounds and their cleanup is one of the major tasks in this project, since the methanation catalyst will be deactivated by sulfur. Source: UC San Diego

Table 3 shows that the main oxides in the ash are CaO, K₂O, SiO₂, and Al₂O₃. Table 4 shows the RCRA elements in the ash for some of the feedstocks, and Source: UC San Diego

Table 5 shows the volatile metals in the feedstocks themselves.

Table 2: Ultimate Analysis of Feedstocks

	C [kg / kgbiomass (dry)]	H [kg / kgbiomass (dry)]	N [kg / kgbiomass (dry)]	S [kg / kgbiomass (dry)]	O [kg / kgbiomass (dry)]
Almond Prunings	49.97%	5.82%	0.47%	0.0290%	41.78%
Forest Thinnings	52.15%	6.12%	0.12%	0.0010%	40.17%
Forest Tops/Limbs	51.94%	6.14%	0.18%	0.0250%	40.40%
Forest Residue	52.11%	6.17%	0.09%	0.0120%	41.08%
Redwood	52.36%	6.17%	0.05%	0.0130%	41.12%
Average	51.62%	6.07%	0.19%	0.0168%	41.07%

Source: UC San Diego

Table 3: Elemental Analysis of Ash (w%)

	SiO₂	Al₂O₃	TiO₂	Fe₂O₃	CaO	MgO	Na₂O	K₂O	P₂O₅	SO₃	Cl	CO₂
Almond Prunings	9.93	2.91	0.16	1.61	27.7	3.42	5.78	10.4	6	1.46	4.62	11.19
Forest Thinnings	27.29	11.28	1.13	7.31	26.2	2.4	0.38	11.7	2.26	0.62	0.01	3.55
Forest Tops/Limbs	19.82	10.15	1.02	6.3	27.7	4.31	0.45	15.5	3.44	0.75	0.03	6.01
Redwood	16.3	3.99	0.36	2.85	27.5	3.55	1.93	17.1	5.62	2.53	<0.01	12.93

Source: UC San Diego

Table 4: RCRA Metals in Ash

	Barium [mg/kg]	Cadmium [mg/kg]	Chromium [mg/kg]	Lead [mg/kg]	Silver [mg/kg]
Almond Prunings	270	9	281	33	16
Redwood	10100	11	353	160	10

Source: UC San Diego

Table 5: Volatile Metals in Feedstock

	Arsenic [mg/kg]	Mercury [mg/kg]	Selenium [mg/kg]
Almond Prunings	1.53	0.02	<0.05
Forest Thinnings	0.23	0.01	0.08
Forest Tops/Limbs	0.12	0.01	0.23
Redwood	0.61	0.01	0.08

Source: UC San Diego

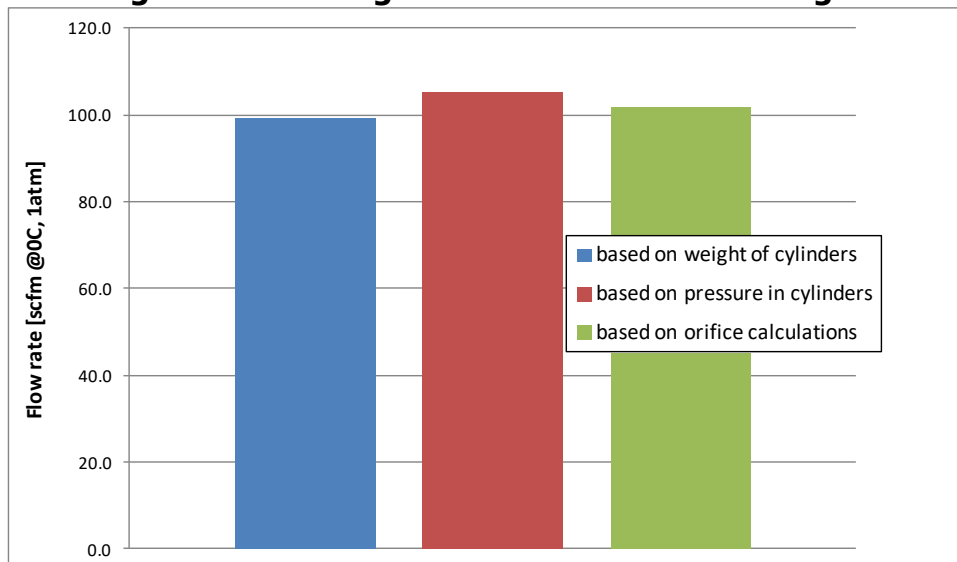
Summary of Gasifier Tests

As part of this project, three gasifier tests were conducted. During these tests, several parameters were evaluated, and measurements were conducted with consideration of using this type of gasifier for the production of RNG. Besides energetic efficiency and operating costs, the main factors for RNG production via fluidized-bed methanation are the main gas composition and the amount and type of impurities that affect the methanation catalyst.

Gasification Parameters

Several parameters influence the operation of the gasifier and product-gas composition. Some important ones are the biomass feed rate, steam/biomass ratio, and temperature. The biomass rate is controlled by the speed of the compression screw. All other devices along the feed train are adjusted accordingly. The feed rate is measured by a scale underneath the biomass bin. The steam rate is measured by the flow rate of the feed water into the steam generator. The steam/biomass rate is calculated by the overall steam amount (into gasifier and upper loop seal) divided by the biomass rate (wet). The temperature of the gasifier is influenced by various factors, such as biomass rate and composition, steam rate, bed-material circulation rate, air-flow rate to the combustor, and extra fuel flow to the combustor. Extra fuel to the combustor is the simplest way to affect the temperature. It can be a fuel such as propane, or a portion of the producer gas that is recycled to the combustor. The temperature of the gasifier is measured with several thermocouples that are inserted into the gasifier vessel. The main output variables during gasification are the producer-gas flow rate and composition. The flow rate was measured with an orifice plate after the biodiesel scrubber. The method followed ASME MFC-15-2003, and was once verified with nitrogen (Figure 10).

Figure 10: Testing of Orifice Plate with Nitrogen



Results of testing of flow-rate measurement using an orifice plate. The test was conducted with nitrogen cylinders and determining the flow rate based on the weight of the cylinders as well as the pressure and volume inside the cylinders. It compares well with the calculation of the flow rate from the pressure drop across the orifice plate (ASME MFC-15-2003).

Source: UC San Diego

The producer gas composition was measured with various instruments and is presented in the next sections. One quantity readily calculated from the producer-gas composition is the molar H₂/CO ratio. Table 6 shows the H₂/CO ratio that was achieved during the gasifier tests, and also the other key parameters are summarized.

Table 6: Overview of Gasifier Results

H₂/CO Ratio [mol/mol]	Biomass Rate [t/day]	Steam/Biomass Ratio [kg/kg]	Gasifier Temp. [C]	Producer Gas Flow [scfm@0C,1atm]	Feedstock	Date [yyyy/mm/dd]
1.53	2.88	0.83	868	71.43	Almond Prunings	2016/03/30
1.14	4.34	0.69	848	112.85	Almond Prunings	2016/10/26
1.26	2.79	0.87	852	65.65	Almond Prunings / Forest Thinnings	2018/02/22

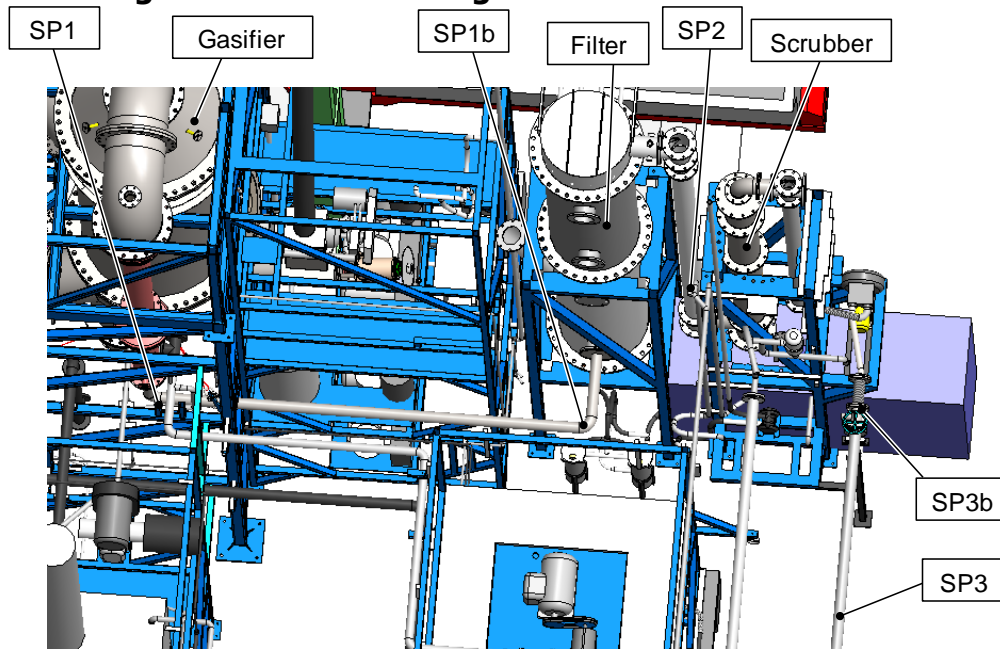
Source: UC San Diego

It is shown that the highest H₂/CO ratio was achieved when the steam/biomass ratio and the temperature of the gasifier were high. A higher amount of steam shifts the water-gas-shift equilibrium towards hydrogen, and a higher temperature helps those reactions since the composition is usually not close to equilibrium. For fluidized-bed methanation, H₂/CO ratios below 3 are acceptable, since steam can be added to the methanation for further water-gas-shift activity, and coke formation is less of a problem in fluidized-bed methanation compared to fixed-bed methanation. The demonstration plant in Güssing has regularly achieved a H₂/CO ratio of 2. The reasons for the higher ratio may be the catalytic activity of olivine sand which is used there as bed material, and the large scale, which usually increases the temperature and residence time in the gasifier slightly.

Producer Gas Composition

Figure 11 and Figure 12 show additional details of the sampling locations. The focus for sampling locations 1-3 was the measurement of tars, while for locations 3-6, it was the measurement of sulfur compounds.

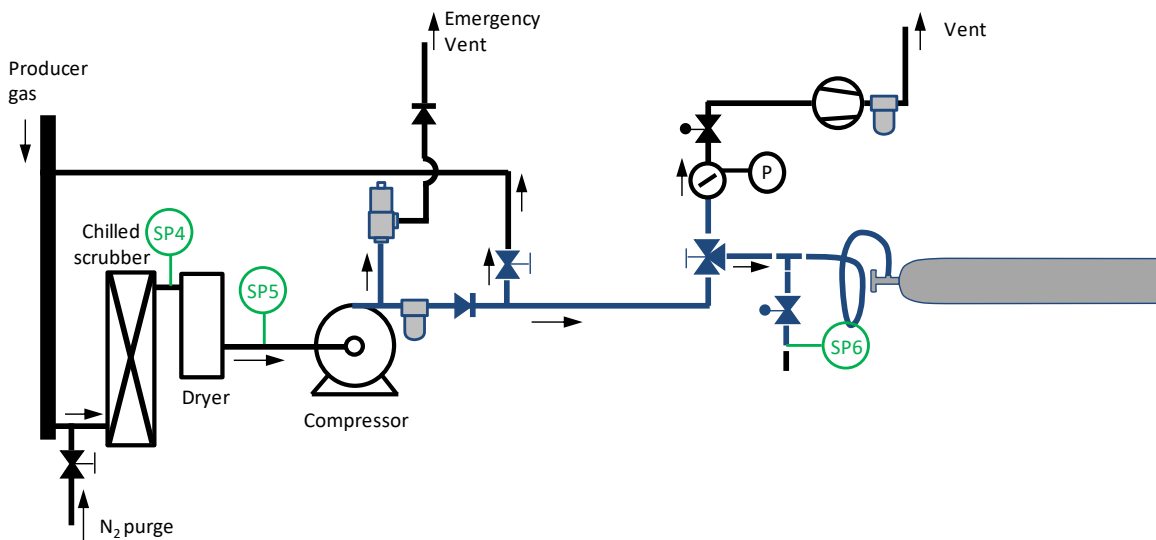
Figure 11: CAD Drawing of Pilot Gasification Plant



CAD drawing of pilot-plant gasification plant with gas sampling points. Sampling points SP1, SP2, and SP3 are used for tar measurements; SP1b is used for water moisture measurement. SP3b is used for the measurement of permanent gases and sulfur compounds.

Source: UC San Diego

Figure 12: Gas-Sampling Points after Chilled Scrubber



Gas sampling points after chilled scrubber (SP4), after dryer (SP5), and after compressor (SP6). Sulfur compounds were measured at these sampling locations.

Source: UC San Diego

Measurement of Major Gas Composition

A Micro Gas Chromatograph was used to measure the dry-gas composition of the producer gas. Three major methods were used to collect the gas samples:

- 1) For sampling point SP3b, a direct sampling line was available all the way to the Micro GC. To condense out tars and water, an impinger in an ice bath was used along the

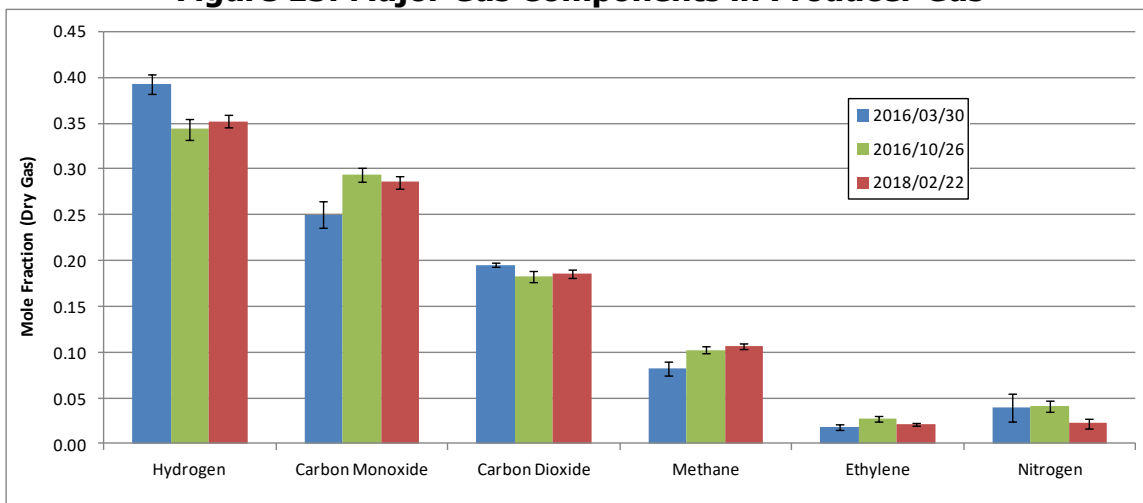
sample line. The impinger was either filled with toluene or isopropanol, and the loaded liquid was exchanged at regular intervals.

- 2) Gas-tight syringes (plastic or glass) are employed at sampling points SP3-SP6. The permanent-gas composition does not significantly change across those sampling points, and therefore sampling point SP3b is typically used. A 0.22-micron, 25mm diameter Teflon prefilter was used to prevent tars and aerosols entering the syringe. Other condensables adhere to the syringe wall, and only the dry-gas composition is considered from the Micro-GC result. For compounds such as hydrogen sulfide and benzene, a glass syringe is better than a plastic syringe, since these compounds are readily absorbed into plastic materials.
- 3) Tedlar sampling bags are an alternative to syringes and provide a larger volume/surface ratio than syringes. They work well for gases and sulfur compounds. It is not recommended to store the bags for more than a few hours, and hydrogen can be lost due to diffusion.

For methods (2) and (3), a representative measurement requires that the concentrations of compounds of interest are below the vapor pressure at the sampling temperature. This means that for less volatile compounds such as tars, other methods, such as heated lines or wet-sampling are required.

Figure 13 shows the major gas components in the dry producer gas for selected intervals during the gasifier tests. Hydrogen and carbon monoxide are the components that will be converted to methane in the synthesis. Carbon dioxide appears due to the water-gas shift equilibrium. An advantage of the FICFB gasifier is that the gas already contains about 10 percent methane which corresponds to nearly 25 percent of energy content of the gas. It also contains a few percent ethylene which can easily be converted to ethane or methane and add further to the heating value of RNG. Nitrogen was found to be lower than 5 percent, and on an industrial scale, this would be even lower due to lower gas leakage across the fluidized-bed connecting chutes and if carbon dioxide was used as purge gas instead of nitrogen.

Figure 13: Major Gas Components in Producer Gas



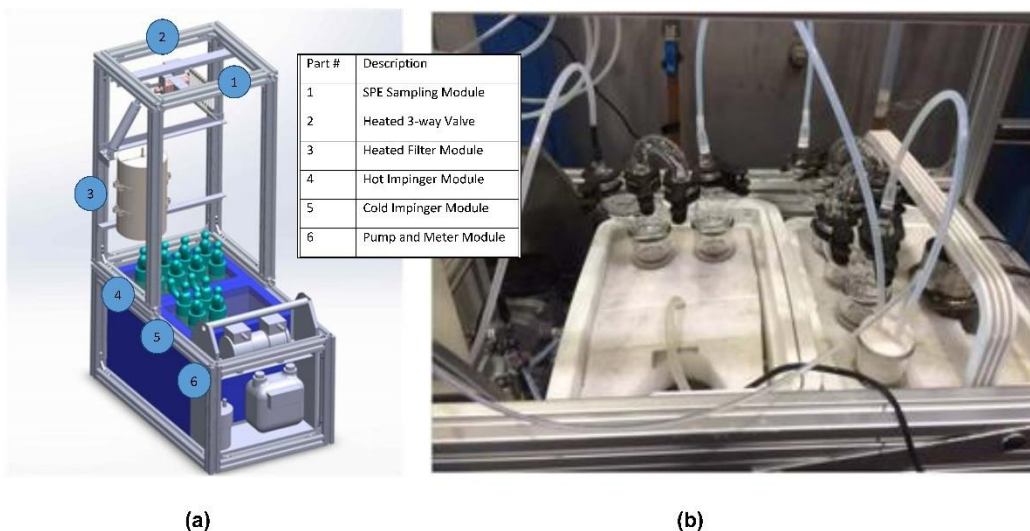
Dry-gas composition measured by Micro Gas Chromatograph. The averages plus/minus one standard deviation are shown for the steady-state intervals of the gasifier tests. The figures that include all measurements are shown in Appendix D.

Source: UC San Diego

Measurement of Tars

Tars were measured at sampling points SP1, SP2, and SP3 following the European guideline CEN/TS 15439:2006. The alternate method was used with the first four impingers at 40C and the last two at -20C. For sampling point SP1, a heated filter is used, and particulates are measured as well. Figure 14 shows one complete setup for the measurement of tars and particulates. This setup was designed to be portable so that it can be moved close to any sampling point.

Figure 14: Portable Tar Sampling Equipment



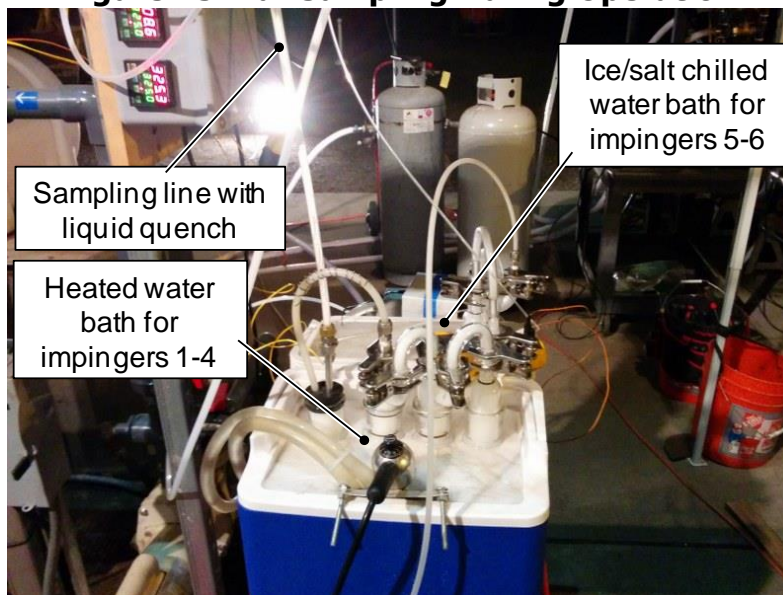
Portable tar sampling equipment including heated filter, impinger train, pump, and flow meter. a) Engineering design of portable unit. b) Photograph of the impinger section of the constructed unit.

Source: UC San Diego

Figure 15 shows another setup that was used on sampling points SP2 and SP3, where the gas stream is already cleaned of particulates. Here, solvent from the first impinger was recirculated to the sampling nozzle (liquid quench), in order to capture all tars in one step. To make the equipment further compatible with the measurement of sulfur tars, nozzle, sampling lines, and impinger parts were either made of Teflon, FEP, or glass.

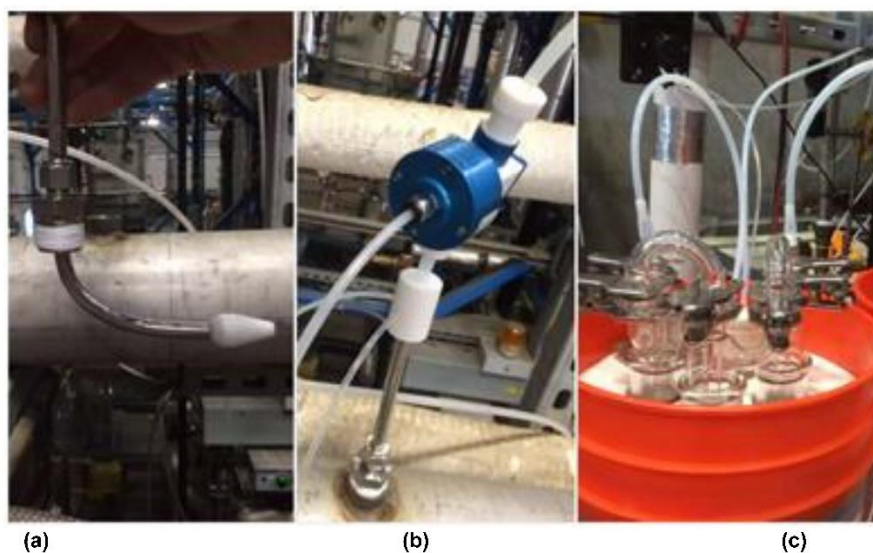
Figure 16 shows photographs of the parts used for the sampling of sulfur tars.

Figure 15: Tar Sampling During Operation



Source: UC San Diego

Figure 16: Sampling Equipment for Tars and Sulfur Tars



Setup for measurement of tar and heavy organic sulfur compounds from the producer-gas stream. The sampling location is after the ambient biodiesel scrubber for bulk removal of tars. Materials in contact with the sampled gas stream are Teflon (a, b) or glass (c) to prevent loss of sulfur compounds due to reactions. The stainless steel tube (a, b) has a Teflon liner inside.

Source: UC San Diego

Table 7 shows the results of particulate and tar measurement during gasifier run 2016/03/30. Tars were evaluated using the gravimetric method. The solvent is evaporated in a rotary evaporator (Rotovap), and benzene is not included in the tar values. The results show tar levels of around $10\text{g}/\text{Nm}^3$ before the biodiesel scrubber which is typical for a fluidized-bed gasifier. After the biodiesel scrubber, the tars were reduced to less than $0.5\text{g}/\text{Nm}^3$. Sulfur tars were evaluated from the same samples and are described in the next section.

Table 7: Test Results of Tar and Particulate Measurements

Sampling ID	Sampling Location	Time	Tars [g/Nm ³]	Particulates [g/Nm ³]
SP1-EUTAR-1	Before product gas filter	4:24pm - 5:05pm	8.2	128
SP1-EUTAR -2	Before product gas filter	10:38pm - 10:59pm	16.4	105
SP2-EUTAR -1	After product gas filter	5:33pm - 6:10pm	11.8	n/a
SP3-EUTAR -1	After RME scrubber	5:11pm - 6:02pm	0.25	n/a
SP3-EUTAR -1	After RME scrubber	10:43pm - 11:06pm	0.41	n/a

Results of tar and solid analysis for gasifier test (2016/03/30) following CEN/TS 15439.

Source: UC San Diego

Measurement of Sulfur Compounds

The main instrument for the analysis of low-level sulfur compounds is a gas chromatograph with chemiluminescence detector (GC-SCD), see Figure 17. In this instrument, sulfur compounds are first separated in a chromatographic column and then analyzed in the SCD burner/detector. Details on the instrument, calibration, analysis, and sampling procedure are given in Appendix E.

Figure 17: GC-SCD for Sulfur Analysis

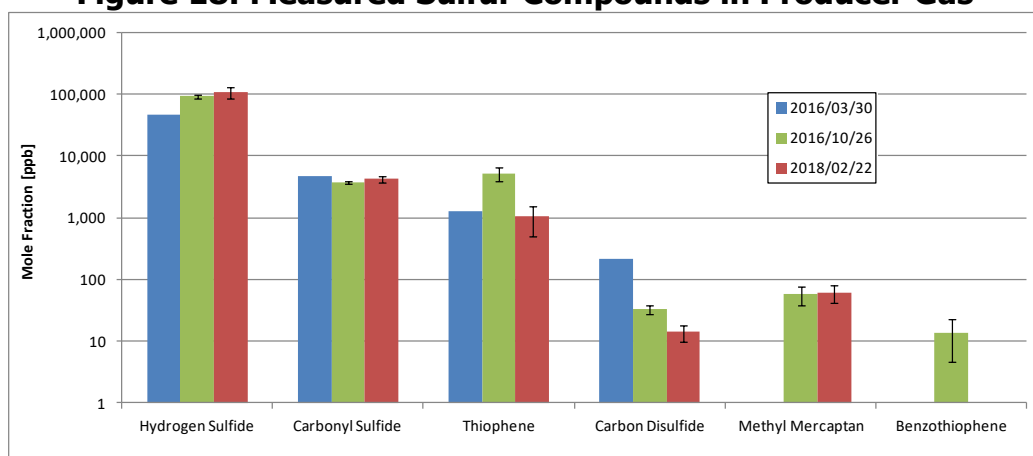


Setup for analysis of sulfur samples with a GC-SCD (gas-chromatograph with sulfur-chemiluminescence detector).

Source: UC San Diego

The analysis in the gas phase was conducted using Tedlar bags and sampling producer gas generated from the FICFB gasifier. The sampling location was after the ambient biodiesel scrubber that is used to remove tars and water from the gas (Sampling Point 3b). **Error! Not a valid bookmark self-reference.** shows the results of these sulfur measurements. Several sulfur compounds are present in the gas, and they are formed from the sulfur present in biomass. While the main compound is hydrogen sulfide, other compounds such as carbonyl sulfide and thiophene also occur in significant concentrations. The total concentration of sulfur needs to be reduced below a certain level to ensure a long enough lifetime of the nickel catalyst that is used in the methanation reactor.

Figure 18: Measured Sulfur Compounds in Producer Gas



Result of measurement of sulfur compounds during gasifier test. The gas was sampled with Tedlar bags and analyzed in a GC-SCD. Samples from 2016/03/30 were analyzed at a commercial laboratory. Samples from 2016/10/26 and 2018/02/22 were analyzed in house. Error bars show plus/minus one standard deviation for cases where multiple samples were taken.

Source: UC San Diego

The analysis in the liquid phase was conducted on the liquids collected using the tar protocol (isopropyl alcohol as solvent). The liquids showed mainly thiophene and benzothiophene. Another analysis with a GC-SCD that is optimized for analyzing liquids showed thiophene, benzothiophene, and dibenzothiophene.

Measurement of Other Compounds

For certain compounds in the producer gas, Draeger tubes are available. These tubes contain indicators that are highly sensitive to a certain compound. For this project, Draeger tubes for three compounds were used, for hydrogen sulfide, hydrogen chloride, and ammonia. Draeger tubes work by pulling a certain amount of gas through the test tubes. This can be performed with the use of a syringe. The temperature and pressure in the syringe can be used to calculate the standard volume drawn through the test tube. For different concentration levels, different indicators may be available. These can be combined with the amount of gas sampled through the test tube. For example, if the indicator is only discolored by a few percent after one stroke with the syringe, multiple strokes can be taken to increase the total volume. Table 8 shows the results of the measurements on producer gas. The column "Volume Sampled" indicates if multiple syringe strokes were used or only a partial stroke. The main result, the mole fraction in the gas, is calculated from the type of Draeger tube, volume sampled, and indicator change.

Table 8: Results of Draeger Tube Measurement

Sampling ID	Sampling Location	Time	Tube Type	Mole Fraction [ppmv]	Volume Sampled [% of nominal]	Indicator Change [% of capacity]	Typical COV [%]
SP3b-H2S-1	After RME scrubber	5:40pm	H2S 100/a	57.1	350%	10%	±5-10%
SP7-H2S-1	After compressor	7:02pm	H2S 100/a	< 30	100%	0%	±5-10%
SP7-H2S-2	After compressor	7:06pm	H2S 1/d	12.0	500%	3%	±15%
SP3b-HCl-1	After RME scrubber	5:54pm	HCL 2/a	< 0.05	500%	0%	±10-15%
SP3b-NH3-1	After RME scrubber	5:48pm	NH3 5/b	555.6	18%	100%	±10-15%
SP7-NH3	After compressor	7:20pm	NH3 5/b	0.2	500%	1%	±10-15%

Results of Draeger tube samples from gasifier test 2016/03/30. Mole fraction indicates the calculated mole fraction in the gas stream. Volume sampled reports how many syringe strokes were performed, pulling gas through the Draeger tube. Values less than 100 percent indicate a partial stroke. Indicator change shows the portion of the Draeger tube indicator that was discolored (larger numbers are more accurate).

Source: UC San Diego

Hydrogen sulfide was also measured by GC-SCD, and the Draeger results show values of a similar order of magnitude, albeit slightly smaller on average. Hydrogen chloride was virtually undetectable. This is because with a lot of calcium in the biomass, the preferred product is Calcium chloride. Ammonia was measured to be around 550ppm after the first biodiesel scrubber, but was nearly not detectable after the compressor. Ammonia is highly soluble in water and may have been absorbed in any condensate in the chilled scrubber or desiccant (LiCl).

Collection of Producer Gas

Compression of Producer Gas

A compressor was donated to the project by the Parker-Hannifin Veriflo Division and setup to compress the producer gas into pressurized gas cylinders. This was done to be able to evaluate the gas more thoroughly and use it later in longer-term methanation experiments. Figure 19 shows a photograph of the 4-stage compressor after it was received, and Source: UC San Diego

Figure 20 shows the compressor installed and in operation.

Figure 19: Testing of Gas Compressor



Source: UC San Diego

Figure 20: Producer Gas Compression during Gasifier Operation

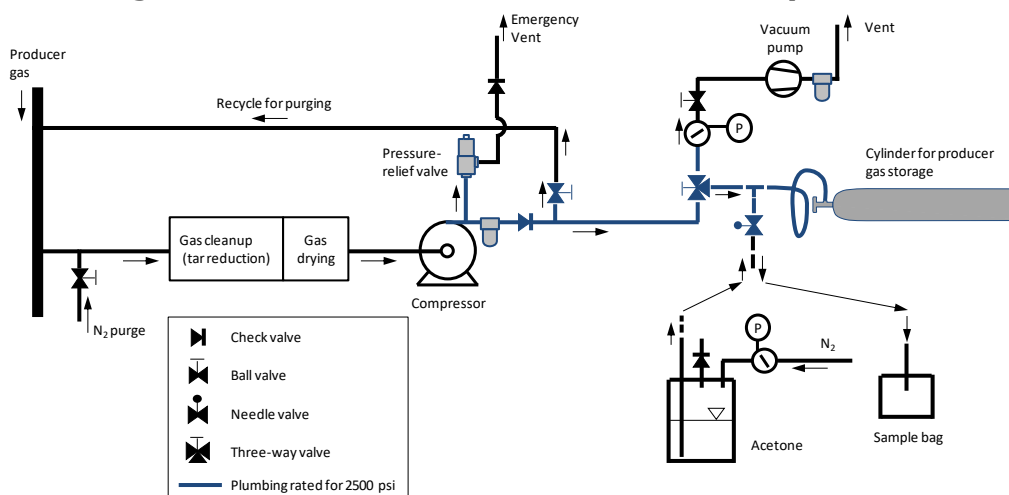


Photograph during operation of the FICFB gasifier. To the left, the chiller and chilled scrubber are shown. To the right, the compressor and producer gas cylinders are shown.

Source: UC San Diego

Figure 21 shows a schematic of the producer-gas compression. After purging the compressor with nitrogen, a slip stream of producer gas is drawn from the main producer gas pipe and cleaned and dried before compression. The pressure cylinders are cleaned with acetone and evacuated before filling them. Some of the cylinders were deliberately filled with 1L of acetone before adding the producer gas, to test what sulfur and tar compounds are absorbed in the solvent and to prevent deposition on the cylinder walls.

Figure 21: Schematic of Producer Gas Compression



Schematic of producer gas compression and collection in gas cylinders. The gas was cleaned of tars and heavy sulfur tars in a chilled biodiesel scrubber ("Gas cleanup") and dried with LiCl pellets. The setup also allowed for evacuating cylinders before use and filling them with acetone.

Source: UC San Diego

Producer Gas Cylinders

The cylinders storing the producer gas were purchased from cylinder vendors and equipped with stainless steel valves (CGA330). The cylinders themselves were made of steel and of a size of 300scf (T-type). The cylinders were filled up to a pressure of 2000 psi. The gas was subsequently used in analysis, adsorbent studies, and methanation experiments. For this, stainless steel regulators/valves and FEP tubing were used (see Figure 22).

Figure 22: Use of Compressed Producer Gas



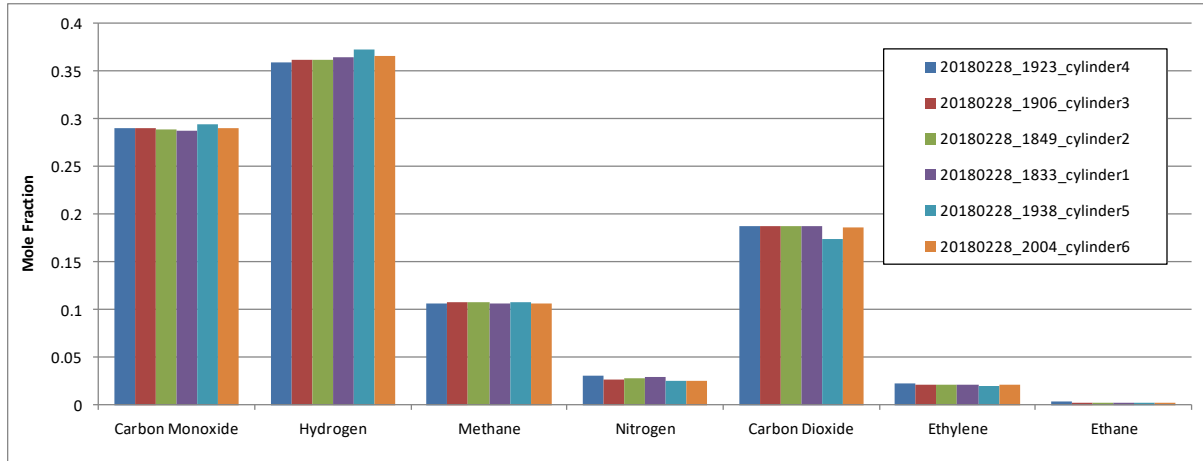
Photo of gas cylinder with collected producer gas from gasifier test (2016/03/30) together with stainless regulator and FEP line to adsorption experiment.

Source: UC San Diego

Composition of Collected Producer Gas

Figure 23 shows the analysis of permanent gases in the producer gas collected during gasifier test (2018/02/22). The analysis was performed six days after collection. The results shows a good repeatability across the different cylinders and good agreement with the gas-phase measurements during the gasifier test.

Figure 23: Major Gas Components in Producer Gas Cylinders

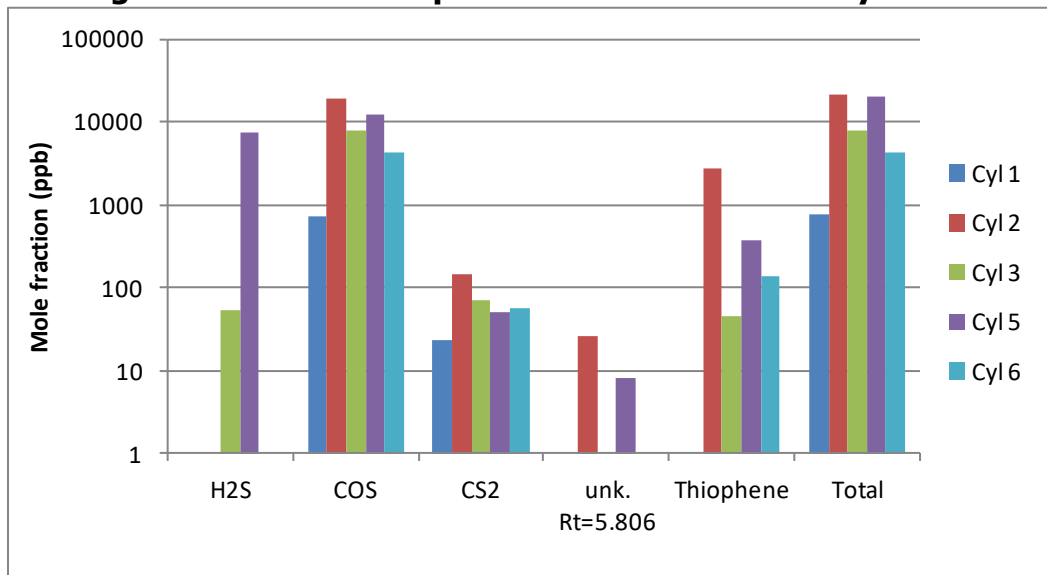


Analysis of the major composition of the producer gas collected during the gasifier run on 2/22/2018. The cylinders were analyzed by micro gas chromatograph. They are reported in the order they were filled.

Source: UC San Diego

Figure 24 shows the analysis of various producer gas cylinders from the first two gasifier tests (2016/03/30 and 2016/10/26).

Figure 24: Sulfur Components in Producer Gas Cylinders



Analysis of sulfur compounds in stored producer gas. Gas samples were taken on 3/24/2017. Cylinders 1 and 3 were filled with producer gas on 3/31/2016. Cylinders 2, 5, and 6 were filled with producer gas on 10/26/2016. Cylinders 1,3,5 and 6 contain 1L acetone, Cylinder 2 is dry. COS, CS₂, and thiophene are present in the gas. H₂S has mostly reacted away.

Source: UC San Diego

The results show that COS and thiophene are the major sulfur compounds in the cylinders. H₂S, which is the largest compound in the original producer gas, was not well preserved and was mostly reacted away. Some H₂S was detected in cylinders that used acetone as wash fluid. The H₂S was either absorbed into the acetone or prevented by a liquid film from reacting with the steel walls. The acetone was analyzed by GC-SCD, and H₂S was found as well as thiophene. The lower values of thiophene in the gas phase of the cylinders using acetone is consistent with this.

CHAPTER 3:

Gas Cleanup

Appropriate gas cleaning is necessary to ensure reliable operation of the fluidized-bed methanation, specifically for preventing the deactivation of the catalyst by sulfur compounds. The main sulfur compounds were measured to be hydrogen sulfide, carbonyl sulfide, and thiophene, and other sulfur compounds included methyl mercaptan, carbon disulfide, and benzothiophene. Different gas sulfur cleanup technologies are available, especially for large scale plants, but the goal of this project was to test technologies that are either relative simple or have low capital requirements so that they could be used for medium-scale gasification plants (30-100MW_{biomass}). Two of such techniques are scrubbing (without solvent regeneration) and adsorption (regenerable or non-regenerable).

Chilled Biodiesel Scrubber

The typical FICFB biomass plant employs a biodiesel scrubber at ambient temperature to condense and remove tars from the producer gas. Biodiesel is an excellent solvent for naphthalene, one of the main tar compounds in the raw producer gas. Heavier tars, even if not soluble, condense in the scrubber and get washed down into the collection vessel, where they accumulate in an emulsion zone that continuously gets recycled to the combustor section of the FICFB gasifier. Since biodiesel is a costly consumable, it would be advantageous to use the fresh biodiesel first in a colder downstream stage, and then as it removes some of the condensable sulfur compounds, use it in the regular biodiesel scrubber instead of the regular clean makeup flow. Operationally, there would be no additional cost for the biodiesel, but only the added cost for chilling the gas. This latter cost is substantial, but chilling is standard technology and will benefit other stages of the plant that rely on tar-free gas, such as compression and control equipment, and subsequent adsorbent stages that often work better at low temperature and with less moisture.

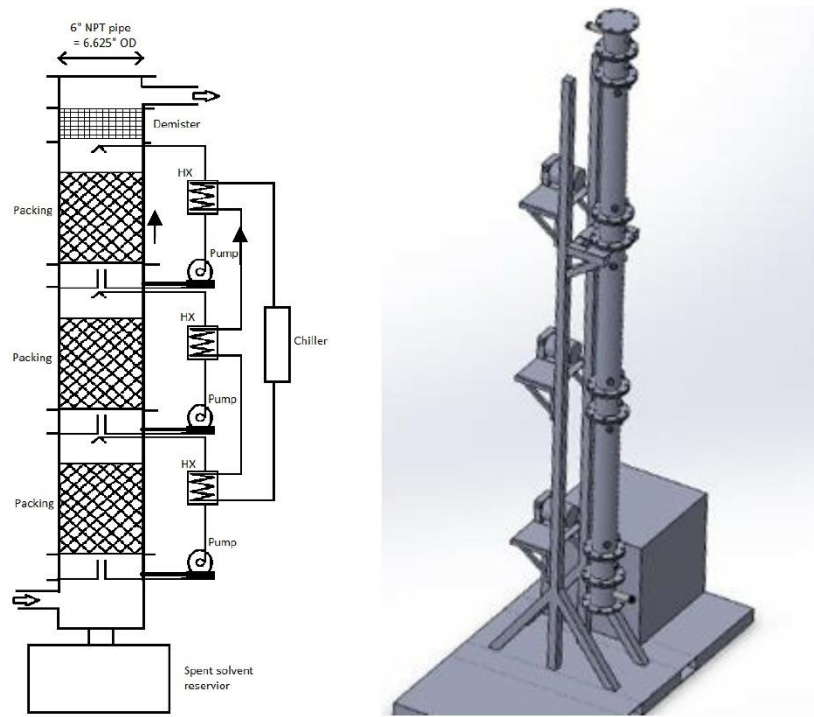
Since additional stages could be employed between the ambient and chilled scrubber, the design was made to allow for expansion to several stages, and the drawings are shown in Figure 25. New biodiesel would be added at the appropriate rate to the last (uppermost) stage, and then automatically overflows to earlier stages.

Design and Construction of Scrubber

For testing in this project, a single-stage scrubber was built and evaluated. The size of the scrubber was designed based on the flow rate of the downstream compressor which is 12 scfm compared to 150 scfm from the gasifier. It therefore uses a slip stream of the plant. Figure 26 shows the construction and installation of the chilled scrubber.

Figure 27 shows the installed scrubber with insulation, plumbing, and cooling units. The inside of the scrubber is filled with stainless-steel pall rings, and above the spray nozzle, a demister (stainless-steel mesh) was placed. To cool the biodiesel, and intermediate propylene-glycol loop is used with a plate heat-exchanger. One reason was that if the biodiesel was cooled directly by the chiller, crystallization of tars on the cold surfaces inside the chiller could occur.

Figure 25: Design of a Multi-Stage Version of a Scrubber



Schematic and engineering designs of a multi-stage chilled scrubber. Each stage has a circulating pump and a heat exchanger for circulating and cooling of the biodiesel. The last stage (top) has the coldest temperature and cleanest biodiesel. Makeup biodiesel would be added near the inlet of the top pump, and contaminant-laden biodiesel will overflow gradually to lower stages. Biodiesel from the spent solvent reservoir will be recycled to the ambient biodiesel scrubber and subsequently to the combustor section of the gasifier.

Source: UC San Diego

Figure 26: Construction and Installation of a Single-Stage Scrubber



Source: UC San Diego

Figure 27: Installed Chilled Scrubber



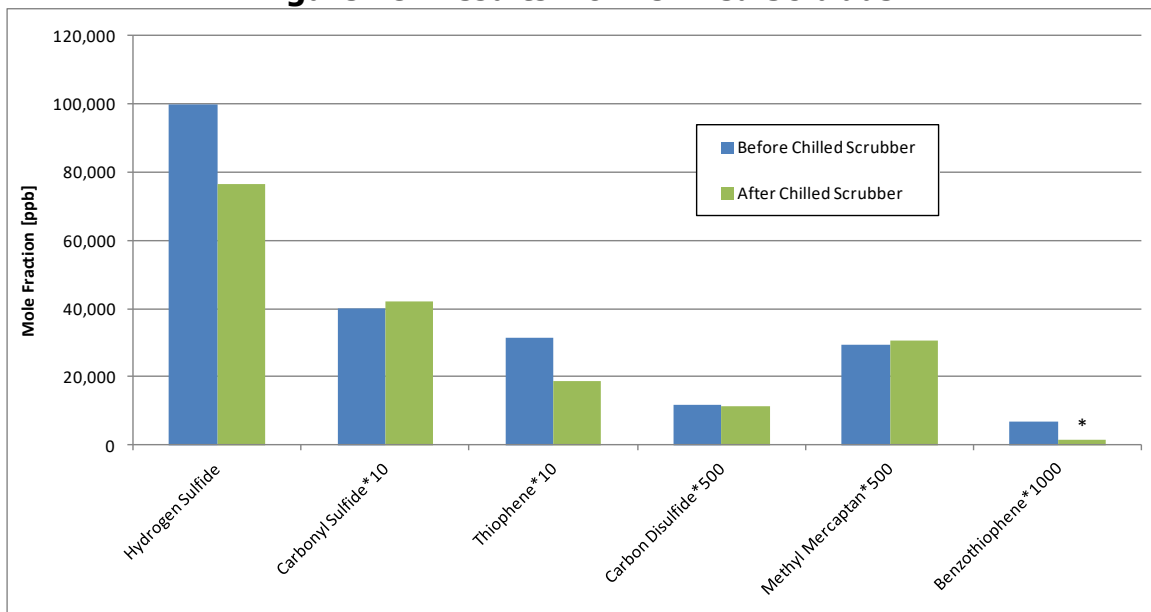
Photograph of installed chilled biodiesel scrubber (right vessel) with piping and chilling equipment. Producer gas enters near the bottom of the chilled scrubber. On the left side, an adsorbent vessel is shown, used for moisture removal before the piston compressor. Gas sampling ports are available after each unit for the analysis of gas, sulfur, and tar compounds.

Source: UC San Diego

Results from Operation of Scrubber

Figure 28 shows the results of sulfur measurements before and after the scrubber. The main compounds that were significantly reduced were thiophene and benzothiophene. Benzothiophene was below the detection limit after the scrubber. Hydrogen sulfide is also reduced, but since it is a very reactive molecule, reduction may be due to reaction on surfaces of piping and vessels between the two sampling points. Temperature recordings during the operation of the scrubber show that the gas/liquid heat transfer was not optimal, with a significant temperature between the gas leaving the scrubber and the liquid entering. Also, the intermediate glycol loop temperature was higher in some runs than the design value. In order to improve the performance, a pacing and drip tray from Sulzer Inc., and improved insulation and chiller control are recommended. The results show that the chilled scrubber has the potential to work well as bulk removal of thiophene, one of the main sulfur contaminants in producer gas. The scrubber also removes water and tars, which will help with fine-removal stages, compression, and other in-line equipment before the methanation.

Figure 28: Results from Chilled Scrubber



Results of sulfur measurements during operation of chilled scrubber. The data show averages from the last two gasifier tests. The values are multiplied with different factors to allow for a linear scale. *) Benzothiophene after the scrubber was below the detection limit and was plotted as the detection limit.

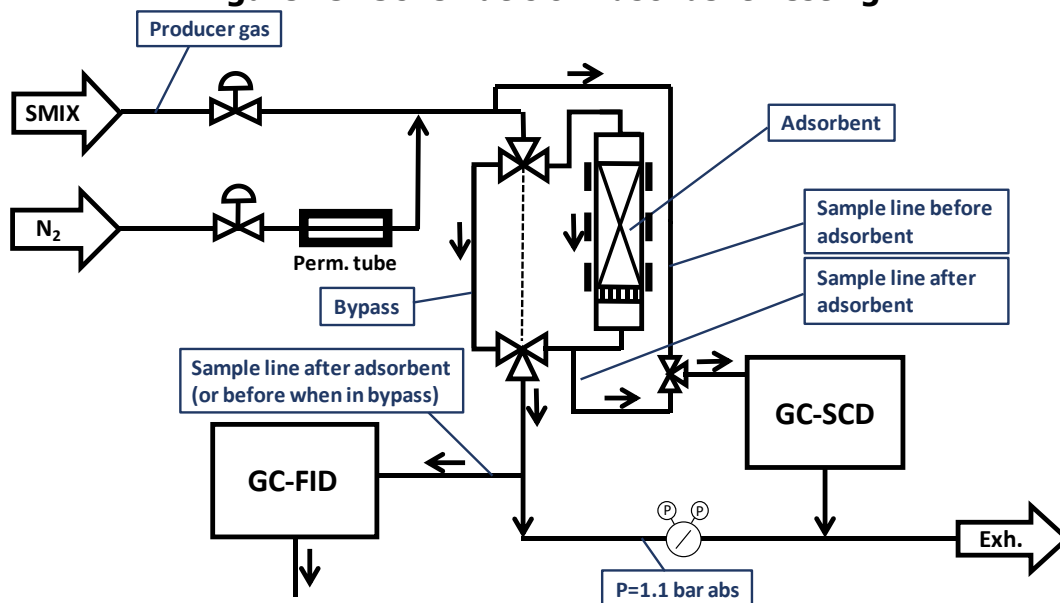
Source: UC San Diego

Adsorbent Studies

Materials and Methods

Figure 29 shows the schematic of the setup used for adsorbent testing. A sulfur-containing gas is diluted with nitrogen and flows into a vessel filled with adsorbent. In order to introduce small amounts of liquid or solid sulfur compounds, a permeation oven is placed in line with the nitrogen flow. The adsorbent vessel can be bypassed with two three-way valves in order to add adsorbent or to perform a calibration without flowing through the adsorbent. A GC-FID was installed later during the test program to measure benzene, either after the adsorbent or before the vessel when it is in bypass. For measuring sulfur compounds, short sample lines were installed before and after the adsorbent vessel with a selection valve to alternate between them without stopping the main flow through the adsorbent.

Figure 29: Schematic of Adsorbent Testing



Schematic of adsorbent testing with sample lines for GC-SCD (sulfur) and GC-FID (benzene).

Source: UC San Diego

Figure 30: Installed Adsorption Vessel



(a)

(b)

a) Heated and insulated adsorption vessel made of Teflon for adsorption studies. Two sampling lines lead to the GC-SCD (on the left), one for sampling before and one for sampling after the vessel. b) Disassembled Teflon vessel with end caps containing a FEP-coated silicone o-ring and Viton o-ring.

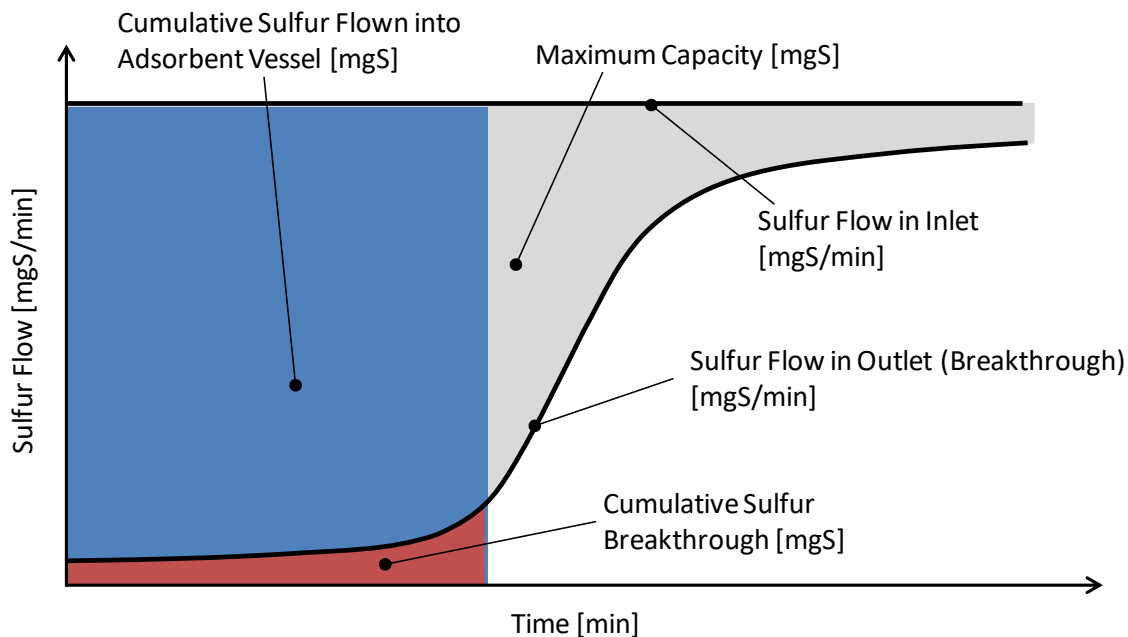
Source: UC San Diego

Figure 31 shows the definition of quantities used in the adsorbent studies. The breakthrough of sulfur can be expressed on an instantaneous or cumulative basis. Dividing the outlet flow of

sulfur by the inlet flow gives the instantaneous breakthrough of sulfur in percent. Dividing the cumulative sulfur breakthrough (red area in Figure 31) by the cumulative sulfur inflow (blue rectangle in Figure 31) gives the cumulative breakthrough in percent. For the current studies, a cumulative breakthrough threshold was specified at which point in time the adsorbent capacity was determined (in mgS). It is calculated as the cumulative sulfur inflow minus the cumulative breakthrough. This adsorbent capacity is always below the maximum adsorbent capacity if only a certain cumulative sulfur breakthrough is allowed. By placing several adsorbent stages in series, and moving the adsorbent upstream as it gets loaded with sulfur, the adsorbent capacity can approach the maximum capacity and the overall breakthrough can be decreased. The trade-off is a higher pressure drop.

For the experiments in this study, a cumulative breakthrough threshold was specified for each material depending on the length of bed, gas concentration, measurement accuracy, and efficacy of the material. Even if a high threshold is chosen to evaluate one stage, a projection can be made for more stages in series to bring the overall breakthrough down to desired levels.

Figure 31: Definition of Quantities in Adsorbent Studies



Time history during adsorbent studies. The solid lines show sulfur inflow and outflow in [mgS/min] (or [ppm] if the flow rate is constant). The grey area between the two lines illustrates the maximum capacity. For a specified time, the red area shows the cumulative sulfur that has left the vessel (broken through), and the blue rectangle shows the cumulative sulfur that has entered the adsorbent vessel. Dividing these two quantities by each other leads to a cumulative sulfur breakthrough in percent. For a given cumulative sulfur breakthrough (e.g. 5 percent threshold), the adsorbent capacity equals the cumulative sulfur flown into the adsorbent (blue) minus the cumulative sulfur breakthrough (red).

Source: UC San Diego

Test Plan

Table 9 shows a summary of the adsorbent tests that were conducted during the project.

Table 9: Summary Adsorbent Tests

Date [yyyy/mm/dd]	Name of Adsorbent	Regenerated	Gas Type	Dilution of Gas	Temperature	Time on Stream [hrs]
2016/11/23	Florisil	No	Smix1+Thiophene	1001	Ambient	23
2016/12/16	SulfaTreat	No	Smix1+Thiophene	500	Ambient	90
2016/12/22	Brightblack	No	Smix1	500, 44	Ambient	870
2017/04/18	Brightblack	No	Producer Gas	21	Ambient	370
2017/05/12	Brightblack	No	Producer Gas	150, 43, 16.1	Ambient	136
2017/07/14	Brightblack	No	Producer Gas	43, 16.7	Ambient	272
2017/12/24	Activated Biochar	No	Smix3	150, 43, 16.7	35 C	67
2018/01/01	Activated Biochar	1x	Smix3	150, 43, 16.7	35 C	124
2018/01/12	Activated Biochar	2x	Smix3	150, 43, 16.7	35 C	90
2018/01/25	Circledraft Biochar	No	Smix3	150, 43, 16.7	35 C	244
2018/02/13	Circledraft Biochar	1x	Producer Gas	43	35 C	38
2018/02/19	Circledraft Biochar	No	Producer Gas	43, 27.3	35 C	56
2018/03/16	Circledraft Biochar	No	Producer Gas	16.7	75 C	20
2018/03/18	Circledraft Biochar	1x	Producer Gas	16.7	75 C	16.5
2018/03/20	Circledraft Biochar	No	Producer Gas	16.7	55 C	26
2018/03/23	Circledraft Biochar	1x	Producer Gas	16.7	55 C	30
2018/03/26	Circledraft Biochar	2x	Producer Gas	16.7	55 C	19
2018/04/30	SulfaTrap R8C	No	Producer Gas	16.7, 5.6	35 C	63
2018/05/04	SulfaTrap R8C	No	Producer Gas	5.6	80 C	89
2018/05/15	SulfaTrap R8C	No	Producer Gas	5.8,1	110 C	108
2018/05/25	FICFB Biochar	No	Producer Gas	16.7	35 C	22
2018/05/27	FICFB Biochar	1x	Producer Gas	16.7	35 C	18
2018/05/29	FICFB Biochar	2x	Producer Gas	16.7	35 C	14
2018/05/31	FICFB Biochar	3x	Producer Gas	16.7	55 C	24

Summary of adsorbents tested: "Date" indicates the starting date of the test series, "Time on Stream" indicates the number of hours during which gas was flowing through the adsorbent. "Regenerated" indicates if the adsorbent was used more than once, in which case it was regenerated by heating between tests. "Dilution of Gas" is the factor by which the sulfur-containing gas was diluted with nitrogen.

Source: UC San Diego

Besides the type of adsorbent, there are several important parameters that define an individual adsorbent test and are:

- **Regenerability.** Specifies if the adsorbent can be regenerated, for example by heating in air. The adsorbent, however, may degrade in capacity after each regeneration. Table 9 indicates if the adsorbent was regenerated before and if yes, how many times.
- **Gas Type.** Two different sulfur gases were used. First, a synthetic laboratory gas mixture containing a variety of sulfur compounds. This is useful when screening what type of sulfur compounds are adsorbed well and which ones are not. The gases were labeled as Smix1, Smix2, and Smix3, and had similar sulfur concentrations (Appendix E). Second, cylinders of producer gas collected from the gasifier tests. This test is important to evaluate an adsorbent for its efficacy under real-world conditions, with other interfering compounds present (matrix effect).
- **Dilution of Gas.** A higher dilution simulates the latter section of an adsorbent bed, where the sulfur concentrations are already low, and to evaluate how low of a sulfur breakthrough can be expected. A lower gas dilution is useful to accelerate the screening of adsorbents and to evaluate the adsorbent capacity.
- **Temperature.** For physisorption, a lower temperature is usually preferable, but different compounds, including non-sulfur compounds, may compete for adsorption sites depending on the temperature. For chemisorption, a higher temperature can increase the reaction rate and lead to a better overall adsorption.
- **Time on Stream.** The time of the test is a function of the adsorbent capacity and dilution of the gas. The tests are usually conducted until the breakthrough of key components have reached a predetermined threshold value of breakthrough.

Test Results

Table 10 shows an overview of the test results, with the main adsorbed compounds listed. The capacity for a given cumulative-breakthrough threshold is reported for each compound. Details for each adsorbent are given in the following sections. The individual breakthrough curves are shown in Appendix F.

Table 10: Adsorbent Testing Results

Date [yyyy/mm/dd]	Name of Adsorbent	Ads. mass [g]	Flow Rate of Gas [slpm]	Compounds Adsorbed	Cumulative Breakthrough Threshold [Sout/Sin]	Capacity [gS/gAdsorbent]	Comment
2016/11/23	Florisil	27.22	5.01	dimethyl sulfide, n-propyl mercaptan	1%	4.78E-6, 1.36E-5	
2016/12/16	SulfaTreat	1.02	1.50	hydrogen sulfide, methyl mercaptan, ethyl mercaptan, n-propyl mercaptan	1%	>2.56E-3, 7.03E-4*, 1.05E-3*, >1.33E-3*	Mercaptans likely formed other sulfur compounds
2016/12/22	Brightblack	9.94	1.50	hydrogen sulfide, methyl mercaptan, ethyl mercaptan, dimethyl sulfide, n-propyl mercaptan	1%	1.12E-3, 2.24E-3, >6.03E-3, 6.57E-3, >6.50E-3	
2017/04/18	Brightblack	10.00	0.74	hydrogen sulfide, carbonyl sulfide, thiophene	15%	>3.00E-4, 6.90E-6, 5.10E-5	
2017/05/12	Brightblack	9.93	1.50	carbonyl sulfide, thiophene	15%	5.64E-6, 1.21E-5	
2017/07/14	Brightblack	10.00	1.50	carbonyl sulfide, thiophene	15%	7.20E-6, 5.50E-6	
2017/12/24	Activated Biochar	11.24	1.50	hydrogen sulfide, carbonyl sulfide, methyl mercaptan, ethyl mercaptan, carbon disulfide, n-propyl mercaptan	1%	2.10E-3, 7.20E-4, 7.98E-4, >1.09E-3, 5.68E-4, >1.20E-3	
2018/01/01	Activated Biochar	11.24	1.50	methyl mercaptan, ethyl mercaptan, n-propyl mercaptan, thiophene	1%	1.45E-4, 2.45E-3, >2.05E-3, 2.22E-3	
2018/01/12	Activated Biochar	11.24	1.50	ethyl mercaptan, n-propyl mercaptan, thiophene	1%	2.56E-4, >2.3E-3, >2.16E-3	

Date [yyyy/mm/dd]	Name of Adsorbent	Ads. mass [g]	Flow Rate of Gas [slpm]	Compounds Adsorbed	Cumulative Breakthrough Threshold [Sout/Sin]	Capacity [gS/gAdsorbent]	Comment
2018/01/25	Circledraft Biochar	17.05	1.50	hydrogen sulfide, carbonyl sulfide, methyl mercaptan, ethyl mercaptan, dimethyl sulfide, carbon disulfide, n-propyl mercaptan, thiophene	1%	2.57E-3, 1.27E-3, 2.96E-3, >4.36E-3, 1.56E-3, 3.22E-3, >4.80E-3, 4.25E-3,	
2018/02/13	Circledraft Biochar	17.05	1.50	thiophene	1%	1.51E-5	
2018/02/19	Circledraft Biochar	11.77	1.50	carbonyl sulfide, thiophene	1%	9.82E-5, 1.95E-5	
2018/03/16	Circledraft Biochar	9.85	1.50	carbonyl sulfide	5%	>4.61E-5	
2018/03/18	Circledraft Biochar	9.85	1.50	carbonyl sulfide, thiophene	5%	1.82E-5, >1.62E-6	
2018/03/20	Circledraft Biochar	10.25	1.50	carbonyl sulfide	5%	>5.09E-5	
2018/03/23	Circledraft Biochar	10.25	1.50	carbonyl sulfide, carbon disulfide	5%	3.04E-5, 5.85E-7	
2018/03/26	Circledraft Biochar	10.25	1.50	carbon disulfide	5%	4.66E-7	
2018/04/30	SulfaTrap R8C	15.18	1.50	carbonyl sulfide, benzene	1%	6.30E-5, 1.29E-2*	Some H ₂ S in outlet
2018/05/10	SulfaTrap R8C	17.14	1.50	carbonyl sulfide, thiophene, benzene	1%	>4.76E-4, 1.99E-5, 1.66E-2*	
2018/05/15	SulfaTrap R8C	16.33	1.5, 0.44	carbonyl sulfide, benzene	1%	>2.05E-3, 3.36E-3*	Immediate breakthrough of thiophene
2018/05/25	FICFB Biochar	7.49	1.50	thiophene, benzene	15%	2.16E-5, 1.30E-1	

Date [yyyy/mm/dd]	Name of Adsorbent	Ads. mass [g]	Flow Rate of Gas [slpm]	Compounds Adsorbed	Cumulative Breakthrough Threshold [Sout/Sin]	Capacity [gS/gAdsorbent]	Comment
2018/05/27	FICFB Biochar	7.49	1.50	thiophene, benzene	15%	1.89E-5, 1.08E-1	
2018/05/29	FICFB Biochar	7.49	1.50	thiophene, benzene	15%	1.95E-5, 1.07E-1	
2018/05/31	FICFB Biochar	7.49	1.50	thiophene, benzene	15%	1.31E-5, 7.9E-2	

Results of adsorbent tests: The capacity for various compounds is expressed for a cumulative-breakthrough threshold. For example, a cumulative breakthrough of 1 percent for a certain compound means that 1g of that compound has flown out of the adsorbent for every 100g of that compound that has flown into the adsorbent.

* Capacity for benzene is reported in gBenzene/gAdsorbent

Source: UC San Diego

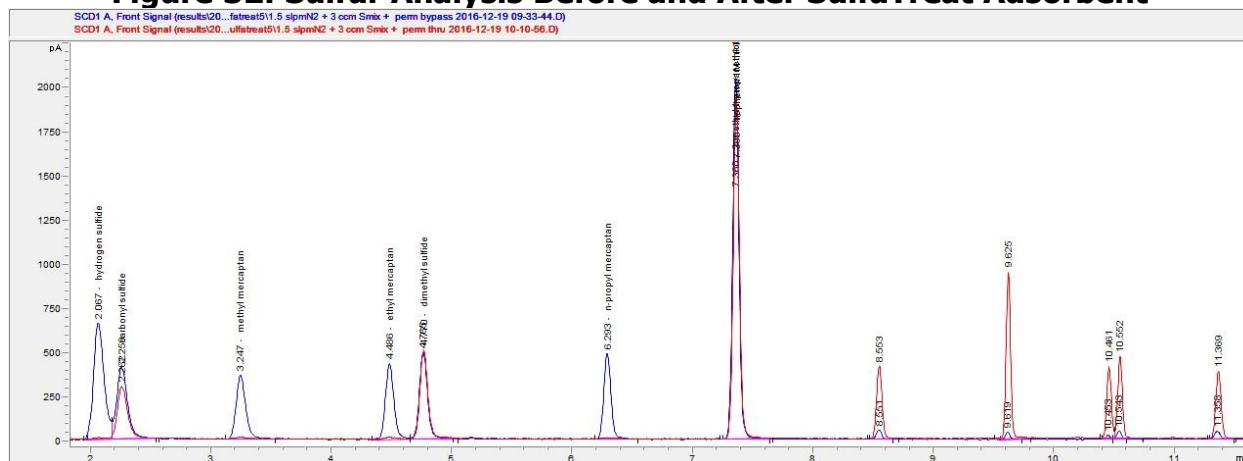
Florisil US Silica A60/100

The porous inorganic adsorbent was tested on a variety of sulfur compounds. A calibration gas (Smix1) containing 6 sulfur compounds was diluted 1000:1 with nitrogen giving mole fractions around 50-100ppb. In addition, thiophene was added to the nitrogen stream by a permeation tube, and quantified with the GC-SCD as 1.04ppm. The adsorbent showed significant adsorption of n-propyl mercaptan and some adsorption of dimethyl sulfide. All other compounds showed very early breakthrough. Since hydrogen sulfide, carbonyl sulfide, and thiophene are the major compounds in producer gas, and these were not well adsorbed, no further tests were conducted on the adsorbent. See detailed results in Appendix F.

SulfaTreat

SulfaTreat Select Premium is a commercial iron-based adsorbent for H₂S removal made by Schlumberger Inc. It is non-regenerable but highly effective. Therefore, a small quantity (1.02g) was used for adsorbent testing in a 3/8" ID Teflon tube. A calibration gas (Smix1) containing 6 sulfur compounds was diluted 500:1 with nitrogen giving mole fractions around 100-200ppb. In addition, thiophene was added to the nitrogen stream by a permeation tube, and quantified with the GC-SCD as 340ppb. Figure 32 shows a chromatogram of the measurement before and after the adsorbent. H₂S and mercaptans were well removed. Some of them were, however, converted to other sulfur compounds, presumably sulfides and disulfides. The adsorbent was not effective for COS and thiophene, two major compounds in producer gas. It may be considered as a guard bed for H₂S, if it is confirmed that only mercaptans are responsible for the formation of other sulfur compounds. The detailed adsorption results are shown in Appendix F.

Figure 32: Sulfur Analysis Before and After SulfaTreat Adsorbent



Measurement of sulfur compounds before (blue) and after (red) adsorbent vessel filled with 1.02g SulfaTreat Select Premium adsorbent. The conditions were 1.5 slpm N₂ with seven sulfur compounds. H₂S and mercaptans were well adsorbed, but other sulfur compounds were formed.

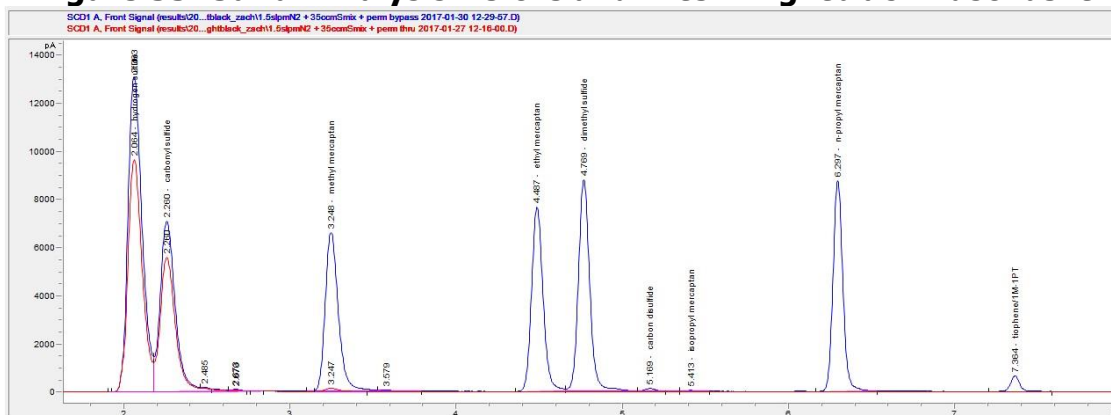
Source: UC San Diego

Brightblack

Brightblack is a microporous synthetically-produced carbon product made by ATMI Inc. It has been employed for CO₂ separation in pressure-swing adsorption (PSA). The material comes in different forms, but the one tested in this study is in powder form. Therefore, the pressure drop was higher, and a shorter bed selected (1in high and 1in wide). The first test was to use

a calibration gas (Smix1) containing 6 sulfur compounds (diluted 500:1 with nitrogen, and later 43:1 to accelerate the experiment). In addition, thiophene was added to the nitrogen stream by a permeation tube and measured as approximately 179ppb. Figure 33 shows that mercaptans and thiophene were well adsorbed but H₂S and COS not as well.

Figure 33: Sulfur Analysis Before and After Brightblack Adsorbent



Measurement of sulfur compounds before (blue) and after (red) adsorbent vessel filled with 9.94g Brightblack adsorbent, approximately half-way through the test. The conditions were 1.5 slpm N₂ with seven sulfur compounds. H₂S and COS have reached breakthrough, while mercaptans and thiophene are still well adsorbed.

Source: UC San Diego

To investigate the material further in regards to thiophene adsorption, three tests were conducted with producer gas. For this, Cylinder 5 was used, that had been filled with producer gas during gasifier test 2016/10/26. Since the producer gas also contained benzene and toluene, the gas has to be diluted to avoid coking of the element in the SCD burner. This dilution simulates a downstream adsorbent stage where the concentrations are already reduced from the earlier stages.

The three tests on producer gas are summarized in the Appendix. In these tests, an earlier version of the setup was used, where the adsorbent vessel was not temperature controlled, and had to be switched into bypass mode to measure the inlet concentrations. For this reason, the results show a high degree of variability, caused by switching of valves, changes in dilution, changes in temperature, or possibly a formation of COS from H₂S, in addition to the uncertainty of the measurement at these low concentrations.

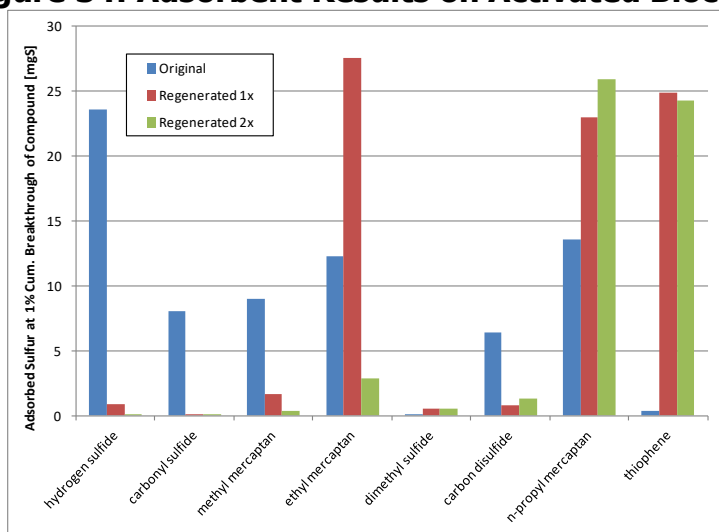
The inlet gas included 2000 ppm of benzene and 30 ppm of toluene which is seen as a major factor why the adsorbent did not perform as well as under the synthetic sulfur mixture (Smix1). This emphasizes the need for testing on real gases. Because of the earlier breakthrough of thiophene, and the poor adsorption of COS, the test intervals were shorter than in the synthetic-gas tests. The exact performance of H₂S adsorption could not be evaluated, in part because H₂S is very reactive and degrades in cylinders, lines, and adsorbent, and levels were much below the original content in the producer gas. It may also be possible that H₂S was converted to COS in the carbon bed, in which case, the material may still be considered as a H₂S guard bed with subsequent removal of COS in a different adsorbent bed.

Activated Biochar

Activated carbon is a common adsorbent for many contaminants. Typically, an inexpensive carbon source such as coconut shells is activated with steam to increase its surface area. During the project, a similar activation was performed on biochar from a CircleDraft gasifier. The biochar has already undergone heating near 800C, before it was withdrawn from the gasifier, and therefore it is expected to have low amount of volatiles. A small sample of biochar was activated, first with steam and then with CO₂, to further enhance the porosity of the biochar. The biochar was then tested for its adsorption properties with various sulfur compounds in the synthetic gas mixture Smix3. Since the activation of char is an expensive process, it would be of great advantage if the adsorbent could be regenerated after use. This was done as part of the test series, and between every test, the char was heated under a flow of air to 110C. The adsorbent tests were therefore conducted three times: on the original activated biochar, on the regenerated, and on the 2x regenerated material. The individual breakthrough curves are shown in Appendix F.

Figure 34 shows the summary of adsorption of sulfur compounds, once a 1 percent cumulative-breakthrough threshold for each component is applied. It is interesting to observe that the behavior changes dramatically between regenerations.

Figure 34: Adsorbent Results on Activated Biochar



Adsorbent results on activated biochar using a laboratory gas mixture (Smix3). The flow rate was 1.5slpm, and the adsorbent amount was 11.24g. The test was accelerated by diluting the gas 150x, 43x, and 16.1x during each test before regenerating the adsorbent. Regeneration changed the behavior of the material as to which compounds were best adsorbed.

Source: UC San Diego

While initially many sulfur compounds are adsorbed well, after two regeneration cycles, only n-propyl mercaptan and thiophene are adsorbed well. In fact, thiophene was not adsorbed well in the original activated biochar, but improved after regeneration, which indicates a change in adsorption sites/pores after a adsorption/regeneration cycle.

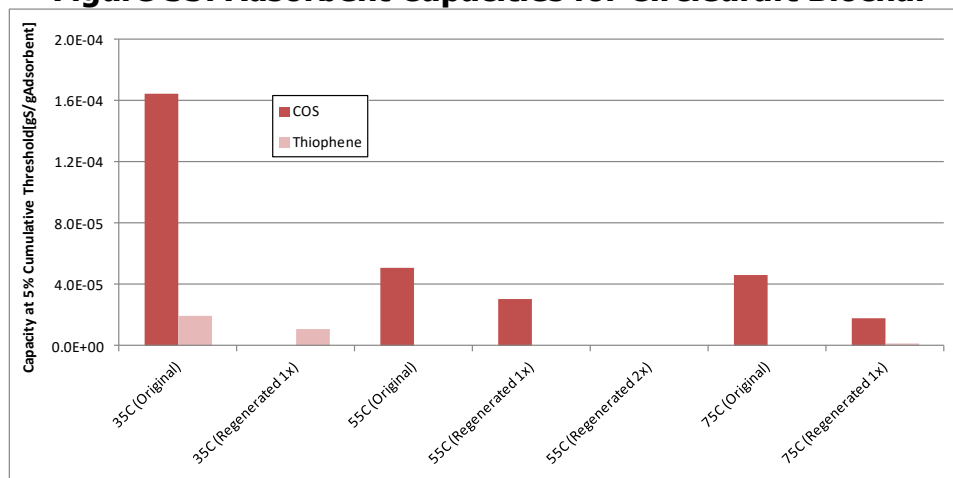
Biochar from Fixed-Bed Gasifier

Original Biochar from a Circledraft gasifier was tested without any activation. While the char may show decreased capacity compared to an activated char, it would be less expensive. The

biochar from the fixed-bed gasifier was tested on the synthetic sulfur mixture and on producer gas, at different temperatures, and for regeneration.

On initial screening using the synthetic sulfur mixture (Smix3), the biochar showed adsorptive capacity for all sulfur compounds. It showed especially good values for ethyl mercaptan, n-propyl mercaptan, and thiophene, nearly to 1%wt of sulfur per mass adsorbent. With producer gas, however, the results were by two orders of magnitude lower. This is attributed to other impurities in the producer gas, such as benzene and water. Higher temperatures and regeneration did not improve the balance among adsorbates and generally lowered the capacity for sulfur compounds (Figure 35). Therefore, for cleaning producer gas, this biochar is best to be used in original form at 35C.

Figure 35: Adsorbent Capacities for Circledraft Biochar



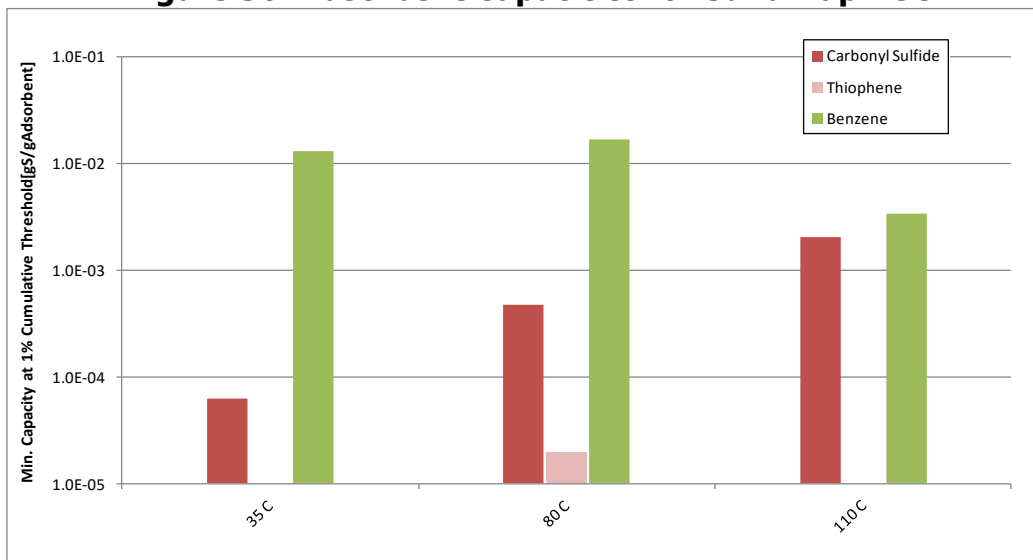
Adsorbent capacities for Circledraft biochar at different temperatures and before and after regeneration. The flow rate was 1.5slpm of diluted producer gas, and the adsorbent amount was between 9.85g and 11.77g.

Source: UC San Diego

SulfaTrap R8C

The previous tests showed that carbonyl sulfide was not well adsorbed on many of the tested adsorbents, and it might even be formed from other sulfur compounds in carbon based materials. For this reason, an adsorbent for COS was acquired and tested. SulfaTrap R8C is a commercial adsorbent based on an impregnated char, especially designed for the adsorption of COS. At lower temperatures, it was found that benzene was also adsorbed. In general, the adsorption of benzene is not desired for the current project, since it takes away pore space from other sulfur compounds. The fluidized-bed methanation is capable of handling benzene, and therefore there is no need to remove benzene, which is present at much larger concentrations in the producer gas than any of the sulfur compounds. Increasing the temperature to 110C reduced the adsorptive capacity of benzene (Figure 36). At the same time, it increased the adsorption of COS. Thiophene is not reported at 35C due to measurement uncertainty and since it was not the focus of this adsorbent. It was adsorbed at 80C, but not at 110C, thus responded more to temperature than benzene. All detailed figures are in Appendix F. Among the temperatures tested, 110C gave the best performance and makes the SulfaTrap R8C a good choice for effective removal of COS.

Figure 36: Adsorbent Capacities for SulfaTrap R8C



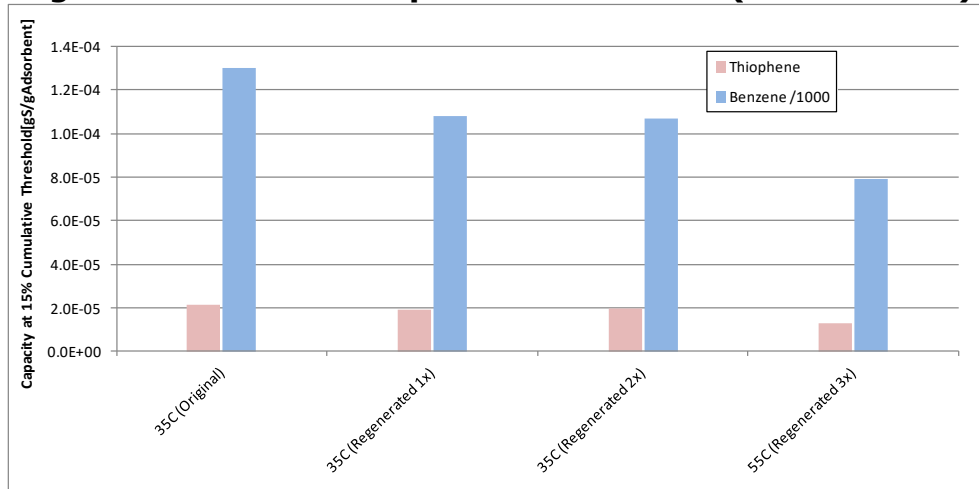
Adsorbent capacities for SulfaTrap R8C. The adsorbent amounts were 15.18g, 17.14g, and 16.33g. The dilution of producer gas ranged from 16.7x to undiluted. The flow rate was 1.5slpm, except when the producer gas was undiluted, it was 0.44slpm. The undiluted producer gas contained 4-10.7ppm COS, 440-940ppb thiophene, and 1300-1650ppm benzene. The range resulted from a change in producer gas cylinders between the experiments. Benzene is shown as g_Benzene/g_Adsorbent. The COS capacities are slightly larger than the values in the graphs, because the cumulative breakthrough was still below 1 percent at the end of the experiment.

Source: UC San Diego

Biochar from Fluidized-Bed Gasifier

Biochar was collected from the FICFB gasifier after the test 2014/12/08 when the gasifier was shut down without burning out the remaining char in the bed. The char was tested for its adsorbent capacity using producer gas, and the results are summarized in Figure 37. The results show that the char adsorbed thiophene and benzene, and it did not adsorb COS. Benzene is three orders of magnitude larger than thiophene, and in Figure 37, it is divided by a factor 1000. The tests show that the char still performed well after it was regenerated twice with nitrogen at 110C. The char also adsorbed benzene which competes with thiophene. An increase in temperature to 55C, decreased the capacity more for thiophene than it did for benzene and thus is not advantageous. The biochar from the fluidized-bed gasifier could be an option for a scenario where benzene should also be removed from the gas stream. In this case, an online withdrawal of the biochar from the FICFB gasifier would have to be developed, and this would provide a steady source of the biochar at the same location as the RNG plant.

Figure 37: Adsorbent Capacities for Biochar (Fluidized Bed)



Adsorbent capacities for biochar from a fluidized-bed gasifier before and after regeneration. The adsorbent amount was 7.49g, and the flow rate of producer gas (16.7x diluted) was 1.5slpm. The undiluted producer gas contained 8.6ppm COS, 710ppb thiophene, and approximately 1500ppm benzene. Benzene is shown as g_Benzene/g_Adsorbent/1000.

Source: UC San Diego

Gas Cleanup of Producer Gas Before Methanation

Two adsorbent vessels were installed before the methanation unit to remove sulfur. The first vessel contained silica gel and biochar. The biochar was obtained from a fixed-bed gasifier and screened to a 0.25-0.5 inch particle size. Silica gel was used to remove moisture from the gas, and biochar was used to remove thiophene. The second vessel contained SulfaTrap R8C in order to remove COS. During the experiments, bag samples were taken before, between, and after the two vessels to monitor the sulfur adsorption performance. Once sulfur breakthrough was detected, the adsorbent in the vessel was replaced.

CHAPTER 4:

Methanation

Methanation is the conversion of a carbon-monoxide (CO) or carbon dioxide (CO₂) containing gas to methane. The reactions require hydrogen, and if less than stoichiometric amounts of hydrogen are provided, the output gas will contain CO₂, which can be removed via separation methods. A too-low amount of hydrogen can also lead to coking on the catalyst surface. This is especially a problem for unsaturated hydrocarbons such as ethylene and benzene, and if fixed-bed methanation is used. Deactivation by carbon deposition or coking can be avoided by supplying sufficient amounts of hydrogen or steam. In the following chapters, different gas compositions and catalysts are evaluated in fixed-bed and fluidized-bed methanation, with the final goal of operating a fluidized-bed methanation reactor on producer gas.

Catalyst Development

The state-of-the art catalyst for methanation is nickel-based, and nickel together with promoters are typically deposited as a thin layer on the surface of a catalyst support material. Nickel is subject to contamination by sulfur, and therefore the gas needs to be cleaned of sulfur compounds (see Chapter 3). Deactivation by coking is another problem, and this is addressed later in the current chapter. The activity and deactivation are influenced by the catalyst amount, formulation, dispersion on the surface, and surface area of the catalyst support.

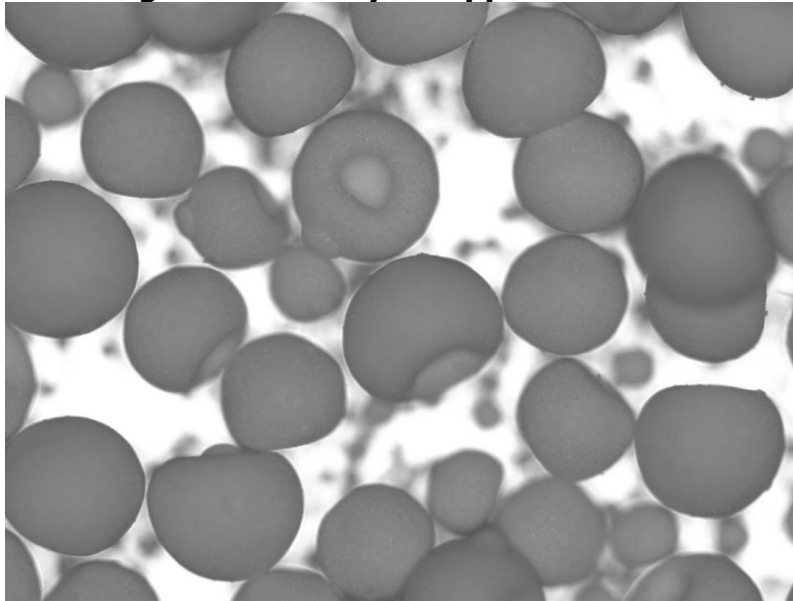
Catalyst Support

For catalyst support, an alumina-based bed material (AD90) was acquired from Coorstek Inc. This bed material has a relatively small surface area, but superior attrition resistance. The same support material was used in tar reforming by NREL (National Renewable Energy Laboratories), by coating it with a Ni-based catalyst (Magrini, 2012). Figure 38 shows a microscope image of the bed material, and Figure 39 shows the size distribution.

Fluidization Tests

To characterize the bed material for a fluidized-bed, a cold-flow experiment was conducted. Figure 40 shows the experimental setup. In this experiment, the minimum fluidization velocity can be measured by finding the velocity at which the pressure drop no longer increases, starting from a packed bed. Figure 41 shows the result of the measurement, and Table 11 shows a summary of the measured and predicted minimum-fluidization velocity. After adding the nickel catalyst to the bed material, the weight of the particles will be increased by the amount of nickel added, while the envelope volume does not significantly change. Using the formulas for predicting the minimum-fluidization velocity, the experimental values can be adjusted upwards by the appropriate factor (with catalyst/without catalyst).

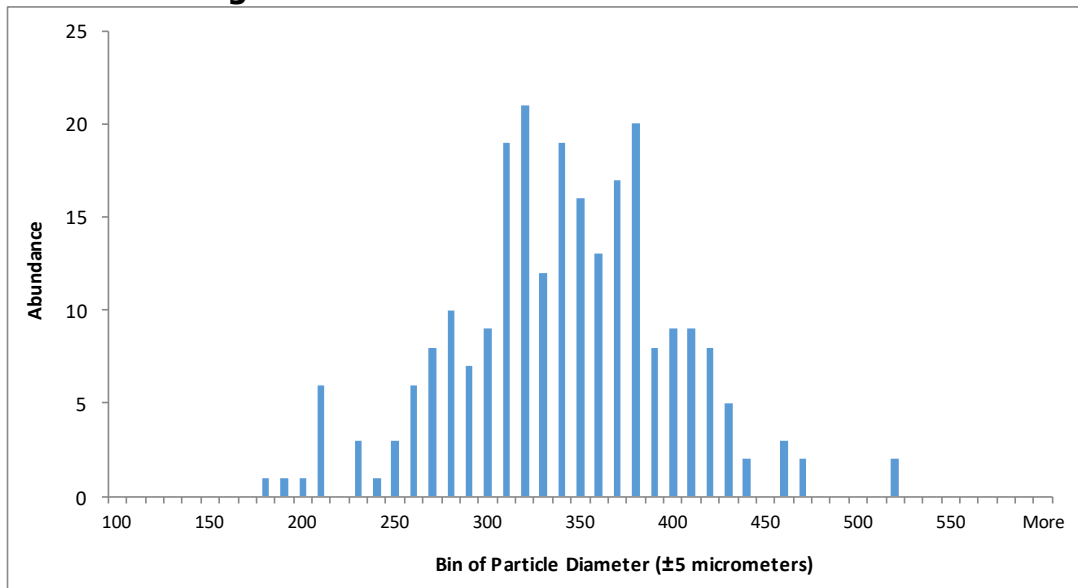
Figure 38: Catalyst Support Material



Microscope image of CoorsTek catalyst support material (AD90) without catalyst coating. The outer envelope is nearly spherical, but there is an inner half-spherical cup-shaped hollow section observable for most particles.

Source: UC San Diego

Figure 39: Size Distribution of Bed Material



Histogram showing the size distribution of the bed material. The abundance of each particle-size bin was determined by counting the particles in a series of microscope images.

Source: UC San Diego

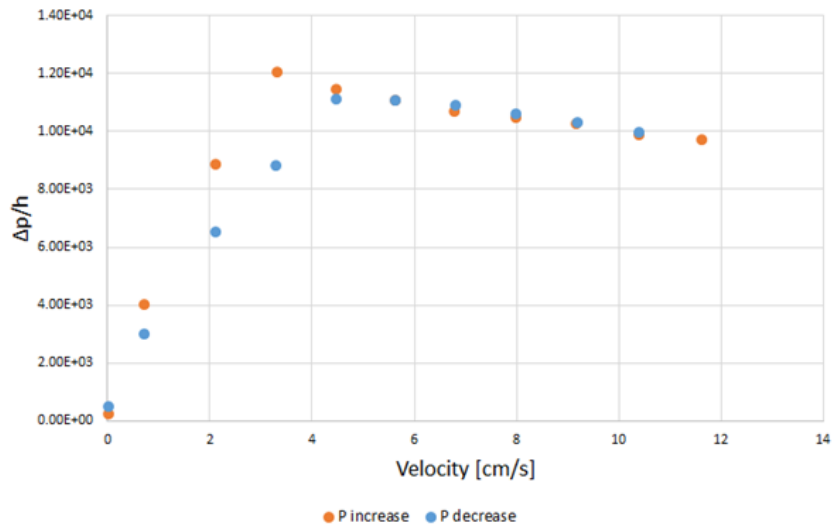
Figure 40: Cold-Flow Experiment



Photo of vertical fluidized bed experiment, along with four pressure probes in the fluidized bed. The cold-flow model is used to determine fluidization parameters for gasifier and methanation bed materials.

Source: UC San Diego

Figure 41: Determination of Minimum Fluidization



Normalized pressure gradient plotted as a function of superficial gas velocity for AD90 bed material. The plot shows the hysteresis when pressure at the bottom of the bed is either increased or decreased.

Source: UC San Diego

Table 11: Summary of Minimum Fluidization

U_{mf} Determined from Pressure Drop [cm/s]	U_{mf} Determined from Void Fraction [cm/s]	U_{mf} predicted from theory using $\phi_s = .658$ [cm/s]	Archimedes number [-]	U_{mf} Determined from flow regime diagram [cm/s]
2.82	2.19	3.57	4817.7	8.96

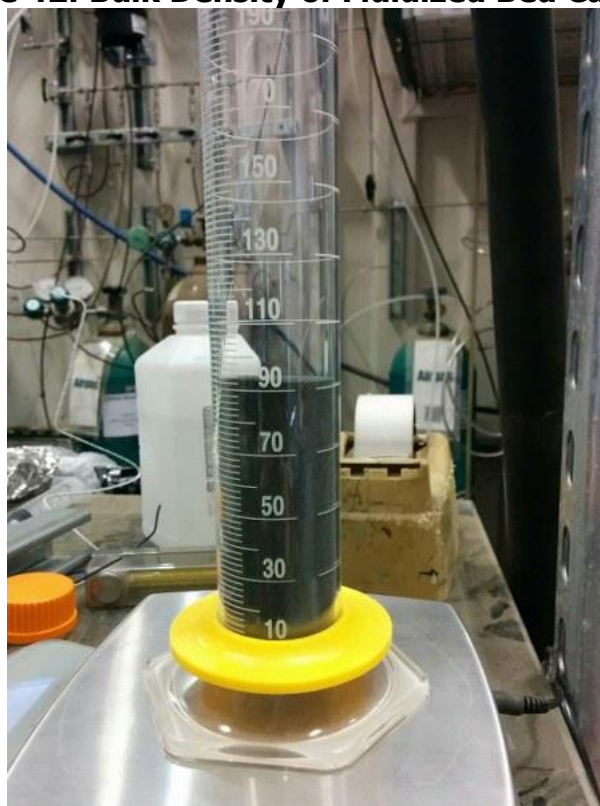
Experimental and calculated minimum fluidization velocities for AD90 bed material. This bed material is used as support material for nickel-based reforming and methanation catalysts.

Source: UC San Diego

Fluidized-bed Catalyst

During this project, a nickel-based catalyst was impregnated on top of the AD90 alumina bed material. Several formulations were tested in bench-scale fixed-bed reactor, and the best one was selected for testing in the fluidized bed. Figure 42 shows the catalyst that was selected and produced in larger quantities for the fluidized bed experiments. The bulk density was measured with a graduated cylinder and a scale.

Figure 42: Bulk Density of Fluidized Bed Catalyst



Catalyst for fluidized-bed methanation. The Ni-based catalyst was impregnated on top of small alumina particles (AD90). A measuring cylinder and a scale were used to determine the bulk density of the catalyst.

Source: UC San Diego

Fixed-Bed Characterization

Figure 43 shows the fixed-bed flow reactor used for characterizing the nickel-based catalyst produced for fluidized-bed methanation. A small amount of catalyst particles is mixed with quartz chips to reduce the reaction rate and heatup. CO conversion is then significantly less than 100 percent and can be precisely measured.

Figure 43: Fixed-bed Flow Reactor

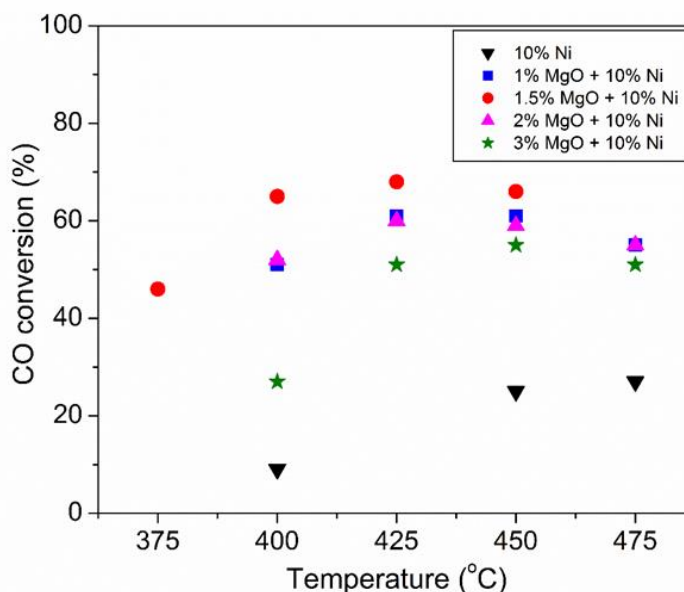


Setup for characterizing methanation catalysts in a laboratory fixed-bed reactor.

Source: UC San Diego

Error! Not a valid bookmark self-reference. shows the results of one experiment comparing different magnesium-promoted nickel catalysts.

Figure 44: Catalyst Screening Results



Screening of different catalyst formulations in a fixed-bed reactor. Temperatures are generally higher than in a fluidized-bed reactor because coke formation has to be avoided. Addition of small amounts of MgO increases the CO conversion.

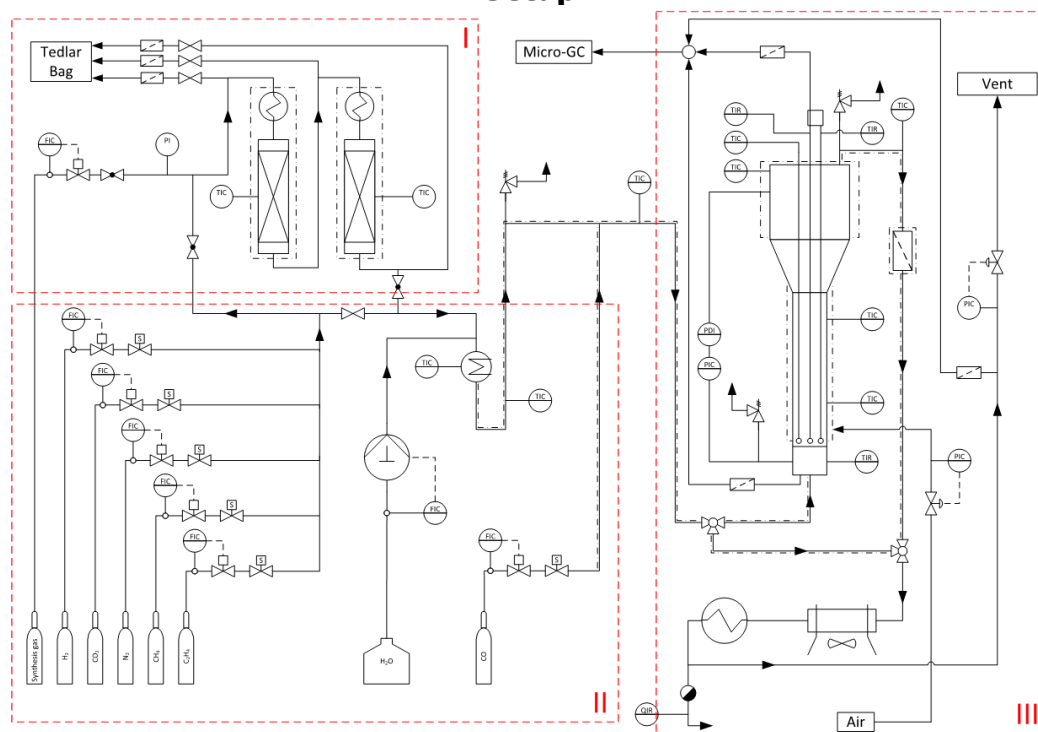
Source: UC San Diego

During the project, many catalyst formulations were investigated, including formulations that reduce the coking behavior. All detailed experiments are shown in Appendix J. The final catalyst formulation was submitted for patent disclosure. In this report, the catalyst is denoted as UCSD and refers to a loading of 0.015g MgO, 0.095g Ni, and 0.005g Ru per gram of AD90 alumina support (Mg-NiRu05 in Appendix J).

Methanation Testing Experimental Setup

A major focus of the work in this project was the development of a versatile catalyst synthesis unit for research purposes. A flexible system based on independent subsystems was designed, fabricated, and commissioned. The unit was designed for fully automated operation with 3-25 slpm gas flow rate, 1-5 bar, a design pressure, 20 percent moisture content, and up to 1 percent BTX content. All gas-distribution tubing after vaporization (see below) is constructed of 1/4" OD stainless steel (SS316) and maintained at an elevated temperature to avoid condensation. The unit is framed in 2" structural steel tubing to provide protection and allow for simple relocation, or loading and unloading, via a forklift skid type base. The primary subsystems of the unit are: 1) The gas generation unit which serves to generate the desired test gas as well as meter and condition the flow of synthesis gas - or any other carbon containing gas of interest - from a real gas source. 2) The gas cleaning unit which removes sulfur containing species from the incoming gas stream while allowing investigation of the sulfur removal properties of various sorption materials. 3) The methanation reaction unit which is effectively the heart of the system where the methanation reaction takes place. Figure 45 gives a process diagram of the full system as designed.

Figure 45: Process Flow Diagram for the Laboratory Fluidized-Bed Methanation Setup



Process flow diagram for the laboratory fluidized-bed methanation setup. The setup consists of a gas-cleaning unit (I), gas-generation unit (II), and methanation-reaction unit(III).

Source: UC San Diego

Gas-Generation Unit

This module is responsible for accurate generation of the gas stream that feeds the methanation reactor. The unit consists of six mass flow controllers for bottled gases, one mass flow controller for synthesis gases operation from the gas producer, and two piston pump systems with associated vaporization units for controlled liquid flow and evaporation into the gas stream (see Figure 46). All gas streams are setup with normally closed solenoid shut-off valves to provide automatic cutoff of gas flow in the event of a power failure. System plumbing has been arranged to minimize tracer concentration diffusion bleed issues through series arrangement of the gas input streams, from greatest to least; this allows for minimal dead space and a sweeping of smaller flow paths by upstream gases. Further, mass flow controllers are held in place by a laser-cut plate designed with universal bolt patterns to simplify replacement of mass flow controllers with any of the major brand controllers in the event of required controller change out. Vaporization is provided by a Bronkhorst CEM (Controlled Evaporator Mixer) unit followed by heated capillary injection for steam and tars, respectively; both placed downstream of the gas mixing arrangement. Distilled water is delivered to the evaporator at a controlled rate via an HPLC pump. All gas distribution lines after vaporization are maintained at an elevator temperature. Carbon monoxide is kept separate from the rest of the mixture just before the Methanation Unit in an attempt to avoid carbonyl formation.

Figure 46: Gas and Steam Generation Components for the Laboratory Methanation Setup



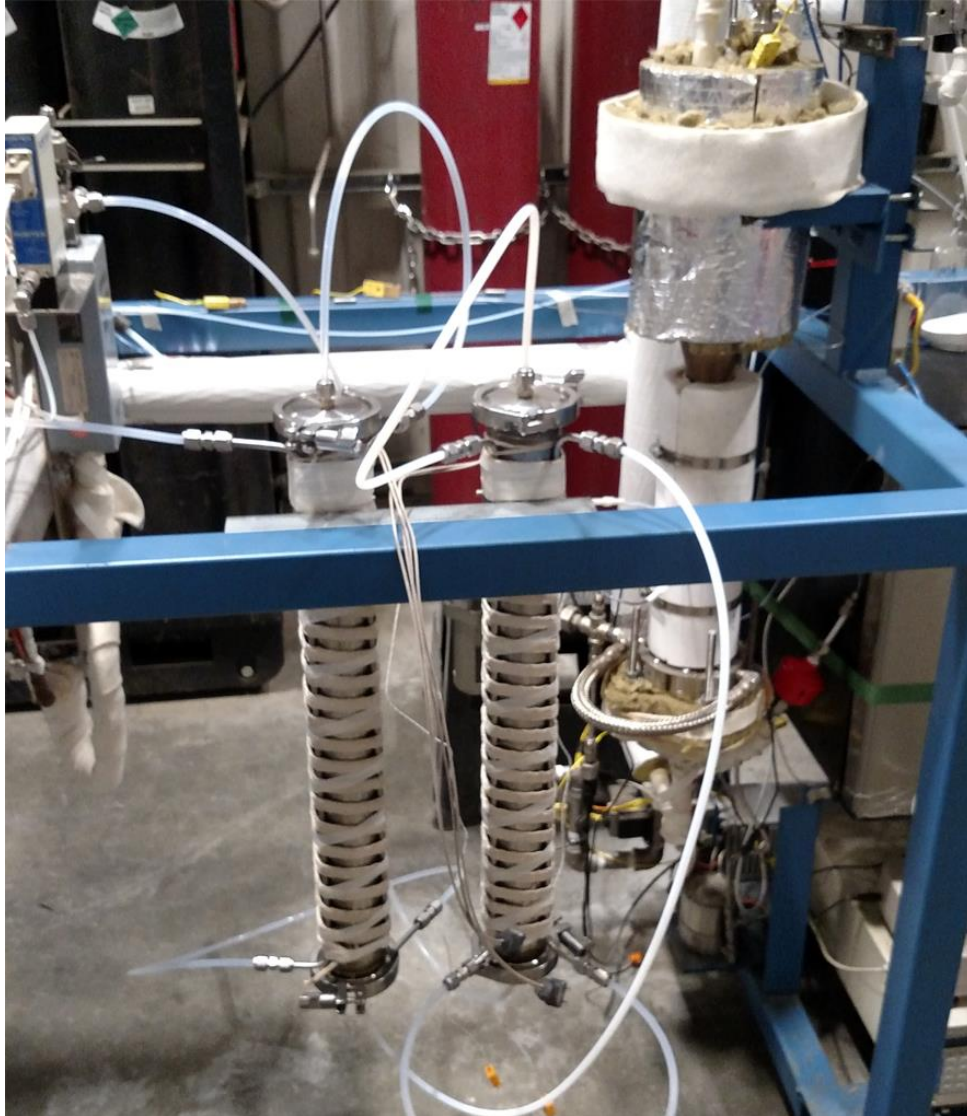
Gas and steam generation components. A micro-boiler is used to evaporate water and the system can be setup with up to 9 mass flow controllers (MFCs) for control of up to 9 gases. The picture shows 6 MFCs installed and ready for operation.

Source: UC San Diego

Gas Cleaning Unit

This module is responsible for removal of sulfur species down to low ppb levels. As seen in Figure 47, the unit consists of two temperature-controlled adsorption columns placed in series arrangement. The columns can be run with various sorption materials to optimize removal for the current process requirements. Sampling ports are located before, between, and after the columns for measurement of Sulfur species removal efficiencies. In practice, the gas cleaning unit is only used when operating the methanation on synthesis gases produced from woody biomass via gasification.

Figure 47: Installation of Two Adsorbent Vessels Before the Fluidized-Bed Methanation Reactor



Installation of two adsorbent vessels before the fluidized-bed methanation reactor. Both vessels are heated and insulated (insulation not shown). The purpose of the adsorbents is to remove sulfur from the producer-gas stream before it reaches the methanation catalyst.

Source: UC San Diego

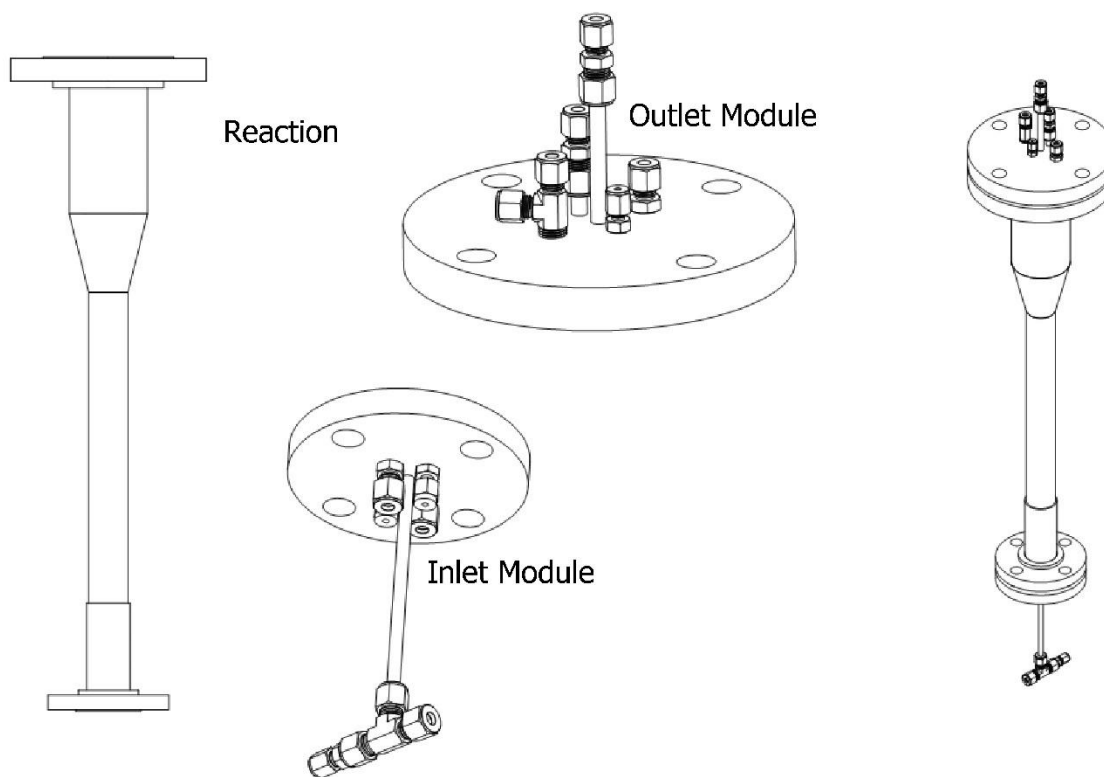
The inlet module was fabricated around a 1-1/4" standard 150# flange and consists of ports for temperature, pressure, pressure safety relief, gas inlet, and gas sampling. A removable

38.1 [mm] diameter, 10-micron porous plate distributor along with graphite seal is held in place by a spring system that is held in-place by the inlet flange itself.

The reaction module consists of a 34.8 [mm] diameter main reaction tube of 304.8 [mm] length, preceded by a windbox of 38.1 [mm] diameter, and followed by a disengagement zone of 72.9 [mm] diameter and 152.4 [mm] of length; all of welded construction.

The outlet module was designed around a 3" standard 150# flange consisting of gas outlet, pressure sensing and safety relief, main control thermocouple, and two 5/16" bed sampling probe entry ports. Bed sampling ports have been oversized to allow use of sampling probes up to 1/4" in diameter. The main control thermocouple is 1/8" in diameter and reaches to a location of 5mm above the distributor plate.

Figure 48: CAD Figures of the Engineered Main Reactor



CAD figures of the engineered main reactor with sub-modules. Sub-modules can be replaced updated and replaced on an individual basis to allow for simple adjustments as needed for future experimental requirements.

Source: UC San Diego

Axial Sampling Unit

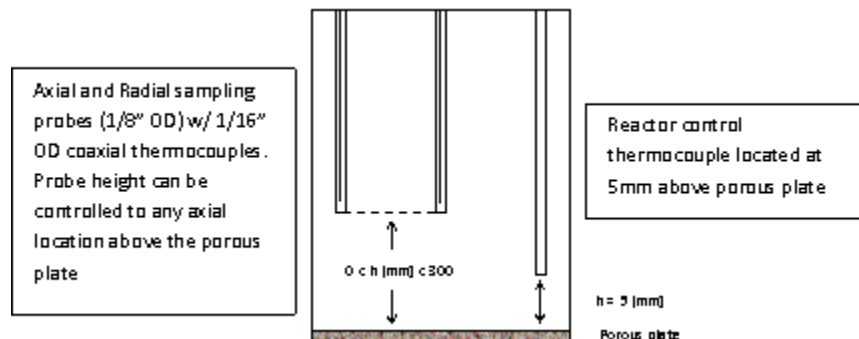
An axial sampling unit was developed to allow for gas sampling and temperature measurement at any location within the bed along the center axis and at 0.8 of the bed radius. The probes are of a coaxial design with 1/16" thermocouples terminating at 38 mm above the probe inlet, inside 1/8" sampling tubes. Probes are held by a Thompson MS25LA0 series linear positioning slide allowing for sampling within the bed to a precision of 0.03 mm and an accuracy of 0.18 mm. Figure 49 gives a diagram of the probes within the bed. Sealing for the probes to outlet

module interface was originally of a PTFE ring seal type, but after finding a lack of sealing, the seals were replaced with graphite tube ferrules which were found to work much better.

Source: UC San Diego

Figure 50 is a picture of the axial sampling unit with associated upper probe bodies being held in place by the probe carriage atop the linear slide.

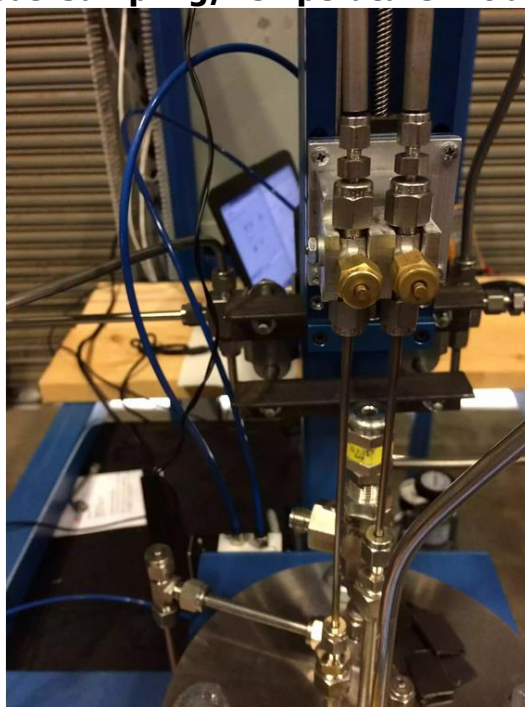
Figure 49: Diagram of sampling probe locations



Location of the three sampling probes in the laboratory fluidized-bed methanation reactor. The first two sampling probes include a thermocouple for temperature measurement. Both can be moved up and down inside the fluidized bed. The third probe consists of a thermocouple only and is used for temperature control of the reactor.

Source: UC San Diego

Figure 50: Axial Sampling Unit for Two Combined Gas-Sampling/Temperature Probes



Axial sampling unit for two combined gas-sampling/temperature probes. The probe locations can be adjusted to any height in the fluidized bed.

Source: UC San Diego

Post Reactor

Post reactor gas conditioning includes filtering, condensation, cooling, and pressure regulation. The high temperature filter was designed and fabricated to use standard analytical gas sampling thimble-type filters. The filter captures any entrained fines and allows for quantification of bed particle losses. Following the filter, a 3/8" OD stainless steel air cooled product gas condensing coil and similar product gas cooling coil, located inside a refrigerated box, serve to first condense then minimize the vapor pressure of any condensables in the gas stream. Condensate is removed and weighed, while dried product gas is run to a backpressure regulator before being exhausted. Condensate weight is determined by mass gain principle on an electronic balance. The back-pressure regulator is of pilot type allowing for automated control of the system pressure by the control system.

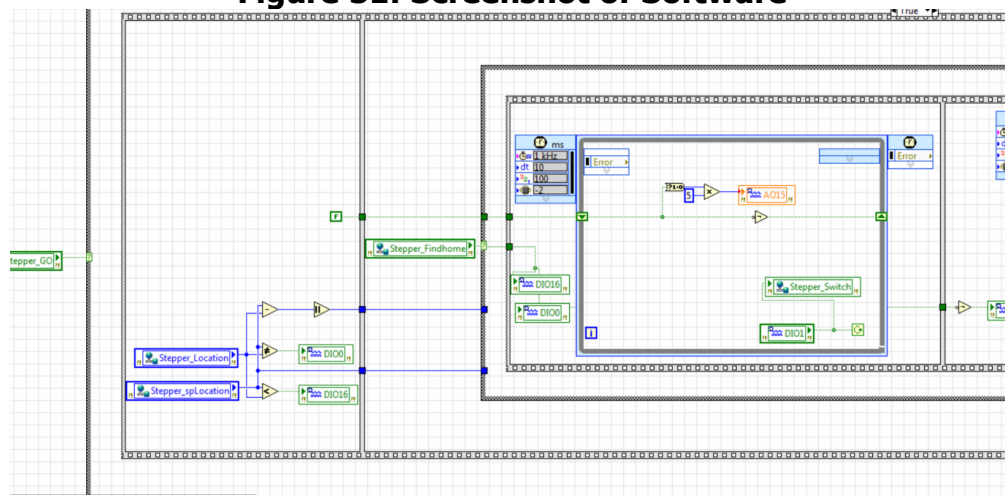
Control

Automated control of the entire system is provided by National Instruments cRIO modules. Modules gather thermocouple signal, voltage, and digital inputs from sensors as well as create control voltage and digital output signal that are sent to system control devices.

Software

A system control program was developed using National Instruments Labview software. The program is based on two independent system; an underlying control program and a supervisory control and data acquisition (SCADA) program. The control program simply maintains the active control parameters, such as setpoint temperatures and axial sampling unit probe location, while the SCADA system gives setpoint information to the active control program and has direct control of less fundamental control parameters, such as mass flow controllers, gas shut-off valves, uGC sampling command, sampling port selection. The SCADA program also collects and logs all data. Due to the extremely exothermic nature of the methanation reaction, the control program has been setup with priority processing to the main reactor temperature control PID. A rudimentary scheduling function has also been included in the SCADA program to allow for complete scheduling of an experiment's run conditions and times at each condition. An image of the control program is shown in Figure 51.

Figure 51: Screenshot of Software



Screenshot of software (in Labview) for controlling the gas sampling probe linear positioning stage.

Source: UC San Diego

Thermal Control – Cooling

Reactor cooling is provided by compressed air using an Exair Super Airwipe radial air multiplier. The unit evenly delivers a sheet of air to the reactor walls at the location of the distributor plate to maximum cooling at the location of maximum heat release. Delivered air causes a venturi effect, leading to a multiplication of the air flow over the reactor walls which after impact travel upward along the entire length of the main reaction tube before dispersing into the surrounding area. Cooling control is provided by PID algorithm sensing the control temperature and generating a signal to a pressure regulator that controls the flow of air to the Airwipe device. The Airwipe air multiplier along with related control equipment as shown in Figure 52 and Figure 53. The reactor control temperature is measured by a 1/8" OD fixed thermocouple located 5mm above the distributor plate as shown in Figure 49.

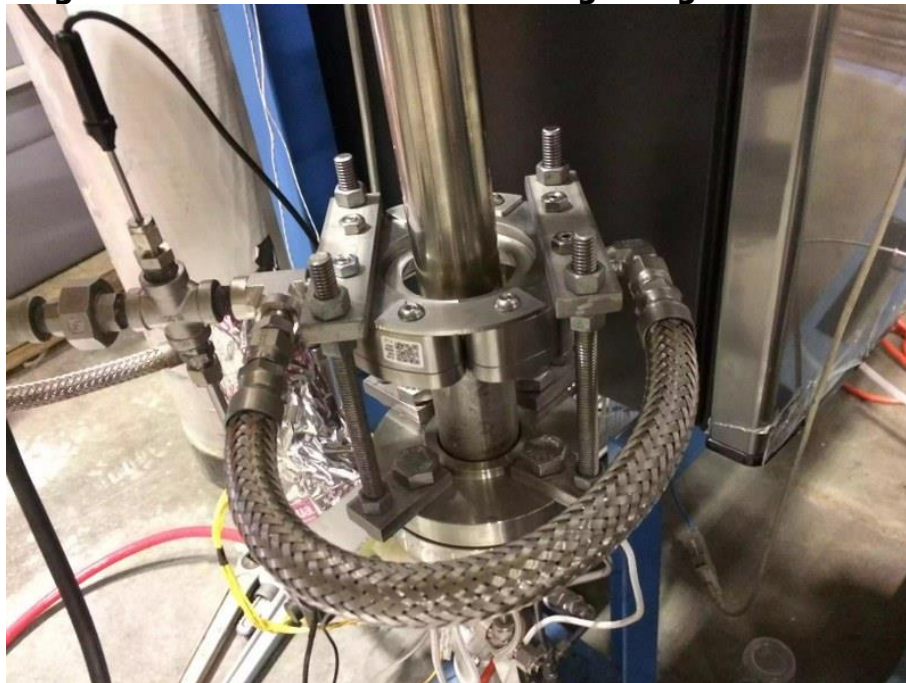
Figure 52: Control of Reactor Cooling by Compressed Air



Control of reactor cooling by compressed air. Shown in the figure are a constant-pressure regulator with dryer, an electronically controlled pressure regulator, and the methanation reactor (from left to right).

Source: UC San Diego

Figure 53: External Reactor Cooling Using an Air Knife



External reactor cooling using an air knife. The high-velocity annular sheet flows upwards along the outer reactor wall to provide a means of removing the reaction heat.

Source: UC San Diego

Thermal Control – Heating

Heating is required to heat the reactor to reaction temperatures prior to methanation and for maintenance of all heating lines. An inline air heater was first included in the original design to deliver pre-heated air to the air multiplier; thus in effect changing the cooling system to a pre-heating system. However, during commissioning it was found that heat losses through the delivery plumbing was excessive for such a heating method. Accordingly, a set of two stacked 2" ID 6" tall ceramic tube heaters were added to allow for two zone heating control along the reactor and serve as flow channels for the cooling air during typical operation. The tube heaters are mounted directed atop the Air-wipe system as seen in Figure 54.

Pressure

System pressure must be measured for determination of experimental pressure effects and to maintain safe operating conditions. Total pressure and bed differential pressure are measured using a 100 [psi] Druck 9x2 series and a bidirectional ± 511 [mbar] Druck LPM series sensors, respectively. Three mechanical pressure relief valves are also located throughout the reactor system to ensure safe release of pressure in the event of a controller malfunction or system blockage. Control of system pressure is maintained through a pilot type back-pressure regulator that receives a control pressure signal from a pneumatic pressure regulator which is control via voltage signal from the control system.

Figure 54: Ceramic Heater for Preheating of Laboratory Methanation Reactor



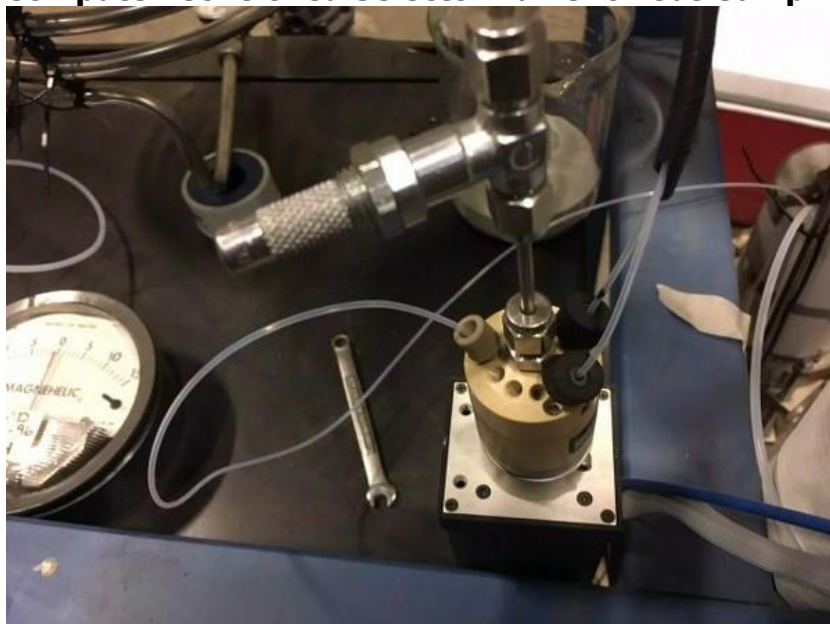
Ceramic heater for preheating of laboratory methanation reactor. The heater is mounted above the air knife that provides the cooling flow. The heater is used to preheat the reactor and to compensate for heat loss to keep the reactor at operating temperature.

Source: UC San Diego

Gas Sampling

Gas sampling is accomplished by porting all 4 sampling streams (inlet, axial probe, radial probe, and dried outlet) to a VICI actuated selection valve for selection of which stream will be allowed to pass to the uGC sampling system. The valve is controlled by an Arduino based sub-controller which interprets that control signal from the Labview NI cRIO control module into a rapid pulse-based control that signal that drives a VICI valve's stepper motor to the desired sampling position. A precision needle valve is placed on the outlet of the sampling valve which acts, along with an analog pressure indicator placed just before the uGC inlet, to limit flow from the reactor to a minimal but sufficient stream. Figure 55 shows the sample selection valve. Gas Chromatography (GC) is provide by a 4-channel Agilent 3000 Micro GC. A desiccant vessel filled with MgSO₄ is located at the outlet of each sampling port to ensure no condensation within the sampling lines. The vessel system consists of a main body followed by a section of clear desiccant filled tubing to allow for simple indication of spent desiccant. Figure 56 shows one such desiccant vessel setup.

Figure 55: Computer-Controlled Selector Valve for Gas Sampling Location



Computer-controlled selector valve for gas sampling location. The three outside tubes lead to the gas sampling locations of before the reactor, inside the reactor in a center location, and inside the reactor in an off-center location. The tube in the center leads to the gas chromatograph.

Source: UC San Diego

Figure 56: Laboratory Methanation Setup with Gas Sampling to Gas-Chromatograph



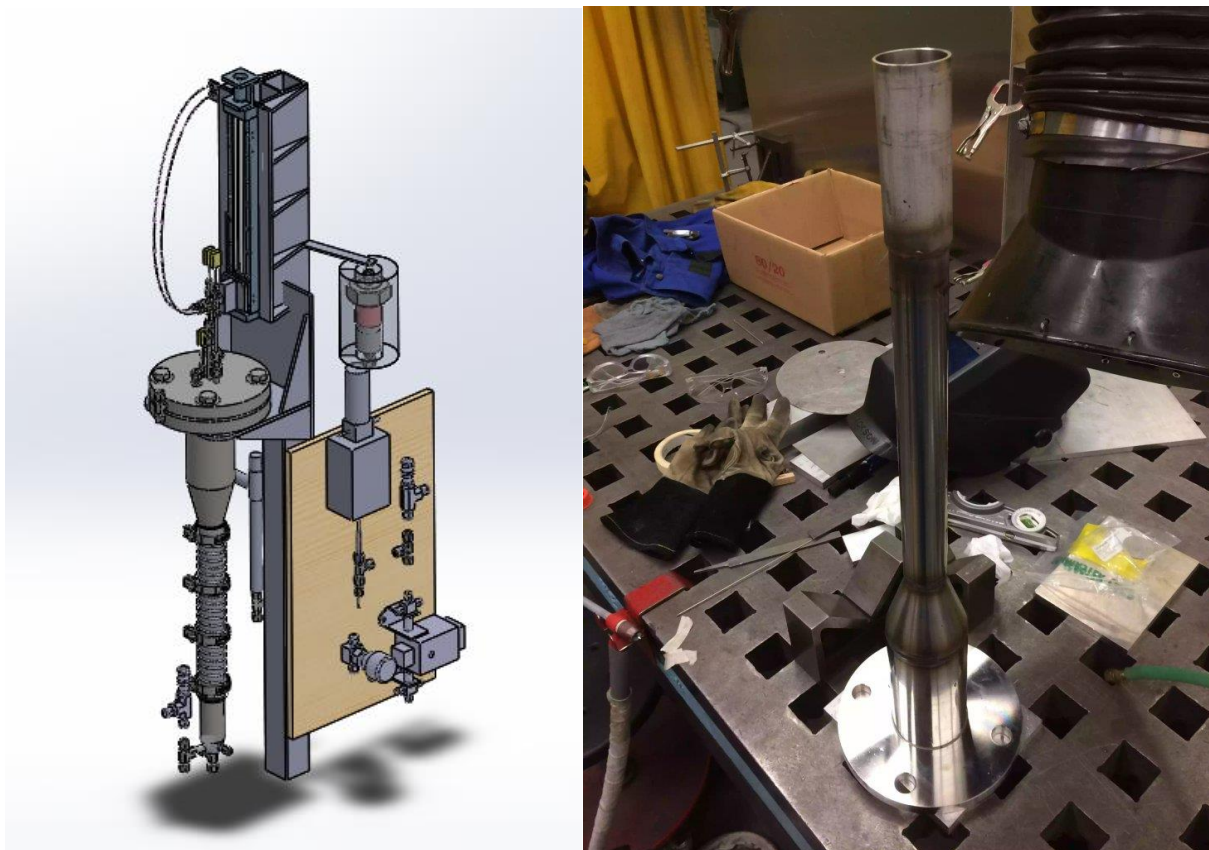
Laboratory methanation setup with gas sampling to gas-chromatograph. The red vessel contains desiccant to dry the sample before being analyzed by the gas chromatograph. The insulated part shows the top of the methanation reactor.

Source: UC San Diego

Fabrication

System fabrication was completely done in-house. A 2" square structural tube frame was developed to protect and house all system components while leaving room for unforeseen future additions. The frame has fork lift points below to allow for simple loading and unloading in the event of future deployment to field study sites. Engineering design of the main system components included modeling in Solidworks 3D modeling software. An image of an earlier system arrangement and a picture of the main reactor unit during fabrication are given in Figure 57. The main tube components are shown having been completely welded with the inlet windbox complete and before welding the inlet flange (not shown).

Figure 57: Engineering Design and Fabrication of Fluidized-Bed Methanation Reactor



Engineering design of fluidized-bed methanation reactor with thermocouples mounted on a computer controlled positioning stage for measuring in-bed reactor temperatures (Left). Fabrication of methanation reactor (Right).

Source: UC San Diego

Figure 58 gives four pictures of the frame during fabrication catalytic synthesis unit assemble process as various steps with the inlet module first being completed followed by a picture of the system at an intermediate stage of development, and finally a picture of the system in its mostly complete and under commissioning stage.

Commissioning

Commissioning involved shakedown of all systems, calibration of sensors, tuning of PID control algorithms, and investigations of factors such as catalyst fluidization properties.

Figure 58: Catalytic Synthesis Unit Fabrication and Assembly



Catalytic synthesis unit fabrication and assembly. Fabrication from 2" structural tubing with fork lift channels (top left) and assembly through time (top right, bottom left, and bottom right).

Source: UC San Diego

Sensor Calibration

All mass flow controllers were calibrated against a wet-test gas meter during reactor commissioning and periodically checked during experimentation. Pressure sensors were calibrated against gauges of known accuracy prior to installation. The condensate electronic balance was calibrated using standard weights and the HPLC pump for distilled water delivery was calibrated by mass difference rate determination using the condensate electronic balance.

PID Controller Tuning

The system has many thermal control systems that are used to maintain line temperature, reactor sub-system temperatures, and main reactor temperature. Each heated maintenance zone is controlled using a PID algorithm that varies the on/off time of the electric heaters.

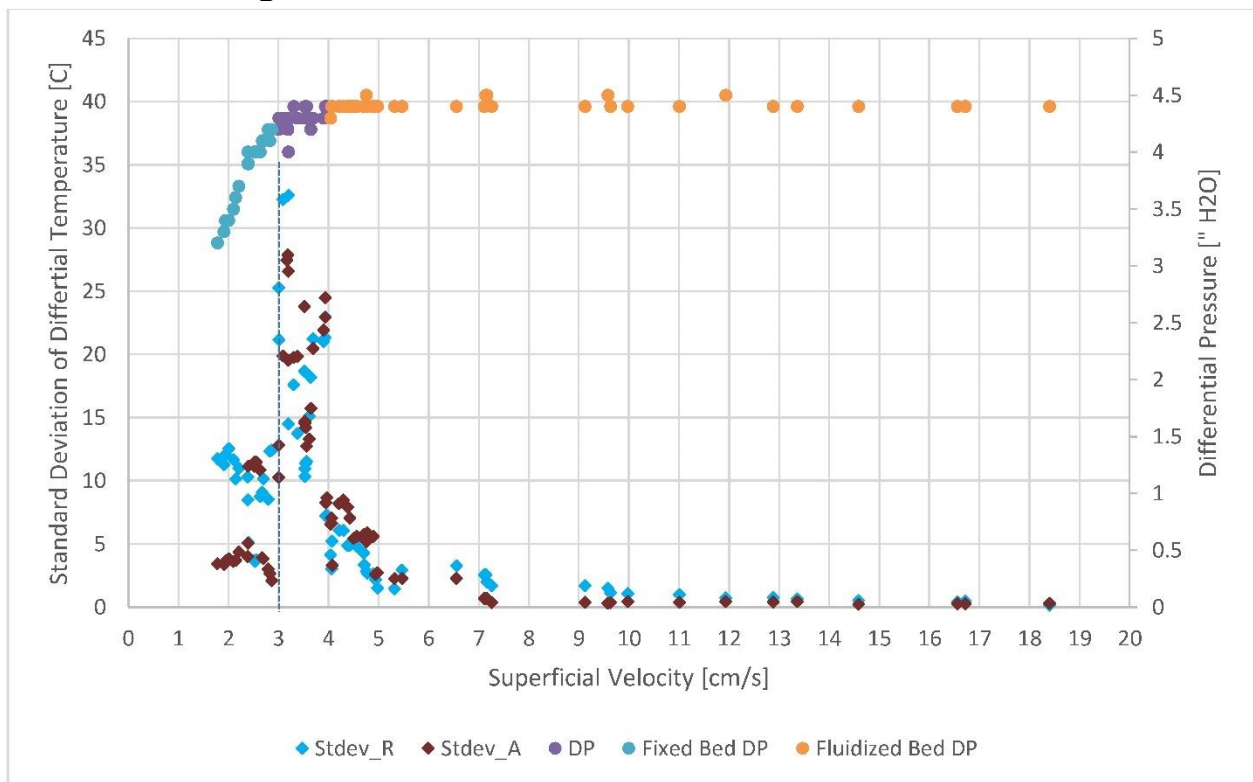
The unique thermal properties of each heated zone required that each PID loop be calibrated by operationally determined PID parameters to provide the best control of the zones to the desired conditions. Similarly, the cooling control loop required unique PID parameter characterization to allow for rapid cooling air response to changes in reactor heat production – caused by changes in operating conditions – while also avoiding a control that was too jumpy for stable operation. The back-pressure regulator's control loop also required careful PID tuning to prevent over pressurization during increased in flow, while at the same time to

prevent rapid pressure loss from overly aggressive control that can lead to ejection of bed material into the particle filter.

Fluidization

Catalyst material properties were measured and tested for fluidization behavior for comparison to theoretical models. The minimum fluidization velocity is typically found by measuring the bed pressure drop over a range of fluid velocities. A plot of the generated data then shows two distinct trend lines; one of the fixed bed pressure drop gradually increasing with velocity, and another of the fluidized bed pressure drop, which remains nearly constant regardless of velocity. The intersection of the two lines is defined as the minimum fluidization velocity. The experimentally found minimum fluidization plot for the UCSD-provided catalyst showing pressure versus superficial fluid velocity is given in Figure 59. The spatial temperature difference between thermocouples was also measured to investigate the potential use of temperature measurement in fluidization detection. Accordingly, one can see in the figure that the standard deviation of the differential temperature between two thermocouples sharply increases as the minimum fluidization velocity is reached.

Figure 59: Determination of Minimum Fluidization



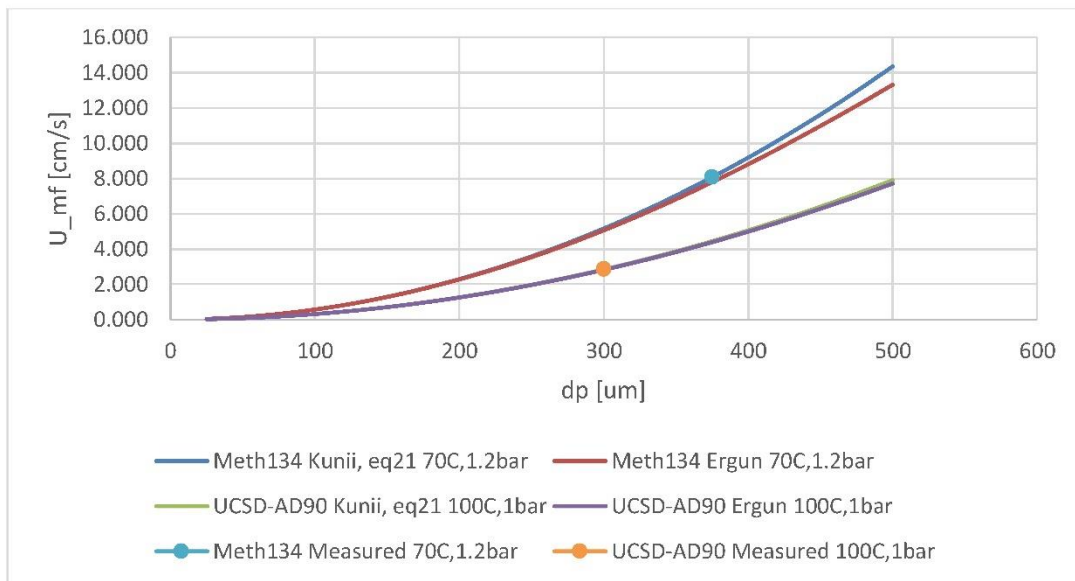
Differential pressure and standard deviation of differential temperature versus superficial velocity. The typically agreed point of minimum fluidization is found by the intersection of the two pressure curves: fixed and fluidized behavior. Note the maxima of thermal data occurs at the same superficial velocity as the intersection of the pressure curves.

Source: UC San Diego

Experimental data was collected for both catalyst materials used in this study and compared with multiple theoretical models in Figure 60. Parameters that effect the theoretical fluidization models are particle size, particle envelop density, fluid density, fluid viscosity, bed void fraction

at minimum fluidization, and particle sphericity; most of which are hard to accurately measure. It is for this reason that fluidization data was collected for comparison and tuning of the model. Bed expansion from bulk density was determined by graduated cylinder and scale under loose pack conditions. Minimal expansion before fluidization beyond the measured bulk density was assumed as the loose packed density was measured thus an expansion of 10 percent was assumed at minimum fluidization conditions. Particle envelop density is typically measured for non-porous particles by fluid displacement methods; however with porous particles there is a need to exclude the inter-particle volume. Consequently, the particle envelop density was determined by measuring the ellipsoid volume of pre-ground fixed bed Meth134 using calipers on three axis and the particle mass. Both particle densities were determined with the catalyst in the oxidized state, thus a correction to the densities for the reduced active state was then applied. Finally, the particles were not perfect ellipsoids; so a correction factor was applied to the particle envelop density for model tuning to agreement with measured data.

Figure 60: Model Curves Compared to Experimental Data for UCSD and Meth134 Catalyst



Theoretical fluidization models with experimentally found points of minimum fluidization for two catalysts.

Source: UC San Diego

Confidence in the correction factor is gained from investigating the resulting particle voidage fraction as defined as

$$\epsilon_{mf} = 1 - \frac{\rho_{bmf}}{\rho_p}$$

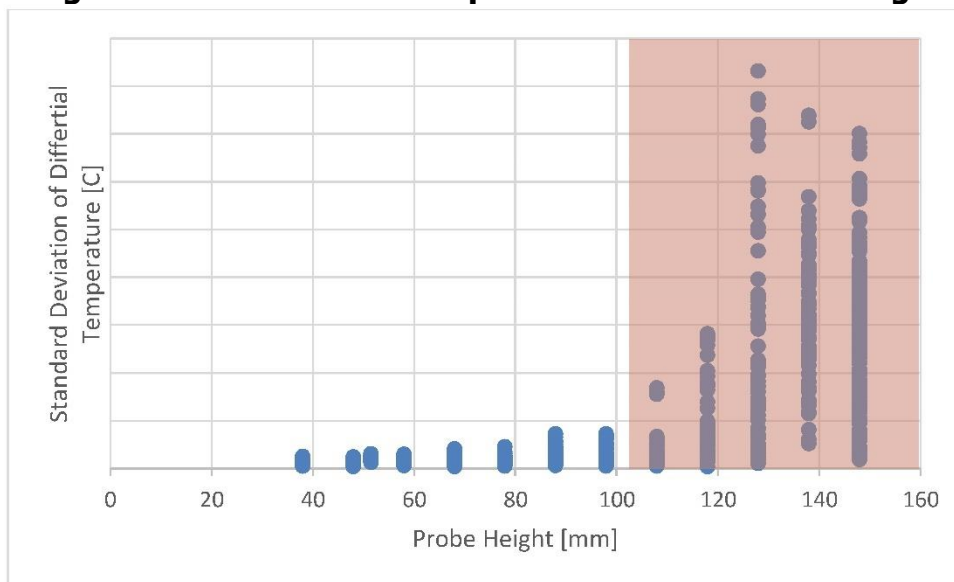
Typical voidage fraction for particles of similar diameters to the ground Meth134 range between 0.41 and 0.56, while the calculated voidage fraction after application of all correction factors as described above is 0.466 suggesting good agreement.

Thermal Data for Fluidization Detection

In considering differences between fixed and fluidized bed behaviors; particle mixing is known to increase from no mixing in fixed beds to very high values in well mixed beds. The thermal mass of the mixing particles in fluidized beds leads to near elimination of thermal gradients in well mixed bed. This can be easily seen with temperature measurements at various points in the bed. Given the difference in the difference in thermal gradients between fixed and fluidized bed behavior, thermal data from fluidization trials of the catalyst during commissioning of the reactor was overlaid atop the minimum fluidization plot of differential pressure vs. fluid velocity plots. As shown in Figure 59, the standard deviation of the difference in temperature between spatial measurement locations within the bed shows a maxima at the point of minimum fluidization. This finding suggests that thermal data could supplement pressure data to increase confidence in reactor fluidization related determination and provide need fluidization information in situations where pressure measurements are unfeasible. Further investigation of this detection method is recommended.

Of similar consideration to the above thermal fluidization detection, the difference in thermal mass of the particles in the bed and gas could potentially be employed to detect the active bed height in a thermal fluidized bed reactor. Gas, having a much lower mass, is expected to rapidly drop in temperature once it has left the bed, while the gas in the bed is known to have a fairly constant temperature as the thermal mass of the fluidized particles will maintain the gas temperature. Accordingly, an experiment was run in which the axial sampling probes were used to transect the bed during operation. Analysis of sampling probe temperatures vs probe height shows temperature measurements can be used to detect bed height through comparison of a movable probe's temperature reading to that of a fixed control thermocouple. Figure 61 shows that when the movable probe leaves the bed a corresponding jump in the differential temperature between the two probes develops.

Figure 61: Differential Temperature Versus Probe Height



Standard deviation of the differential temperature between the fixed control thermalcouple and a movable thermalcouple probe vs probe height. Difference remains fairly constant until probe has left the bed; at which point the value rapidly increases (shaded area).

Source: UC San Diego

Though a clear indication does exist, further investigation is suggestion as the current resolution of this method does not appear sufficient for practical implementation at this time. However, with purposefully developed instrumentation, this method may prove simple and effective.

Methanation Experiments

The experimental focus in this work was on demonstration and characterization of the fluidized bed methanation process. With such a large number of variables that effect methanation, a total of 42 unique experimental conditions were run during the duration of the experimental program. Table 12 shows a summary of the experimental conditions, and Appendix G shows a table of all experimental conditions. The following parameters are considered to have key effects on the process:

- Temperature: Reaction kinetics and thermodynamic equilibrium are largely affected by temperature. At low temperatures, the reactions may be kinetically limited, while at high temperature the reactions may reach equilibrium prior to the desired outlet concentrations.
- Pressure: In gas phase chemistry, pressure is directly proportional to concentration and concentration is well known to effect reaction kinetics and equilibrium. Higher pressures help push the methanation reaction towards the product side.
- H_2/CO ratio: The ratio of hydrogen to carbon monoxide is of high important in all fixed bed methanation theory. In fixed bed systems, a strict ratio of 3 or greater must be maintained in order to avoid catalyst deactivation by coking. The importance here can be understood by considering the partial pressures effect that are being represented by the ratio. Both the dissociation of CO, and the hydrogenation of surface carbon species to methane have reaction rates that are a function of each reagent concentration; the rate of dissociation of CO is matched by the hydrogenation reaction while at typical temperatures and an H_2/CO ratio of at least 3. This strict limit may not be as important in fluidized bed reactions; since particles that may have experience excessive carbon deposition well also experience conditions of hydrogen excess which should lead to hydrogenation of the previously deposited species.
- Nitrogen dilution: The dilution of a reaction stream can effectively lower the reacting concentration, while maintaining a set residence time and in fluidized bed a fixed mixing ratio - U/U_{mf} .
- Steam addition: Being a product of the methanation reaction, H_2O hinders production of methane by pushing the thermodynamic equilibrium towards the reactants. Further, the water gas shift reaction is active under methanation conditions which leads to a competition for catalyst surface active sites between the two major reactions. Though this competition may hinder the methanation reaction, the benefits of steam are additional hydrogen generation via in-situ water gas shift reaction and gasification of deposited carbon on the catalyst surface.
- U/U_{mf} : The ratio of a fluid superficial velocity against the fluid superficial velocity at the point of minimum fluidization denoted as U/U_{mf} . This ratio can be thought of as an indicator of the level of mixing with in the reaction, or a mixing ratio. Greater particle mixing within the reaction leads to increased mass and energy transfer; and

consequently, reduced temperature and concentration gradients. This ratio also has large effects on the physical stresses placed a catalyst particle; insufficient mixing would lead to large temperature spikes at the entrance of the reactor which may place large stresses on the particles, while excessive mixing not only reduces the residence time for a reaction but also results in greater attrition of the particles by the rubbing action of moving within the bed.

- **Catalyst:** Two catalysts were investigated in this study. The type of catalyst has a specific effect on the kinetics of reactions. The first catalyst was developed by UCSD on a low-surface area alumina support (see Appendix J). The second catalyst is a commercial catalyst from Clariant (*METH^R 134*), milled to a particle size around 375 micron.
- **Catalyst Charge:** The mass of catalyst within the reactor impacts the reaction as the particles only reacts (at significant rates) while in the presence of catalyst. Increased catalyst charge results in greater residence time; thus, reducing the chance of kinetic limitations. On the other hand, greater catalyst requirements represent an increase in operational costs as catalyst is would eventually have to be replaced.
- **Gas Type:** This study included trials with very pure exact reagents, simulated synthesis gases, and real synthesis gases from a fast internal circulating fluidized bed reactor (FICFB). Pure exact reagents are well understood from the fixed bed literature. Simulated synthesis gases include other reagents such as CO_2 and C_2H_4 which do have impact on the reactions; CO_2 is relevant due to its role as a product in the water gas shift reaction, and C_2H_4 as it is understood to also dissociate to surface carbon and also takes place in another reaction to C_2H_6 under methantation conditions. Synthesis gases contain many impurities that, although removed to low levels in upstream process steps, dissociate into carbon and coke species at the catalyst surface as well as carry catalyst poisoning compounds such as sulfur.

Table 12: Range of Experimental Conditions

Parameter	Units	Range
Temperature	[C]	340 - 385
Pressure	[bar,a]	1.3 - 3
H ₂ /CO Ratio	[mol/mol]	1.24 - 3.02
N ₂ Dilution	[%]	0 - 60%
Steam Content	[%]	0 - 24%
U/U _{mf}	[-]	2 - 12
Catalyst	[-]	UCSD or METH134
Catalyst Mass	[g]	51.7 - 258.9
Syngas Type	[]	Syngas or Simulated Syngas

Source: UC San Diego

Gas Composition Throughout Fluidized-Bed Methanation Reactor

An experiment was conducted in which the gas phase concentrations were sampled throughout the bed of the reactor. Experimental conditions are given in Table 13. Data from sampling shows the development of the reaction through the bed.

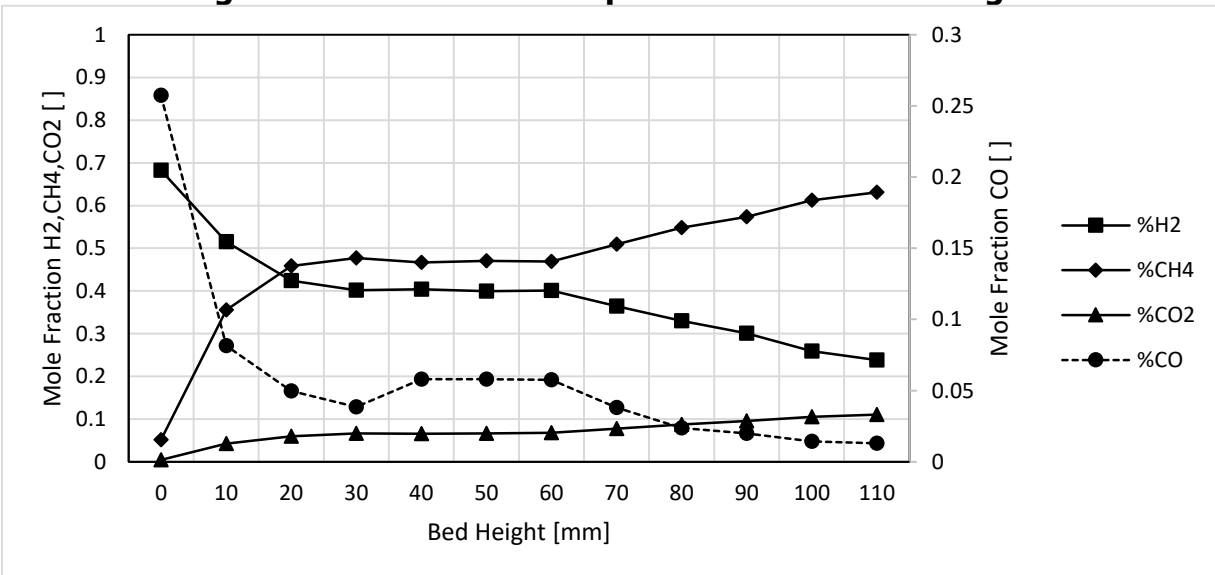
Table 13: Experimental Conditions for Bed Sampling Experiment

H ₂ /CO [mol/mol]	U/U _{mf} [-]	T _{set} [C]	p _{set} [bar]
3.0	6	340	3.0

Source: UC San Diego

The fluidized bed methanation reaction is highly active and exothermic as can be seen in the sharp methane concentration increase over the first 20 mm of the catalytic bed. After an initial active region, the concentration increase in methane and decrease in hydrogen and carbon monoxide is seen to stall, possibly indicating reduced methanation reaction activity, followed by a final active region. Accordingly, it is suggested that the fluidized bed methanation reaction consists of three regions of differing dominating intermediate reactions. The first region is well understood to be dominated by CO dissociation onto the catalyst surface along with significant methanation. Dominating kinetics in the second region are unclear; a balance might be maintained between the volume reducing methanation reaction and the conversion of reagent gases thus resulting in a nearly steady concentration profile. The second stage should be further investigated for better understanding of carbon transport within the reactor. The final region of the reaction is assumed to be the result of mass transfer limitations between dilute, or bubble, and dense phases. Further investigation under non-mass-transfer-limiting conditions - such as lower U/U_{mf} , or increased temperature - would be of interest.

Figure 62: Gas Phase Composition Versus Bed Height



Gas phase composition throughout the catalyst fluidized bed. Conversion is initially very fast, followed by a stall before continuing at a relatively slower rate. Stalling may be caused by mass transfer limitations. This study used the UCSD catalyst.

Source: UC San Diego

Catalyst Comparison

A milled commercial methanation catalyst (METH134) was measured and compared to the UCSD catalyst prepared on a fluidized-bed support material (low-surface area; AD90). A stoichiometric mixture of H₂ and CO was fed into the reactor. For the UCSD catalyst, the last methanation test after several regenerations was chosen. Due to technical circumstances, for the METH134 catalyst, the pressure was set to a lower value, resulting in the experimental conditions listed in Table 14. The small difference in pressure is considered to have little effect on the reaction.

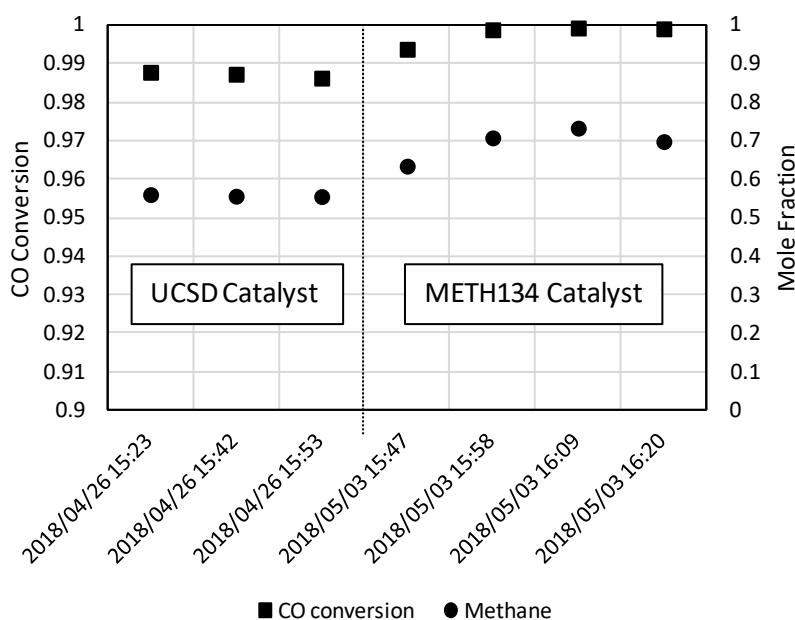
Table 14: Experimental Conditions for the Comparison of the Catalysts

Catalyst	H ₂ /CO [mol/mol]	U/U _{mf} [-]	Steam [mol %]	T _{set} [C]	p _{set} [bar]
UCSD	3.00	2	0	380	1.5
METH134	3.00	3	0	380	1.3

Source: UC San Diego

The outcome of these experiments is plotted in Figure 63 with the first section representing the catalyst from UCSD and the second being the commercial fixed bed type catalyst. The CO-conversion is higher for the commercial catalyst and almost reaches full conversion. The methane concentration in the reactor outlet is also increased but not as constant as the conversion. The observed conversion of CO is at 99.9 percent. To determine if further activation is possible, experiments with increased flow rates would have to be carried out.

Figure 63: Comparison of UCSD and a Commercial Fixed-Bed Type Catalyst



Source: UC San Diego

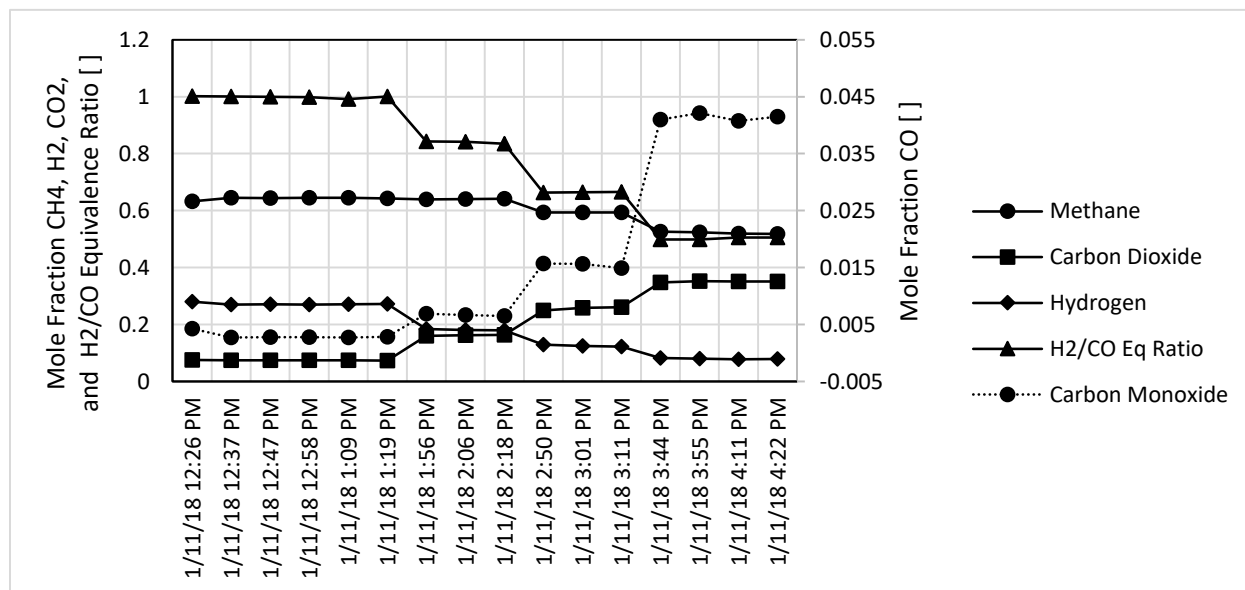
The catalyst provided by UC San Diego reaches a conversion of carbon monoxide of 98.7 percent. This value is taken from the last performance test after several regeneration steps. As described previously, the maximum activity of this catalyst could be even higher, since the regeneration is probably not completely finished. While these results show a much higher CO conversion for the Meth134 catalyst, they do not take in account the different surface areas of the catalysts. The UCSD catalyst was impregnated on a low-surface-area alumina support (<10 m²/g) to test the kinetic limitations and coke formation in a laboratory setting. The Meth134 is a production-ready commercial catalyst with high surface area (>100 m²/g). For future scale-up, the UCSD catalyst will be impregnated onto a high-surface-area alumina material, with the CO conversion rising accordingly.

Parameter Study

During the methanation experiments, a number of parameters and conditions were studied, as described above and shown in Table 12. The results of these tests are shown in detail in Appendix G. A summary of the effects of some of the parameters is provided.

H₂/CO Ratio: Fluidized-bed methanation is able to operate on sub-stoichiometric equivalence ratios, and the UCSD catalyst provided additional protection against coking. At lower equivalence ratios, the breakthrough of CO increases, however, and this becomes one of the limiting factors if pipeline-quality specifications need to be met. CO is an inhalation toxin, and natural-gas standards typically limit CO to below 1000ppm. At larger equivalence ratios, CO breakthrough is minimized, but H₂ breakthrough increases. H₂ breakthrough is not a crucial factor, since it can either be removed from the output gas, or future pipeline standards may allow a larger amount of hydrogen. Figure 64 shows the summary of different equivalence ratios. Because of the low surface area of the UCSD catalyst, the effects are well pronounced.

Figure 64: Effect of H₂/CO Equivalence Ratio



Effect of H₂/CO equivalence ratio on outlet composition. Sub-stoichiometric operation leads to increased CO breakthrough along with decreased CH₄ concentration and a significant increase in CO₂ production. This study was performed using the UCSD catalyst.

Source: UC San Diego

Steam addition: To further avoid coke formation at sub-stoichiometric operation, steam can be added to the inlet gas. Steam has the effect that it provides hydrogen as it influences the water-gas shift equilibrium, thereby reducing CO and increasing H₂ and CO₂. During tests with varying steam amounts, it was found that more steam slows down the CO conversion, and also increases CO₂ in the output gas at the expense of CH₄.

Fluidization: For a given catalyst and operating conditions, there is an optimum for U/U_{mf}. Lower and higher U/U_{mf} cause the CO conversion to drop, since there is either not enough mixing in the bed, or the residence time becomes too short. In a commercial operation, a slightly higher U/U_{mf} could be preferred, since it reduces the reactor size. Again, breakthrough of CO becomes the limiting factor.

Catalyst activation and regeneration: A well-activated catalyst is crucial for optimal conversion. Operating the catalyst with above-stoichiometric equivalence ratio was sufficient for activation. It was observed that sometimes repeating activation was necessary, and that the catalyst kept improving with each step up to an optimum.

Operation on Synthesis Gas From Gasifier

UCSD and METH134 catalysts were tested on synthesis gas, and all detailed results are shown in Appendix G. The METH134 catalyst, with its higher surface area, had a much higher heat release per unit of reactor volume. To be able to keep the temperature in an acceptable range within the set point, the temperature was lowered to slow down the kinetics of the reaction and nitrogen was added. The H₂/CO ratio of the synthesis gas was adjusted by adding hydrogen.

Among various parameters, the effects of steam addition are investigated. In Table 15, the experimental conditions are given. At first, steam was added to the already stoichiometrically-adjusted synthesis gas. Runs three and four featured hydrogen replacement with steam. For this, the hydrogen addition to the synthesis gas was decreased, and the amount of steam increased.

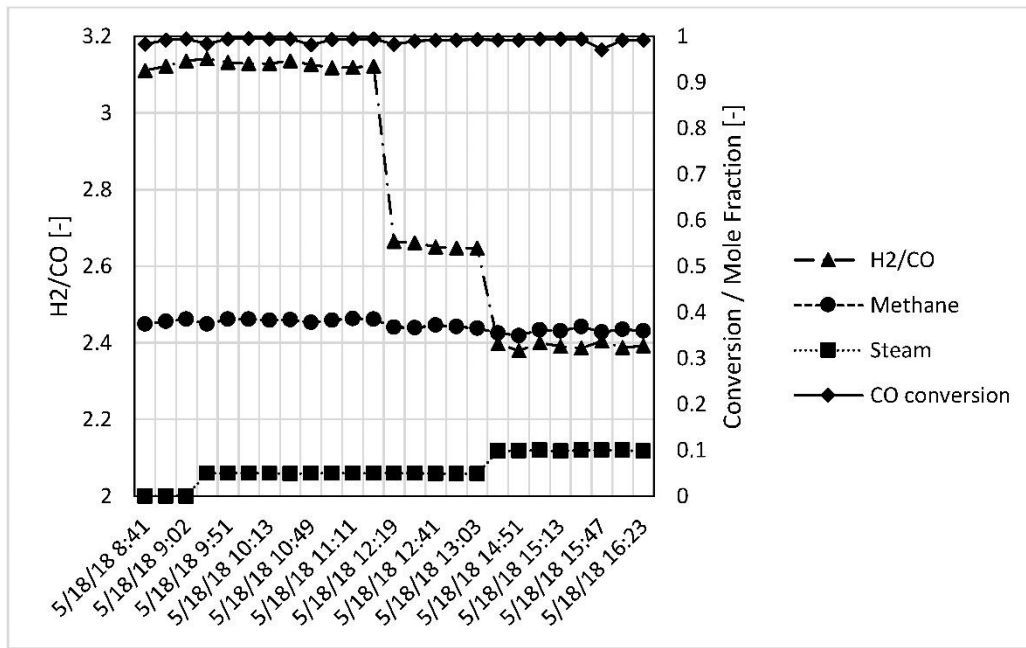
Table 15: Experimental Conditions for the Investigation of Steam Addition

H ₂ /CO [mol/mol]	N ₂ [mol%]	U/U _{mf} [-]	Steam [mol%]	T _{set} [C]	p _{set} [bar]
3.02	20	3	0	360	1.3
3.02	20	3	5	360	1.3
2.54	20	3	5	360	1.3
2.28	20	3	10	360	1.3

Source: UC San Diego

Figure 65 shows the resulting CO conversion and methane concentration in the product gas as well as the H₂/CO-ratio and steam amount at the reactor inlet. The plotted methane concentration is calculated for the nitrogen-free gas. The plot shows that adding steam without replacing hydrogen has little effect on the product gas, and even after lowering the H₂/CO-ratio, the change in CO-conversion is barely noticeable. The amount of CH₄, however, decreases slightly and is affected by less hydrogen at the reactor inlet.

Figure 65: Influence of Steam Addition on Methane Concentration



Methanation reaction characterized by CO conversion and product methane concentration influenced by addition of steam. This study was performed using the METH134 catalyst.

Source: UC San Diego

Because of the high surface area of the METH134 catalyst, the CO conversion stayed very high during most of the experiments. A number of different experiments were conducted and are shown in Appendix G. Occasionally, it happened that steam or hydrogen addition were interrupted for a short time. While CO conversion was not significantly affected thereafter, coke may have been formed on the catalyst surface. If coke formation persists, it can form a permanent deposit that cannot be easily regenerated during fluidized-bed methanation. Therefore, a good control of the quality of the inlet gas composition is required for commercial operation.

Catalyst Surface Analysis

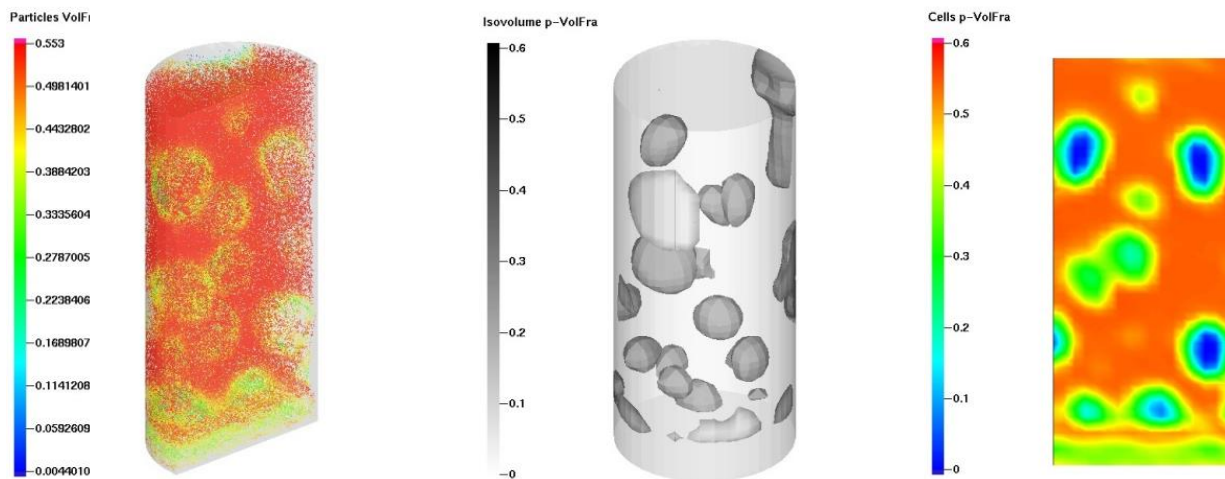
After completion of the experiments, the METH134 catalyst was sent to PSI for analysis of carbon and sulfur on the surface. The catalyst showed no measurable sulfur contamination, but it did show some carbon deposition. Carbon deposition can be explained by operating conditions with too little hydrogen, steam, amount of fluidization, or by too low temperatures. A detailed report on the catalyst analysis is shown in Appendix L.

Modeling of Fluidized-Bed Reactor

Figure 66 shows images obtained from modeling a fluidized-bed using the Barracuda VR software. Modeling has shown that for the expected bed material and flow conditions, there is a significant bubble formation once the gas leaves the distributor plate at the inlet. Large bubbles reduce the mass transfer from the gas to and from the catalyst surface and therefore reduce the methanation activity in an actual reactor. This needs to be considered when scaling up the reactor to larger heights.

A fluidized-bed reactor was simulated with a modeling software (Barracuda VR) to investigate fluidization, bubble behavior, and heat transfer. Figure 66 shows the results of cold-flow modeling without chemistry. Figure 67 shows the results including reaction chemistry and heat transfer. Such models are useful for scaling up the methanation reactor and for implementing the appropriate cooling coils.

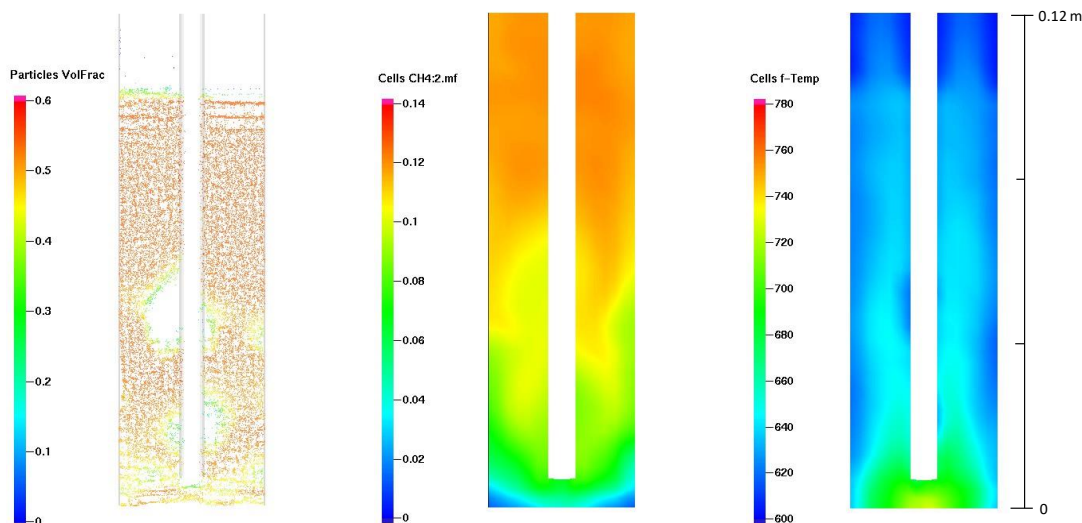
Figure 66: Modeling of Fluidized Bed



Modeling results of a cold-flow model of a fluidized-bed reactor. The bubble-formation is investigated as a function of the boundary conditions.

Source: UC San Diego

Figure 67: Modeling of Fluidized Bed With Reaction and Heat Transfer



Simulation of methanation in fluidized-bed with one-step chemistry and heat loss. An inner tube was added to study the effect on heat transfer. The reaction rate was chosen such that methane is produced within a few cm of bed height. The wall temperature is kept at 600 K. The first image shows the particle volume fraction, the second image shows the methane mole fraction, and the third image shows the gas temperature in K.

Source: UC San Diego

Concluding Remarks

During the project, methanation of synthesis gas to raw RNG was successfully demonstrated for several hundred hours. For a given catalyst and reactor geometry, there are optimal operating parameters, and the most important ones are shown in Table 16. The table indicates the effects if the parameters deviate from the optimums. Besides these parameters, there are several other quantitative and qualitative criteria. Limiting the amount of sulfur in the inlet gas is one of the most important ones. It is estimated that a concentration of near 50ppb would allow the catalyst to perform well for 1-2 years, with catalyst addition or replacement required thereafter. To quantify this more precisely, longer term testing in the order of a few thousand hours would be required. Long operating times will also give more insight into other operating factors, such as fluctuations in flow rate, gas composition (including), and attrition of the catalyst in the fluidized bed. Activating and regenerating the catalyst needs to be considered as well, especially after adverse operating conditions or shutdowns. All these issues should be investigated in long-duration tests at the pilot scale in order to provide all the necessary data for commercial-scale operation.

Table 16: Summary of Experimental Parameters

Parameter	Units	Effect if too low (below optimum)	Effect if too high (above optimum)
H ₂ /CO equivalence ratio	[mol/mol]	Coke formation and catalyst deactivation; increased CO breakthrough.	H ₂ breakthrough; Increased costs due to H ₂ supply or water-gas shift reactor.
Steam addition	[mol%]	Coke formation and catalyst deactivation.	Increased CO breakthrough and reduced CH ₄ content.
Fluidization number, U/U _{mf}	[-]	Increased CO breakthrough due to reduced mixing; increased capital costs due to larger reactor.	Increased CO breakthrough due to reduced residence time.
Temperature	[C]	Increased CO breakthrough due to kinetic limitation; increased coke formation and catalyst deactivation.	Increased CO breakthrough due to equilibrium limitation.

Source: UC San Diego

CHAPTER 5:

Project Benefits and Production Readiness Plan

As part of the study, Black and Veatch analyzed the projected benefits of a first commercial plant and provided a production readiness plan. The report is provided in Appendix B, and details the results as well as the quantitative methods used for calculating the benefits. In the following sections, the qualitative and quantitative project benefits of gasifiers coupled with fluidized-bed methanation are summarized.

Qualitative Project Benefits

The following qualitative project benefits are anticipated if commercial RNG plants based on gasification and fluidized-bed methanation would be constructed in California.

Job Creation

Numerous green jobs would be created along the process chain from harvesting and transporting the feedstock to producing and selling Renewable Natural Gas. This in turn would create further jobs in new methods of forest management and waste collection, and in areas of further technology development, education, and technology export to other states.

Reduction of Operations and Maintenance (O&M) Costs

Plants based on fluidized-bed methanation lead to a smaller economical size ($<100 \text{ MW}_{\text{RNG}}$), because this technology reduces the number of process steps. Compared to fixed-bed methanation, the eliminated process steps are associated with the olefin reformer, water-gas-shift reactor, pre-methanation, and two of the three methanation reactors. A smaller plant size allows for more potential locations in California due to feedstock availability, and the larger number of total capacity leads to economies of scale in supplies, services, and maintenance for the fleet of RNG plants. Smaller plant sizes, in turn, lead to less expensive feedstock transport costs. Concrete benefits achieved during the project were the reduced steam consumption (more coke-resistant catalyst) and the longer catalyst lifetime (lower sulfur levels in clean gas).

Reduction of Capital Costs

The requirement of fewer process steps leads to lower capital costs which includes associated costs such as engineering, physical space requirements, piping, electrical, control, and safety installations. The larger possible number of plants leads to additional cost savings for purchasing larger numbers of identical unit operations, such as vessels, heat exchangers, steam generators, electricity generators, compressors, and pumps.

Non-Energy Economic Benefits

Building out the infrastructure for RNG production leads to network effects with other green industries and associated indirect jobs. The improved forest management leads to fewer wild fires, which in turn leads to economic savings in fewer lost homes due to fire and mudslides, and fewer lost working hours of individuals impacted by such events or by the associated psychological and health effects.

Energy Security

An increased domestic production of RNG reduces fuel imports and diversifies the energy resources of the state relative to other green technologies such as solar and wind. Producing RNG on a wide scale provides base-load energy in times of reduced sun or wind, and the storage capacity of the natural-gas grid and infrastructure provides for the availability of peak energy if needed.

Greenhouse Gas (GHG) Emissions Reductions

Converting renewable resources such as forest thinnings and agricultural wastes to RNG leads to the associated reductions in greenhouse-gas emissions. Offering a cleaner fuel compared to diesel or gasoline will incentivize the adoption of RNG in trucks and cars, leading to further greenhouse-gas-emission reductions. Carbon black emissions due to wild fires and field-side burning increase the global warming potential and this can be avoided by converting these biomass resources to RNG which is then used in clean-burning engines and heating applications.

Criteria Air Pollution Emission Reductions

Criteria emissions include nitrogen oxides (NO_x), particulate matter (PM), non-methane organic compounds (NMOC), and CO. Nitrogen oxides are typically generated at high combustion temperatures. Using controlled combustion by fuel staging, exhaust-gas recirculation, very lean combustion (low fuel-to-air ratio), or installed after-treatment devices significantly reduce NO_x emissions. Particulate matter (PM), non-methane organic compounds (NMOC), and CO are typically formed during incomplete combustion, where low air-fuel ratios, non-premixed flames, or low combustion temperatures occur. Since natural gas can be burned in a very controlled manner, all of the above emissions will be much lower compared to the combustion of liquid fuels such as diesel and fuel oil. RNG production provides an avenue to switch away from higher-polluting combustion equipment, as long as such equipment is still widely used in transportation, power-production, industry, and building heating. Utilizing biomass that would otherwise be burned in an uncontrolled manner (wild fires, open-pile burning) will significantly reduce unnecessary criteria emissions. The emissions at RNG plants are generally limited to auxiliary equipment or regenerators, which can be controlled.

Habitat Area Disturbance Reductions

Sustainable forest management is generally considered to have positive impacts on reducing habitat disturbance compared to the alternatives of harvesting for timber or prescribed and unwanted burning. Active management is an important tool to protect California's forests, and it can work hand-in-hand with the utilization of biomass for the production of RNG.

Quantitative Benefits for a Single 60MW_{RNG} Plant

Black and Veatch has analyzed a potential RNG production facility in California, located in Sacramento near SMUD's Cosumnes combined-cycle power plant. As owner of both plants, SMUD is able to derive benefits related to energy security and reduction of criteria pollutant emissions. Other benefits to the project and to the state were quantified as well for this 60-MW_{RNG} plant. The plant would provide a GHG reduction of 86,658 metric tons of CO₂ per year, worth \$4.7M/yr. It would further provide an estimated wildfire prevention of \$650,000/yr, energy security of \$1.5M/yr, and 2,400 direct and indirect jobs. Avoided criteria pollutant

emissions were calculated by utilizing forest biomass for the production of RNG and then using that RNG in a clean-burning combined-cycle power plant compared to the case that the woody biomass would be burned in an uncontrolled manner (open-pile burning and sustainable forest biomass that would otherwise burn in wildfires). The avoided emissions per year are 8.2 tons of NO_x, 36.4 tons of PM, 28.7 tons of NMOC, and 351 tons of CO. They result in emission reduction credits of \$134.30/MWh_{el} and a value of \$31.7M for SMUD as the operator. Table 17 shows a summary of these quantitative benefits.

Table 17: Quantitative Benefits for a 60MW_{RNG} Plant

Benefit	Units	Quantity
Direct Jobs	#	1,400
Indirect Jobs	#	1,000
Induced Economic Activity	\$	\$154M
Wildfire Reduction	Project \$	\$0.65M
Energy Security	SMUD \$	\$1.5M
GHG Emissions Reduction	Project \$	\$4.7M
Criteria Air Pollutant Emissions Reduction	SMUD \$	\$31.7M

Quantitative benefits calculated by Black and Veatch for a RNG production plant and co-located combine-cycle power plant owned by SMUD. Details are provided in Appendix B.

Source: UC San Diego

Potential Project Benefits to California

Using the technical availability of forest and urban biomass in California (26 million dry tons/yr), 150 plants would provide 60 MW_{RNG} each, for a total capacity of 9,000 MW_{RNG} or a production of 260 PJ_{RNG}/yr (245 million MMBtu/yr). These plants would avoid greenhouse gas emissions of 13 million metric tons CO₂ per year for a value of \$705M/yr. They would benefit California in the amount of \$98M/yr for wildfire reduction (associated cost from damages caused by wildfires) and \$225M/yr for energy security (from avoided energy imports). All plants would provide 360,000 direct and indirect jobs, and induced economic activity of \$23B/yr.

Production Readiness Plan

Two reports from Black & Veatch were made available for this project to evaluate a production readiness plan and expected levelized costs for RNG. The first report was commissioned by SMUD with the goal of evaluating different gasifier technologies and studying the conversion of syngas to RNG at a site in SMUD territory. SMUD contributed the report to this project as part of its match funds. The report is attached as Appendix A. The second report looked specifically at the FICFB gasifier technology coupled with fluidized-bed methanation. This report was created by Black & Veatch for this project as part of Task 7 (Project Benefits) and Task 9 (Production Readiness Plan). It is provided as Appendix B.

Levelized Costs of RNG

Part of both reports was the assessment of the levelized cost of RNG. It includes capital costs, operating costs, and feedstock costs and is expressed in \$/MMBtu. The reports address the capital costs for fixed-bed methanation and fluidized-bed methanation and find a 15 percent lower costs for fluidized-bed, leading to a 11 percent lower levelized cost of RNG. All cost

estimates are for a pioneer plant which is the first of its kind, and costs for an n^{th} plant would be significantly lower. Aranda et al. (2014) have estimated that the capital-cost reduction for an n^{th} plant would be approximately 30%. This would mean that the capital cost of the pioneer plant (\$260M) would be reduced to \$182M for the n^{th} plant, which is supported by the fact that engineering and EPC contractor contingency alone accounted for \$53M, and these two items would be significantly reduced by construction of an additional identical plant. Another recent cost estimate based on fixed-bed methanation can be found in Larsson et al. (2018).

The detailed cash-flow analysis was made available by Black and Veatch, and it was compared with the cash-flow analysis tool (Biogas Upgrade Cost Calculator) provided by the solicitation documents (California Energy Commission, 2015). Both gave essentially the same results. Since the Biogas Upgrade Cost Calculator treats all cash flows in real terms (inflation adjusted), the levelized cost of gas (LCOG) is also in real-terms. The Black and Veatch calculation and report used the LCOG in nominal terms (actual or "current" dollars), and it had to be converted to real terms (inflation-adjusted or "constant" dollars) by using the real discount rate in the energy portion of the formula for LCOG (Short, 1995). In the following, the real LCOG is reported, consistent with the Biogas Upgrade Cost Calculator. (The nominal LCOG is several dollars higher than the real LCOG.)

The Biogas Upgrade Cost Calculator was adjusted for the entire process chain, including biomass gasification, gas-cleanup, methanation, and upgrading. Biodiesel for scrubbing and electricity imports are calculated separately and added on top of the variable operating costs reported by Black and Veatch. The calculator was then used to calculate the baseline LCOG for the n^{th} plant (with capital costs of \$182M), and it was further used to calculate the individual cost contributions by varying the inputs around the baseline value. Figure 68 shows a screenshot of the cash flows for the first nine years. Figure 69 shows the projected commercial LCOG for the n^{th} plant scenario. It is \$26.42/MMBtu, before any credits or subsidies. Capital costs are the largest contributing factor (\$12.07/MMBtu). Because the equity returns to investors are the profits of the plant, they are taxed at the corporate tax rate (40.75%), and those taxes (\$1.50/MMBtu) are included in the capital costs. Fixed and variable operating costs are \$10.29/MMBtu. They comprise labor, scrubbing liquids, electricity, and catalysts. Feedstock costs (at \$40/dry ton, including transport) account for \$4.06/MMBtu.

All other details and assumptions are provided in the Black and Veatch report (Appendix B).

Figure 68: Calculation of Levelized Costs

Levelized Cost of RNG

This sheet will provide a levelized cost
 Default inputs are in green. If you wish to modify them, you may do so but provide justification.
 User-required inputs are in blue. Enter these on the previous sheet.

Technology Assumptions	
CAP (MCM/day)	0.166886278
CC (\$/MCM per day)	\$1,088,046,315
FOM (\$/MCM-yr)	\$55,486,887
FOM Escalation	0.0%
VOM (\$/MCM)	\$146,066.45
VOM Escalation	0.0%
Feedstock Cost (\$/MCM)	\$128,135.16
Feedstock Cost Escalation	0.0%
CONV	100%
LHV (Btu/m ³)	31,558
CF	85%
CONV-BY	0%
P-BY (\$/MCM)	\$103,258
DEG	0.0%

Financial Assumptions	
Debt Percentage	60%
Debt Rate	4.0%
Debt Term (years)	15
Economic Life (years)	20
Percent 5-year MACRS	0%
Percent 7-year MACRS	0%
Percent 15-year MACRS	100%
Percent 20-year MACRS	0%
Energy Price Escalation	0%
Tax Rate	40.75%
Cost of Equity	10%
Discount Rate	6.9%

Outputs	
NPV Equity Return	\$0
Levelized Cost of RNG	\$/MMBtu \$26.42

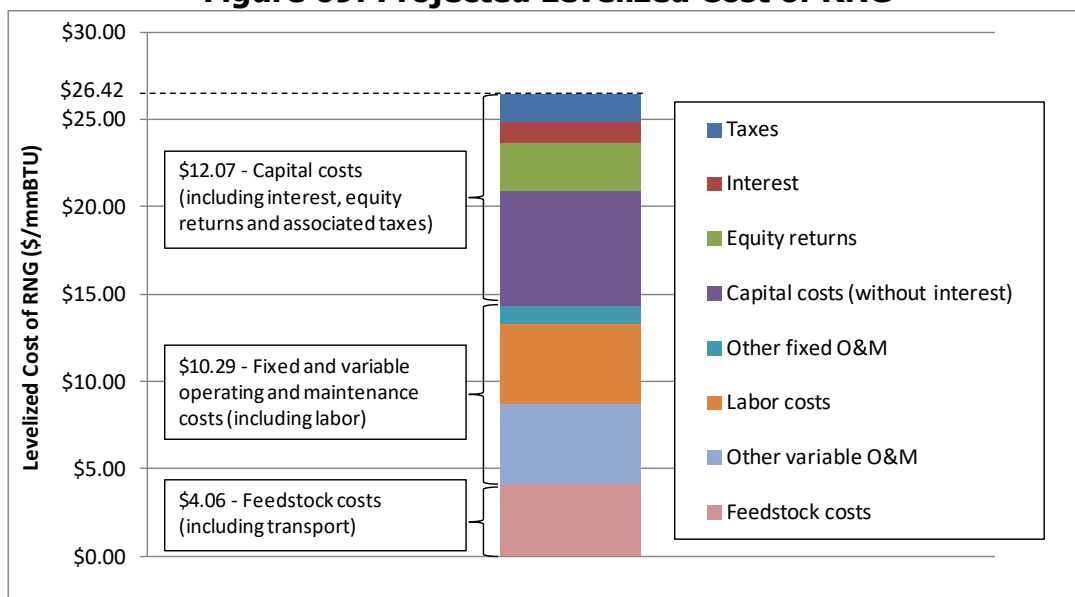
¹ Without incentives for nth plant (30% lower capital cost)

Year	1	2	3	4	5	6	7	8	9
Annual Production (MMBtu)	1,635,060	1,635,060	1,635,060	1,635,060	1,635,060	1,635,060	1,635,060	1,635,060	1,635,060
Gas Price (\$/MMBtu)	\$26.42	\$26.42	\$26.42	\$26.42	\$26.42	\$26.42	\$26.42	\$26.42	\$26.42
Misc Revenue	\$0	\$0	\$0	\$0	\$0	\$0	\$0	\$0	\$0
Total Operating Revenues	\$43,198,792								
Fixed O&M	\$9,260,000	\$9,260,000	\$9,260,000	\$9,260,000	\$9,260,000	\$9,260,000	\$9,260,000	\$9,260,000	\$9,260,000
Variable O&M	\$7,567,985	\$7,567,985	\$7,567,985	\$7,567,985	\$7,567,985	\$7,567,985	\$7,567,985	\$7,567,985	\$7,567,985
Fuel Cost	\$6,638,930	\$6,638,930	\$6,638,930	\$6,638,930	\$6,638,930	\$6,638,930	\$6,638,930	\$6,638,930	\$6,638,930
Operating Expenses	\$23,466,915								
Interest Payment	\$4,357,920	\$4,140,281	\$3,913,936	\$3,678,537	\$3,433,722	\$3,179,115	\$2,914,324	\$2,638,941	\$2,352,542
Principal Payment	\$5,440,983	\$5,658,622	\$5,884,967	\$6,120,366	\$6,365,181	\$6,619,788	\$6,884,579	\$7,159,962	\$7,446,361
Debt Service	\$9,798,903								
Tax Depreciation - 5	\$0	\$0	\$0	\$0	\$0	\$0	\$0	\$0	\$0
Tax Depreciation - 7	\$0	\$0	\$0	\$0	\$0	\$0	\$0	\$0	\$0
Tax Depreciation - 15	\$9,079,000	\$17,250,100	\$15,525,090	\$13,981,660	\$12,583,494	\$11,312,434	\$10,713,220	\$10,713,220	\$10,731,378
Tax Depreciation - 20	\$0	\$0	\$0	\$0	\$0	\$0	\$0	\$0	\$0
Taxable Income	\$6,294,957	(\$1,658,503)	\$292,852	\$2,071,680	\$3,714,661	\$5,240,328	\$6,104,334	\$6,379,717	\$6,647,957
PTC	\$0	\$0	\$0	\$0	\$0	\$0	\$0	\$0	\$0
Taxes	\$2,565,195	(\$675,840)	\$119,337	\$844,210	\$1,513,724	\$2,135,434	\$2,487,516	\$2,599,735	\$2,709,043
Total	(72,632,000)	7,367,779	10,608,815	9,813,637	9,088,765	8,419,250	7,797,541	7,445,458	7,333,240

Calculation of Levelized Cost of RNG. The Biogas Upgrade Calculator (provided by California Energy Commission) was adapted to include all process steps of converting biomass to RNG. The cash flows are shown for the first nine years.

Source: UC San Diego

Figure 69: Projected Levelized Cost of RNG



Levelized cost of RNG for a projected nth commercial plant and the different factors contributing to the costs.

Source: UC San Diego

Sensitivity Analysis of Costs

A sensitivity analysis was performed, during which the major cost parameters were varied and their influence on the levelized costs of RNG recorded. Figure 1 shows the results of the analysis. The base case is the same as that used in Figure 81 and in Figure 82, with a base price of \$26.42 and the corresponding assumptions such as capital and operating costs, cost of financing, and durations of plant operation and loan. The following parameters were varied: capital costs (with associated financing costs and taxes), operating costs (fixed and variable operating costs), cost of capital (weighted-average cost of capital), feedstock costs (including transport), tax rate (corporate tax on equity returns), economic life, and capacity factor.

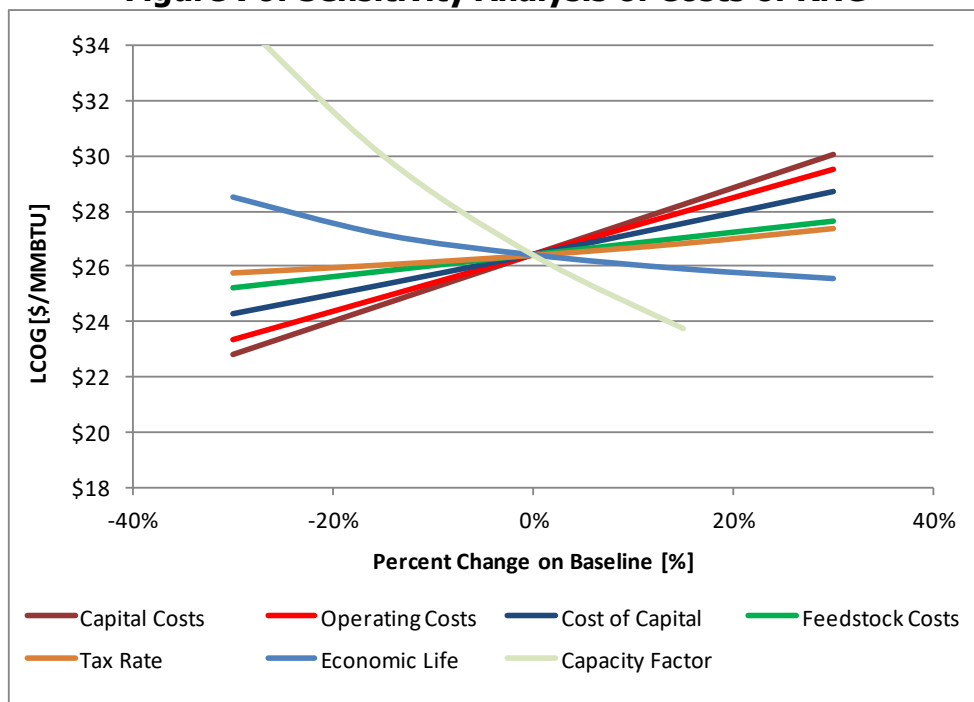
The capacity factor has the largest influence on the levelized costs of RNG. Since the base case has already a capacity factor of 85 percent, further gains are limited, since even limited plant maintenance requires the occasional shutdown of the plant. It shows, however, how important it is to avoid any unnecessary shutdown or idling of the plant, since costs per unit of RNG would increase dramatically. This is due to the fixed capital and operating costs that have to be paid, even if the plant is not producing. An increase/decrease in the process efficiency would have a similar effect.

Capital costs have the second-largest effect. This is not surprising, since the capital costs make up the largest contribution in the levelized costs of RNG (Figure 82). This is partly because any reduction of capital costs will also reduce the interest and taxes on that capital. The sensitivity of the capital costs is slightly less than the one for the pioneer plant in Appendix B, since that pioneer plant had higher capital costs. As the capital costs are reduced by switching from fixed-bed to fluidized-bed methanation, and from a pioneer plant to an nth plant, any incremental reductions of capital costs has less of an effect on the levelized costs of RNG, compared to the other contributing factors.

Operating costs have the third-largest effect. The operating costs include fixed and variable operating costs, and by reducing them, the levelized costs of RNG will be reduced. Fixed operating costs include labor which can be reduced by increased automation, or by employing contract labor during times of plant maintenance only. Variable operating costs can be reduced by optimizing the consumption of catalysts, scrubbing, and adsorption media. For example, improved sulfur cleanup, requiring larger amounts of sulfur adsorbents, will lead to a lower consumption rate of the methanation catalyst.

Cost of capital (interest rate of debt and equity financing; weighed average cost of capital), feedstock costs, tax rate, and economic life of the plant have smaller sensitivities to the levelized cost of RNG. While in the sensitivity study no factor reduced the levelized costs of RNG by more than \$4/MMBTU, it should be pointed out that cost reductions in each of those factors, when combined, can lead to a substantial overall cost reduction per unit RNG.

Figure 70: Sensitivity Analysis of Costs of RNG



Sensitivity of levelized costs of RNG to various parameters. The parameters that were individually varied are capital costs, operating costs, cost of capital, feedstock costs, tax rate, economic life, and capacity factor.

Source: UC San Diego

Comparison to Conventional Systems

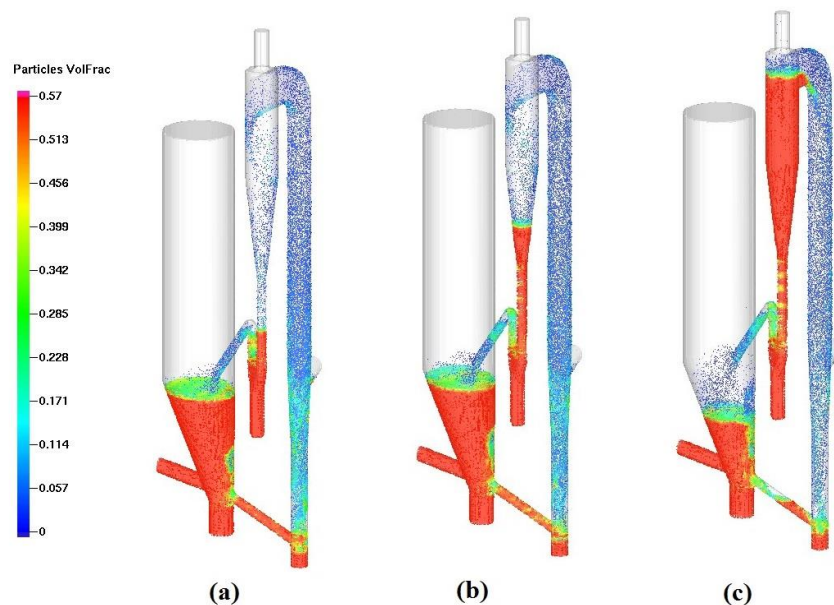
The Black & Veatch study (Appendix B) analyzed fixed-bed and fluidized-bed methanation. Fixed-bed methanation is a commercial technology for large-scale applications such as coal-gasification plants, and has been demonstrated by Haldor Topsoe and Clariant. At smaller scales, the specific costs increase, which makes the technology difficult to succeed economically. For a small-scale plant (20MW_{RNG}) using fixed-bed methanation, such as the GoBiGas demonstration plant, the LCOG may be as high as \$42/MMBtu (Thunman, 2019). For a 60MW_{RNG} pioneer plant employing fixed-bed methanation, Black & Veatch estimated capital costs of \$307.5M. For the same pioneer plant, but using fluidized-bed methanation, capital

costs would be reduced by 15.6%, to \$259.4M. For the n^{th} plant scenario, assuming that capital costs of both technologies would decrease by 30 percent (Aranda et al., 2014), the costs are \$215M (using fixed-bed methanation) and \$182M (using fluidized-bed methanation). With these capital costs, the LCOG in constant dollars translates to \$28.66/MMBtu (fixed-bed) and to \$26.42/MMBtu (fluidized-bed). This difference is solely due to reduced capital costs and does not include any reductions in operating costs. With fewer unit operations, it is likely that fluidized-bed methanation will achieve further operating-cost reductions, which would decrease the LCOG further. A detailed investigation into the savings in operating costs when employing fluidized-bed methanation is recommended for future projects.

Scale-up of Gasification System

Modeling was performed on the pilot-plant FICFB gasifier and a scaled-up version (12x). The results inform on geometric changes that must be considered when scaling up the fluidized-bed reactor. Modeling of the pilot plant was extensively performed and is shown in Appendix I. Figure 71 shows an example of the modeling with different amounts of fluidization in the upper loop-seal. If fluidization is not enough (cases b and c), the bed material fills up in the cyclone. The fluidization numbers between simulation and pilot plant operations showed good agreement.

Figure 71: Modeling of Pilot FICFB Gasifier

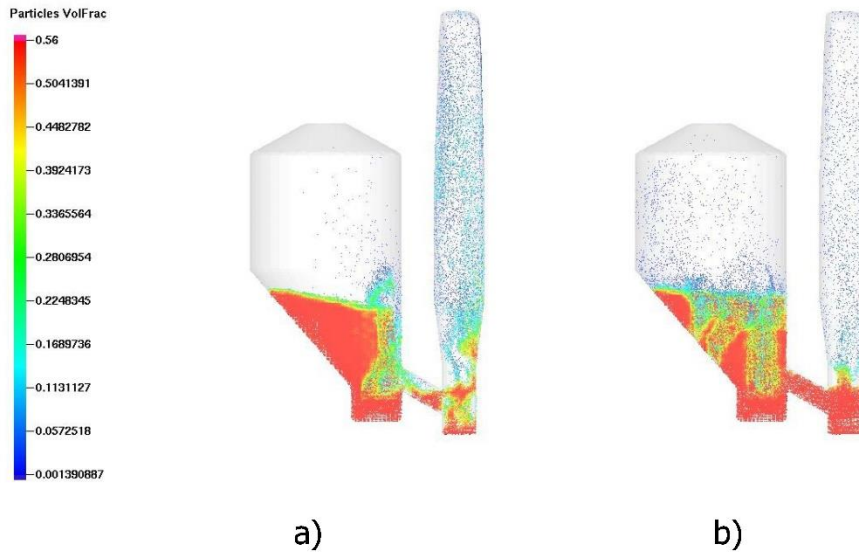


Simulation of pilot-plant FICFB gasifier with different amounts of fluidization in the upper loop seal . a) Large amount of fluidization in upper loop seal, leading to small differences in bed levels. b) Lowest allowable fluidization of upper loop seal. Cyclone dip-leg fills up with bed material. c) Too low fluidization of upper loop seal. Cyclone fills up with bed material.

Source: UC San Diego

Figure 72 shows cold-flow modeling of a 12-times larger FICFB gasifier. It indicates that additional steam nozzles in the gasifier improve the mixing in the bed. Figure 73 shows a study of different amounts of secondary air injection in the combustor section. Larger amounts of air was necessary to properly fluidize this section.

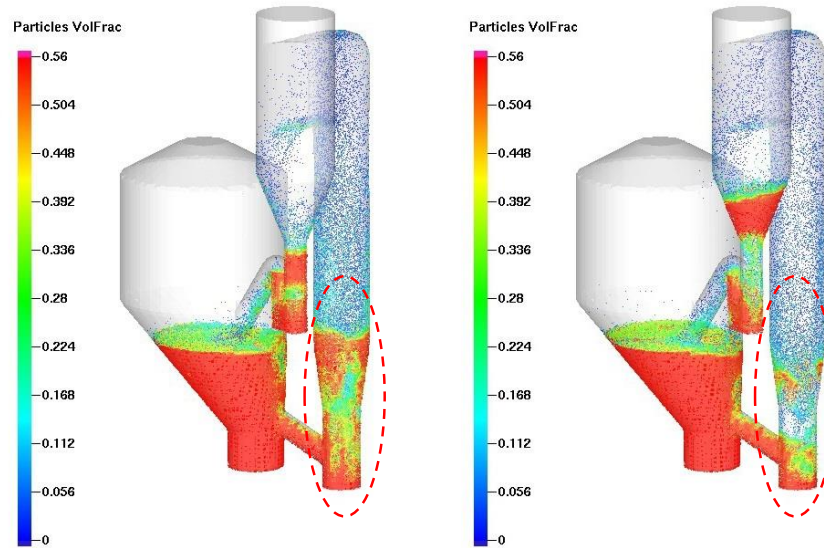
Figure 72: Modeling of Scaled-Up FICFB Gasifier



Simulation of scaled-up FICFB gasifier (cold-flow model, equivalent to 12 MWth). a) Single nozzle bank at bottom of gasifier leads to fluidization along the vertical wall of the cone and steam leakage to the combustor (right vessel). b) Five additional steam nozzles are added to the slanted side of the gasifier cone. Better fluidization is achieved throughout the bed, and steam leakage to the combustor is reduced.

Source: UC San Diego

Figure 73: Modeling of Air Injection in Scaled-Up FICFB Gasifier



Simulation of scaled-up FICFB gasifier (cold-flow model). The size of the gasifier is 12 MWth compared to 1 MWth for the pilot plant. The model shows the potential for accumulation of bed material in the combustor section (left). When the air supply is doubled, the combustor is well fluidized (right).

Source: UC San Diego

CHAPTER 6:

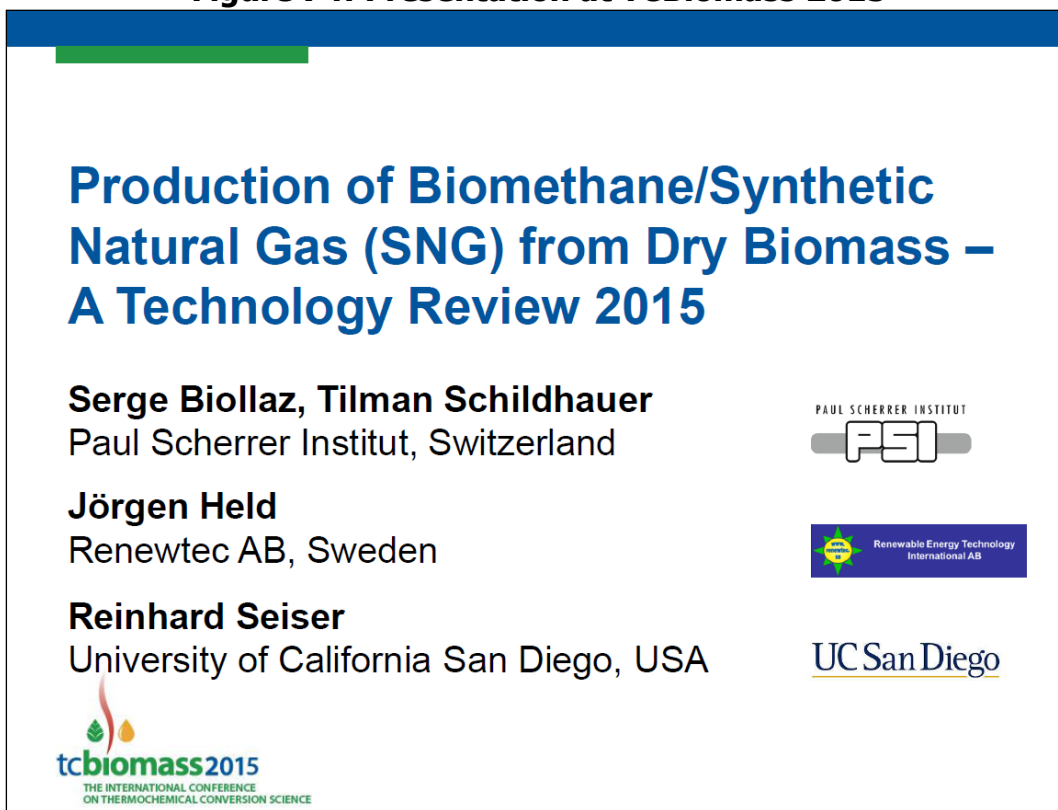
Knowledge Transfer

During the project, many collaborations were formed with other universities, national laboratories, and corporations. The areas of collaboration included gasification, gas cleanup, methanation, and cost projections for future commercial plants. Knowledge was disseminated at conferences, meetings, webinars, workshops, and journal publications. The following shows a summary of the activities.

Conferences

Figure 74 and Figure 75 show the title page of presentations given at two major biomass conferences. TC Biomass is the bi-annual conference held in Chicago, organized by the Gas Technology Institute (GTI). TCS Symposium is held in the years between the TC Biomass meetings. In 2016, the TCS Symposium was held in Raleigh, NC. Figure 76 shows a poster presentation from the TC Biomass 2015.

Figure 74: Presentation at TC Biomass 2015



Screenshot of presentation at TC Biomass 2015 in Chicago, IL. The presentation summarized various RNG technologies around the world.

Source: UC San Diego

Figure 75: Presentation at TCS Symposium 2016

**Detailed Measurement of Sulfur Compounds in
Producer Gas from Fluidized-bed Gasifier**

Zach McCaffrey, Reinhard Seiser, Robert Cattolica
University of California San Diego, USA

Serge Biollaz
Paul Scherrer Institut, Switzerland

Michael Long, Bryan Jenkins
University of California Davis, USA





 University of California, San Diego TCS Symposium, Chapel Hill, November 1-4, 2016

Screenshot of presentation at TCS Symposium 2016 in Raleigh, NC. The presentation summarized the sulfur measurements from the FICFB gasifier and after various gas-cleanup stages.

Source: UC San Diego

Figure 76: Poster Presentation at TC Biomass 2015

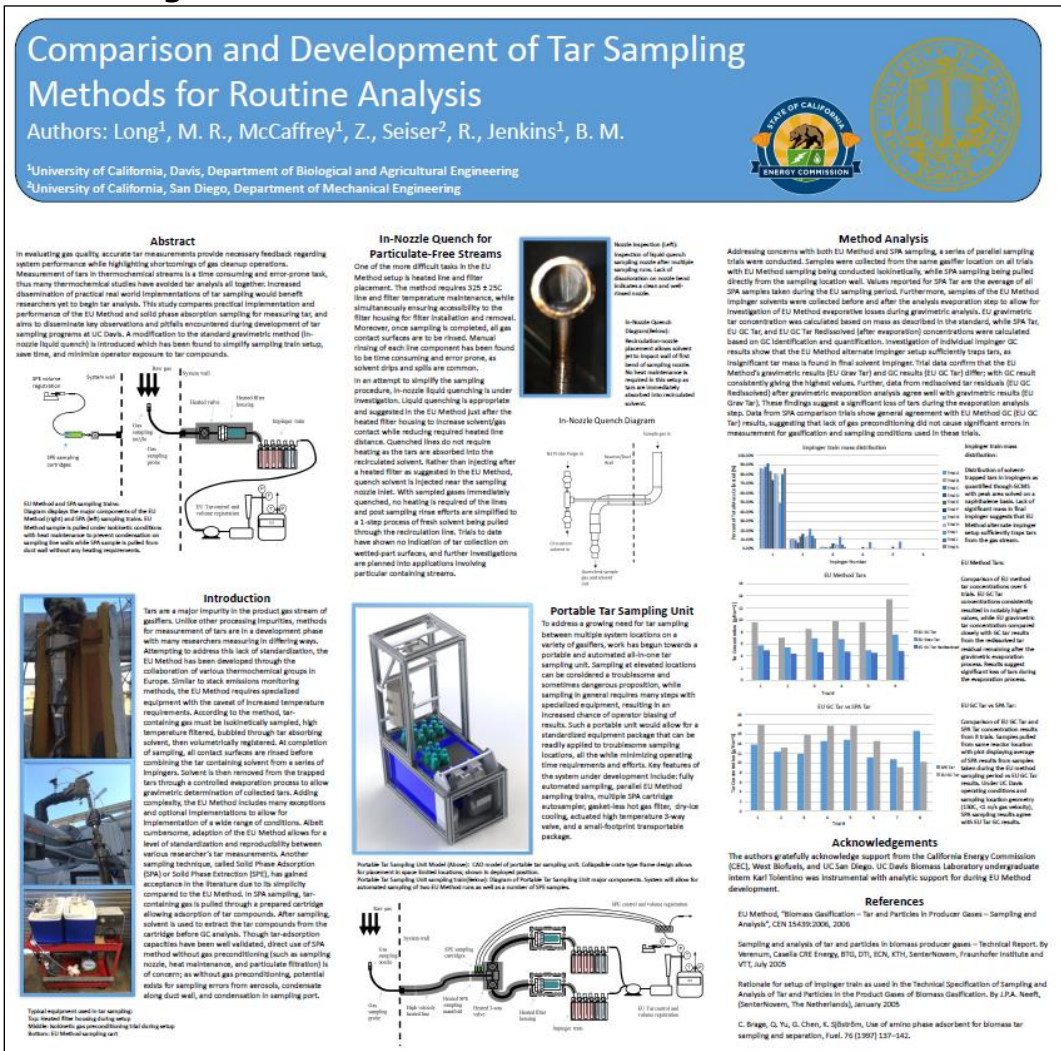


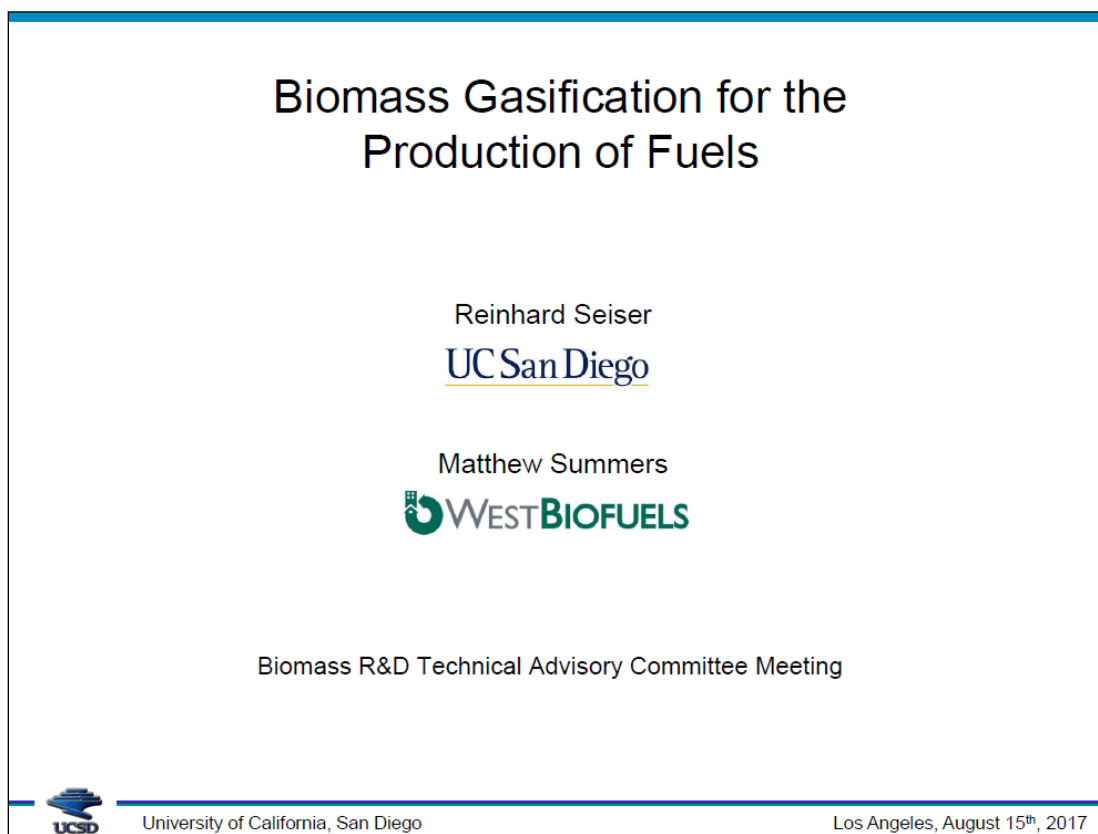
Image of poster presentation at TC Biomass 2015 in Chicago, IL. The poster summarizes various tar measurement techniques that are applied on the gasification plant.

Source: UC San Diego

Meetings

Figure 77 shows the title page of an oral presentation given at the Biomass R&D Technical Advisory Committee Meeting 2017 in Los Angeles, California. The Technical Advisory Committee Meeting is organized by the Department of Energy (DOE).

Figure 77: Presentation at a DOE Biomass Committee Meeting



Screenshot of presentation at the Biomass R&D Technical Advisory Committee Meeting in Los Angeles, California. The presentation summarized various biomass conversion technologies, including biomass-to-RNG.

Source: UC San Diego

Webinars

Webinars summarize the sampling and analysis methods created during the project period. The webinars were either presented online to a group of people or in person where other participants joined online. A summary of the webinars is available in Appendix H. The following webinars were presented:

- Webinar on GC-SCD Measurements
- Webinar on FTIR Measurements of Producer Gas
- Webinar on Sulfur Measurement and Gas Cleaning
- Webinar Adsorbent Testing and Sulfur Measurement
- Webinar on GC-SCD Measurements of Real Gases
- Webinar on Measurement of Sulfur Compounds in Gases and Liquids
- Webinar on Adsorbent Testing

Publications

Three dimensional modeling methods and results produced by this study were published in Chemical Engineering Science:

Hui Liu, Robert J. Cattolica, Reinhard Seiser, Operating parameter effects on the solids circulation rate in the CFD simulation of a dual fluidized-bed gasification system, *Chemical Engineering Science*, Volume 169, 2017, Pages 235-245, ISSN 0009-2509, <https://doi.org/10.1016/j.ces.2016.11.040>.

Collaboration with Paul-Scherrer Institute

A collaboration with the Paul-Scherrer Institute (PSI) in Switzerland allowed the exchange of information on methanation and gas cleanup. PSI pioneered the fluidized-bed methanation technology and has built methanation reactors of four different sizes (laboratory scale, 10kW_{RNG}, 160kW_{RNG}, and 1MW_{RNG}). The laboratory methanation reactor at PSI is shown in Figure 78. During the project, researchers from UC San Diego and UC Davis were able to spend time at PSI and learn about the technology.

Figure 78: PSI microBFB Reactor



PSI microBFB reactor with axial auto sampling system at PSI in Switzerland. The reactor has a flow rate of 1-6 slpm and is air cooled.

Source: UC San Diego

Collaboration with TU Munich

A collaboration with TU Munich allowed the exchange of information on gasification and methanation. TU Munich has several research reactors and also works on the development and characterization of fixed-bed methanation catalysts. Through travel grants from BaCaTeC (Bavaria California Technology Center), researchers and students from both institutes were able to visit the other research facilities. With a separate travel grant from BaCaTeC, the Wolfgang-Hillen Summer School was organized for students at UC Davis and TU Munich with the topic of Energetic Utilization of Biomass. Part 1 of the summer school was held at UC Davis from June 25-30, 2017. The summer school included a gas analysis workshop at the Woodland Biomass Research Center. Figure 79 shows a photograph of the students at the workshop.

TU Munich encourages their engineering students to do their project work abroad. As a result of the collaboration with TU Munich, a student (Elija Talebi) was able to spend several months at the Woodland Biomass Research Center. During this time, he designed the adsorbent vessels for the methanation project, took gas samples, and operated the methanation reactor.

Figure 79: Workshop During BaCaTeC Summer School



Gas Analysis Workshop at Woodland Biomass Research Center. Students are trained in taking gas and tar samples.

Source: UC San Diego

CHAPTER 7:

Conclusions

During the project, woody biomass was successfully converted into raw RNG (before removal of water, carbon dioxide, and excess hydrogen). The results show that fluidized-bed gasification (FICFB gasifier) and fluidized-bed methanation are technically viable methods to convert biomass into RNG with a high efficiency. The FICFB gasifier has several advantages as it pertains to the production of RNG. Because of separate vessels for gasification and char combustion, no oxygen plant is required which allows for smaller economical plant sizes ($<100 \text{ MW}_{\text{RNG}}$). This reduces the distance over which feedstock needs to be transported, and this in turn reduces the feedstock costs. The gasifier is able to generate a hydrogen-to-carbon-monoxide ratio of near 2.0, which the fluidized-bed methanation is able to convert, without the need of an external water-gas-shift reactor to increase the hydrogen content. If renewable hydrogen would become available in the future during certain times of excess electricity generation, this hydrogen could be blended into the methanation without any significant process changes. This would improve the carbon conversion and overall plant efficiency. The intermediate producer gas contains approximately 10 percent of methane and 3 percent of other hydrocarbons. This reduces the amount of methane that needs to be synthesized in the methanation reactor, and creates a small amount of ethane in the final RNG, which helps bringing the heating value into pipeline-quality specifications.

Cleanup of the producer gas is necessary before the methanation step, especially the removal of tars and sulfur compounds. Using scrubbing columns and adsorbent beds, the cleaned gas is able to contain less than 50ppb (parts-per-billion) of sulfur. A level such low is required for fluidized-bed methanation to ensure a catalyst lifetime long enough for commercial application. The major sulfur compounds that need to be removed are hydrogen sulfide, carbonyl sulfide, and thiophene. Several cleanup stages may be required to reduce the sulfur levels by the required amount and be cost effective. This would include a bulk removal and fine removal for each of the compounds, unless future technology improvements allow for simultaneous removal of some of the compounds. During the project, cold-gas cleanup was demonstrated. In contrast, hot-gas and warm-gas cleanup could be more energy efficient, since the gas would not have to be re-heated before the methanation reactor. These gas-cleanup methods, however, currently do not have the technology readiness level to reduce sulfur compounds to ppb levels. During the cold-gas cleanup, water and benzene are two compounds that affect absorption processes. While both compounds are compatible with the fluidized-bed methanation process and would not have to be removed, reducing sulfur compounds to ppb levels is more difficult and less efficient if water and benzene are present at near 1000-ppm levels. Further optimization of absorbent technologies that work in the presence of benzene and water is recommended.

Fluidized-bed methanation was demonstrated during the project to convert the producer gas to raw RNG without major problems. Since this technology was already demonstrated at the 1MW_{RNG} level in Güssing, Austria, a commercial-sized application is considered feasible. The current project showed that the major factors for operation are heat management and coke formation. Coke formation can occur if the temperature, hydrogen-to-carbon-monoxide ratio,

or steam amount are too low. On the other hand, if the temperature, hydrogen-to-carbon-monoxide ratio, or steam amount are too high, the conversion or plant efficiency is reduced. Therefore, a careful study of coke formation, including the effects of ethylene and benzene, is recommended. During the project, a new catalyst formulation was developed that reduces coke formation, and therefore lowers the operational costs.

A cost analysis for a hypothetical 60MW_{RNG} commercial plant, incorporating the above technologies, estimates the levelized cost of RNG to be \$26/MMBtu. This is \$4/MMBtu less than a comparable plant based on fixed-bed methanation, but much larger than the cost of fossil natural gas. The major price components of the RNG costs are capital costs (\$12/MMBtu, including interest, equity returns, and associated taxes), fixed and variable operating costs (\$10/MMBtu, including materials and labor), and feedstock costs (\$4/MMBtu).

To reduce the costs of RNG, all price components should be investigated and improved. The capital costs can be further reduced, as the technology is implemented and improved, such as mass production of units and components for commercial plants at different locations, combining some of the gas cleanup steps into one unit operation, and streamlining administrative efforts for initial development costs (engineering, site development, EPC contingency, and overhead). The operating costs can be further reduced by minimizing consumables and labor, which is largely depending on the development of the knowledge around optimal operation, and developing a detailed maintenance plan. This will increase the automation of the plant and focus labor efforts on the scheduled maintenance periods. Feedstock costs can be reduced by generating relationships with forest management and waste recycling, which over time can increase the availability of feedstocks and decrease transport costs.

The following are recommendations for creating an industry of commercial woody-biomass-to-RNG conversion plants, that are efficient and cost effective:

- Evaluate the size of projected installations and how they interface with feedstock supply and technology suppliers. Different plant sizes (e.g. 50, 150, or 300 MWRNG) result in different optimal technologies for gasification, gas cleanup, and methanation. Plants that are similar in size (e.g. 50-100 MWRNG) may use the same technologies and obtain an economy of scale with providers of equipment, consumables, and maintenance services.
- Provide a path to demonstration-scale using the same or similar technology as in the projected commercial operation. The plants that are smaller than the commercial plant are not profitable and require substantial investment and funds for operations. These costs, however, are less than a commercial plant that turns out to be unprofitable. The smaller plants should test the same technologies that will be used in the commercial plant. The results of the demonstration plant should then be used in multiple commercial plants to mitigate the cost of the demonstration. The demonstration plant may also be used for operator training and may be designed to be reconfigured to test future RNG technologies or other fuel-conversion technologies.
- Investigate the individual circumstances for potential commercial plants. Besides size, other factors are byproducts (char, other fuels), electricity production, district heating, and feedstock type and moisture. Locations in colder climates have more need for district heating, but may also have feedstocks that require drying. A plant design that

can accommodate a wider range of circumstances may be adopted in other states and countries with the opportunity for technology transfer. A larger number of plants will also allow for more collaboration in operation, maintenance, and technology improvements.

In summary, the project has shown that the combination of fluidized-bed gasification and fluidized-bed methanation is able to produce RNG at high efficiency, and that there are no major technical hurdles in scaling-up the technology to pilot, demonstration, and commercial scale. Continuous improvements and optimizations in all aspects of the process, as well as cost reductions in all contributing factors will allow further reductions in the costs of RNG.

LIST OF ACRONYMS

Term	Definition
a.r.	as received
BaCaTeC	Bavaria California Technology Center
BTX	Benzene, toluene, and xylene
FICFB	Fast internally-circulating fluidized bed
GC-SCD	Gas chromatograph with sulfur chemiluminescence detector
GC-FID	Gas Chromatograph with flame ionization detector
LCOG	Levelized cost of gas (RNG)
METH134	Clariant methanation catalyst (developed for fixed-bed methanation)
MMBtu	Million British Thermal Units; equivalent to 0.973 thousand cubic feet (MCF)
PSI	Paul-Scherrer Institute
RNG	Renewable natural gas
SLPM	Standard liters per minute (referenced to 0C and 1atm)
TPO	Temperature-programmed oxidation
UCSD	Catalyst formulation used in fluidized-bed methanation (Mg-NiRu05)
U/U_{mf}	Fluidization number (superficial velocity divided by superficial velocity at minimum fluidization)

REFERENCES

- Aranda, G., van der Drift, A., Smit, R. (2014). The Economy of Large Scale Biomass to Substitute Natural Gas Plants. Petten, Netherlands: Energy Research Centre of the Netherlands. ECN-E--14-008. Retrieved from http://www.biosng.com/fileadmin/biosng/user/documents/reports/The_Economy_of_Large_Scale_Biomass_to_Bio-Methane.pdf
- California Energy Commission (2015), Levelized Cost of Upgrading Biogas to Biomethane, PON-14-505 Addendum 1 Biogas Upgrade Cost Calculator.xlsx. Retrieved from https://www.energy.ca.gov/contracts/PON-14-505/PON-14-505_Addendum_1_Biogas_Upgrade_Cost_Calculator.xlsx
- Hofbauer, H., Rauch, R., Loeffler, G., Kaiser, S., Fercher, E., Tremmel, H. (2002). Six Years Experience with the FICFB-Gasification Process. 12th European Conference and Technology Exhibition on Biomass for Energy, Industry and Climate Protection; Amsterdam, June 2002. Retrieved from http://members.aon.at/biomasse/six_years.pdf.
- Kopyscinski, J., Seemann, M.C., Moergeli, R., Biollaz, S.M.A., and Schildhauer, T.J. (2013). Synthetic Natural Gas From Wood: Reactions of Ethylene in Fluidised Bed Methanation, Applied Catalysis A: General, Volumes 462–463.
- Larsson, A., Gunnarsson, I., and Tengberg, F. (2018). The GoBiGas Project - Demonstration of the Production of Biomethane from Biomass via Gasification. Göteborg Energi. Retrieved from https://www.goteborgenergi.se/Files/Webb20/Kategoriserad%20information/Forskningsprojekt/The%20GoBiGas%20Project%20-%20Demonstration%20of%20the%20Production%20of%20Biomethane%20from%20Biomass%20v%20230507_6_0.pdf?TS=636807191662780982
- Magrini, K. (2012). Prepare, characterize and evaluate 1000 kg of reforming catalyst for use in the 2012 demonstration, NREL Milestone Report.
- Rauch, R., Hofbauer, H., Bosch, K., Siefert, I., Aichernig, C., Voigtlaender, K., Koch, R. and Lehner, R. (2004). Steam Gasification of Biomass at CHP Plant in Güssing - Status of the Demonstration Plant. 2nd World Conference and Technology Exhibition on Biomass for Energy, Industry and Climate Protection, 10-14th May 2004, Rome, Italy. Retrieved from <http://citeseerx.ist.psu.edu/viewdoc/download?doi=10.1.1.462.7303&rep=rep1&type=pdf>
- Short, W., Packey, D. J., and Holt, T. (1995). A Manual for the Economic Evaluation of Energy Efficiency and Renewable Energy Technologies. NREL/TP-462-5173. Retrieved from <https://www.nrel.gov/docs/legosti/old/5173.pdf>.

Thunman, H., Gustavsson, C., Larsson, A., Gunnarsson, I., and Tengberg, F. (2019). Economic assessment of advanced biofuel production via gasification using cost data from the GoBiGas plant. Eng. Sci. Eng., 1–13 <https://doi.org/10.1002/ese3.271>.

APPENDICES

The following appendices are available under separate cover (Publication Number CEC-500-2020-055-APA-L) by contacting Kevin Uy at Kevin.Uy@energy.ca.gov.

- Appendix A: Black and Veatch Report - Biomass Gasification for Pipeline Injection
- Appendix B: Black and Veatch Report - Evaluation of Fluidized-bed Methanation for RNG Production
- Appendix C: Biomass Feeding Failure Modes
- Appendix D: Detailed Gasifier Results
- Appendix E: Sulfur Measurement
- Appendix F: Adsorption Results
- Appendix G: Methanation Data
- Appendix H: Webinars
- Appendix I: Fluidized-bed Modeling
- Appendix J: A New Catalyst for Methanation of Producer Gas
- Appendix K: Analysis of Heavy Sulfur Compounds
- Appendix L: Post-test TPO-Analysis of Methanation Catalysts